Quantum Trajectory Theory of Continuous Variable Quantum Teleportation

Chang-Suk Noh

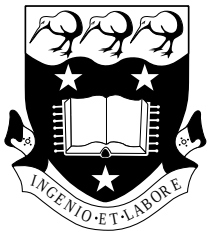

A thesis submitted
in partial fulfillment of the
requirements for the degree of
Master of Science
in
Physics

The University of Auckland
February 2005

Abstract

Quantum trajectory theory of continuous variable quantum teleportation is developed for a single-mode teleportation scheme. Necessary materials are introduced and the theories are developed, which are then applied to the teleportation protocol introduced in the thesis. A stochastic Schrödinger equation is developed from quantum trajectory theory applied to the protocol, and the equation is studied both analytically and numerically. To study the teleportation of non-classical input states, Fock states were chosen; single-shot results are investigated extensively for Fock state inputs. The Wigner function is also used to investigate the protocol analytically. The results show that both methods, quantum trajectory theory and Wigner function analysis, are equivalent.

The Wigner function of the conditional output state is calculated explicitly for a Fock state input with an arbitrary photon number. The conditional output state is also calculated from the stochastic Schrödinger equation for an arbitrary input state, and is shown to be equivalent to the Wigner function of the conditional output state of an arbitrary input state. Conditional fidelities of the single-shot output states are investigated and the results show that the quality of teleportation gets better as the squeezing parameter of the two-mode squeezed state (entangled source) is increased. Also it is shown that for Fock state inputs perfect teleportation can occur for any non-zero squeezing parameter (entanglement), although the chance of it happening is very small for a small squeezing parameter.

Acknowledgements

First of all, I would like to thank my supervisor Howard Carmichael, who has been always willing to listen to me and always answering my questions with tremendous insight. His lectures in 760 was very stimulating and was the primary reason I joined the quantum optics group for my second year of MSc. His thoroughness in proof reading is also very much appreciated. He had corrected hundreds of grammatical mistakes I made, a lot of them being in the use of articles (a's and the's).

Many thanks also to my second supervisor Matthew Collett, who also has a very deep insight on the subject, and whenever I bothered to go down to the 5th floor (my room is on the 7th floor), he had been more than helpful. I am also very thankful for his proof reading, especially when he was so busy moving the house.

Hyunchul Nha, my 'third supervisor', had been a great helper throughout the year. He clarified a lot of concepts I misunderstood, and even more gratefully he introduced me to soccer. His help and friendship has been a great factor for this year.

There are many colleagues and friends who had helped me and cheered me throughout the year. Firstly, I would like to thank Andy Chia for beeing a good peer since 2003. The discussions I had with him aided me greatly in my understanding of physics, and all the funs I had with him prevented me from getting burned out. I would also like to thank Felipe for all the help he gave me. He provided the codes for generating random numbers, gave me the TeXnicCenter with which I wrote my thesis, and taught me how to use the Latex on various occasions. I should thank the members of the soccer group also. Do-Kyung, Won-Keun, Sang-Woo, Sung-Soo, Young-Ho, Benoit and all others who played with us. Playing soccer with you had been a very enjoyable experience. Of course, we should keep playing this year.

Finally, I cannot thank enough my family members. Thank you auntie Hye-Soon and uncle Young-Rok for looking after me since July, and thank you my sisters Hyun-Jung, Ji-Eun, and Young-Eun for cheering me and helping me stay sane throughout the thesis writing period. Biggest thanks goes to my Mum and Dad, for bringing me into this world and for bringing me to New Zealand, where I found my interest in physics.

Chang-Suk Noh
February 22nd 2005

Contents

Abstract **i**

Acknowledgements **iii**

List of figures **viii**

1 Introduction **1**
1.1 General introduction to quantum teleportation 1
1.2 Outline 2

2 Introduction to quantum optics **5**
2.1 Quantized electromagnetic fields 5
2.2 Quadrature operators 7
2.3 Coherent states 9
2.4 Density operator 10
2.4.1 Properties of density operators 12
2.5 Wigner distribution 13
2.6 Squeezed light 17
2.7 Photoelectric detection 20
2.7.1 Semi-classical treatment of photoelectric detection 20
2.7.2 Photon counting distribution for quantized optical field . . . 25
2.7.3 Balanced homodyne detection 28

3 Quantum trajectory theory **31**
3.1 Dissipation and master equations 32
3.1.1 Master equations 32
3.1.2 Example: damped harmonic oscillator 35
3.2 Quantum trajectories 39
3.2.1 Exclusive photon counting distribution 40
3.2.2 Unravelling the master equation 41

3.2.3 Connection between the exclusive counting probability and the master equation . . . 42
3.2.4 Photoelectric detection of a Fock state in a cavity . . . 48
3.2.5 Balanced homodyne detection . . . 51

4 Quantum teleportation **57**
4.1 Entanglement . . . 58
4.2 Quantum teleportation . . . 61
4.3 Continuous variable quantum teleportation . . . 66

5 Fock state teleportation **71**
5.1 Teleportation protocol . . . 72
5.2 Simulation . . . 78
5.2.1 Stochastic Schrödinger equation for the protocol . . . 78
5.2.2 Numerical simulation . . . 79
5.3 Analytical methods . . . 83
5.3.1 Wigner function analysis . . . 83
5.3.2 Solving the stochastic Schrödinger equation . . . 84
5.3.3 Equivalence between the simulation and the Wigner analysis 87
5.3.4 Characteristic function from the output Wigner distribution . 89

6 Fock state teleportation: results **93**
6.1 Single-shot output states . . . 93
6.2 Fidelity . . . 97
6.3 Probability distributions of Q_x and Q_y . . . 105

7 Conclusion and future directions **111**
7.1 Conclusion . . . 111
7.2 Future directions . . . 112

A Evaluation of Eq. (3.26) **115**

B Working out $K(\lambda, 1)$ **117**

C Two-mode squeezed state **121**
C.1 Preliminary . . . 121
C.2 Wigner function for a two-mode squeezed vacuum . . . 122
C.2.1 Two-mode squeezing operator . . . 122
C.2.2 Wigner function . . . 123

D Properties of the characteristic function **127**
D.1 Property 1 . . . 127

D.2 Property 2 128
D.3 Property 3 129
D.4 Property 4 130

E Stochastic calculus **131**

F Computer codes **133**
F.1 Main code 133
F.2 Wigner plot 137

Bibliography **139**

List of Figures

2.1 Wigner distribution of a coherent state, of amplitude 1 + i. 15
2.2 Schematic representation of a coherent state, of amplitude 1 + i. . . 15
2.3 Schematic representation of a squeezed coherent state:
(a) squeezed in the x quadrature, (b) squeezed in the p quadrature,
(c) amplitude squeezed, (d) phase squeezed. 18
2.4 Light beam of cycle-averaged intensity $\bar{I}$ and cross-sectional area A incident on a photoelectric detector. 21
2.5 Sequence of photoelectric detections. Each cell represents a subinterval of duration Δt. Black dots represent successive photon detections and vacancies represent no detection. 22
2.6 The Poisson distribution with $\bar{n} = 100$. 23
2.7 Stochastically varying intensity, when the counting time T is short compared with the correlation time. 24
2.8 Schematic representation of the balanced homodyne detection scheme. 29

3.1 Conditioned mean photon number for a damped cavity initially containing a two-photon Fock state. (a) Single trajectory. (b) Average of 10,000 trajectories. 50
3.2 Model of the balanced homodyne detection scheme. 51
3.3 Conditioned photon numbers calculated by the stochastic Schrödinger equation [Eq. (3.92)], for an initial two-photon Fock state. 10,000 trajectories were averaged. 56

4.1 EPR source creates two electrons, traveling in opposite directions and having opposite spins. The electrons go to Alice (A) and Bob (B), who then pass them through Stern-Gerlach magnets. The electrons move up or down depending on their spin. 58
4.2 Schematic representation of teleportation. 63

5.1 Teleportation scheme. 72
5.2 Wigner representation of a one-photon Fock state. 77

6.1 Wigner representation of a one-photon Fock state. 94
6.2 Single-shot results of a one-photon Fock state input obtained from numerical simulations, for (a) $r = 0.1$, $Q_x = 0.5$, $Q_y = 0.46$ and $n_{max} = 10$. (b) $r = 0.7$, $Q_x = -1.55$, $Q_y = 0.41$ and $n_{max} = 20$. (c) $r = 2.0$, $Q_x = 1.37$, $Q_y = 1.50$ and $n_{max} = 190$. 95
6.3 Single-shot results of a one-photon Fock state input obtained from the analytical expression, for (a) $r = 0.1$, $Q_x = 0.5$, $Q_y = 0.46$. (b) $r = 0.7$, $Q_x = -1.55$, $Q_y = 0.41$. (c) $r = 2.0$, $Q_x = 1.37$, $Q_y = 1.50$. . 96
6.4 Conditional fidelity distribution for a one-photon Fock state input and $r = 0.7$. 200,000 trajectories. 98
6.5 Radial conditional fidelity distribution for the vacuum state input. 100,000 trajectories. 99
6.6 Radial conditional fidelity distributions for a one-photon Fock state input. 100,000 trajectories. 100
6.7 Radial conditional fidelity distributions for a two-photon Fock state input. 100,000 trajectories. 101
6.8 Radial conditional fidelity distributions for a one-photon Fock state input. Overlap of the simulation and analytical results. 100,000 trajectories. 102
6.9 Radial conditional fidelity distributions for a two-photon Fock state input. Overlap of the simulation and analytical results. 100,000 trajectories. 102
6.10 Probability distribution of Alice's measurements for a one-photon Fock state input and $r = 0.7$. 200,000 trajectories. 105
6.11 Radial probability distribution for a two-photon Fock state input and $r = 0.7$. Overlap of the simulation and analytical results. 200,000 trajectories. 108
6.12 Radial probability distribution for the vacuum state input. 100,000 trajectories. 108
6.13 Radial probability distributions for: (a) a one-photon and (b) a two-photon Fock state input. 100,000 trajectories. 109

Chapter 1

Introduction

1.1 General introduction to quantum teleportation

In 1935 Einstein, Podolsky and Rosen published a paper entitled 'Can Quantum-Mechanical Description of Physical Reality Be Considered Complete?' [1]. In the paper, as the name suggests, they tried to prove the incompleteness of quantum mechanics; they believed quantum mechanics was not the most fundamental theory that describes Nature. They used what is now called *quantum entanglement* to show the inadequacy of quantum mechanics. Ironically, quantum entanglement was later used by John S. Bell to give a testable inequality, called the Bell inequality, which were tested experimentally by many physicists to show that Nature favours the quantum mechanical description.[1]

Even though their main argument has been in vain, the concept of quantum entanglement, or entangled states, has proved to be very important. In fact, it plays a central role in the field of quantum information theory; Charles H. Bennett, one of the founders of the field, says that maximally entangled states are the 'purest form of quantum information' [2]. Quantum entanglement is *the* enabling resource in superdense coding [3] and quantum teleportation [4].

According to some, quantum teleportation is the disembodied transport of a quantum state from one place to another by the use of quantum entanglement and a classical communication channel [5, 6, 7]. The total information of the state is separated into classical and quantum information and then transmitted through the classical channel and quantum entanglement, respectively. Quantum teleportation was first proposed by Bennett *et al.* [4] for dichotomic variables (living in a two-

[1] More about the Bell inequality is said in Chapter 4.

dimensional Hilbert space) and later extended by Vaidman [8] to continuous variables (living in an infinite-dimensional Hilbert space); then Braunstein and Kimble [9] proposed a practical scheme using quantum optical tools.

We adopt the teleportation scheme of Braunstein and Kimble in this thesis. In their paper Braunstein and Kimble used the Wigner function (introduced in Chapter 2) to analyze the teleportation scheme and showed that it does work. Our object is to give an alternative description of the scheme using quantum trajectory theory and see if the scheme works as expected. Meanwhile, we try non-classical input states, namely Fock states; Braunstein and Kimble illustrated their scheme with a non-classical state, but the two existing experimental realizations [5, 10] of the scheme make use of classical states called coherent states.[2] The Fock states are interesting because they show the features of truly *quantum* states, i.e., states which do not allow a hidden-variable type description (such as stochastic electrodynamics). Unlike other works on continuous variable quantum teleportation (CVQT), we concentrate on single-shot results, trying to see the shot-to-shot quality of teleportation. Visualization of the states is provided by the Wigner function.

1.2 Outline

A large proportion of this thesis is devoted to the introduction of background materials which one must know before a full understanding of the teleportation protocol and its analysis can be attained. No familiarity with quantum optics is assumed, although it would certainly help the reader, but substantial knowledge of quantum mechanics is assumed, preferably first year graduate level. References to textbooks are given in places to help readers with limited background as much as possible.

Chapter 2 introduces basic concepts of quantum optics; a lot of them taken from the quantum optics lectures given in the first year of MSc here at the University of Auckland. A broad range of material is covered, necessarily in sketchy form, with references given for more detailed explanations.

Chapter 3 introduces quantum trajectory theory. Dissipation in open systems is introduced and the description of dissipation via the master equation is given. The latter is applied to the damped harmonic oscillator, which provides an example through which we develop the theory of quantum trajectories.

Chapter 4 explains the teleportation protocol of Braunstein and Kimble. To do

[2]The definition of non-classical states are given at the end of Section 5.1, and the coherent states are introduced in the next chapter.

this, we describe quantum entanglement first, then the original proposal of Bennett *et al.* which is in terms of dichotomic variables, for example spin. The last section of the chapter describes the proposal of Braunstein and Kimble in detail.

Chapter 5 explains the methods of analysis. Largely, there are two methods: numerical simulations and finding analytical expressions. A specific protocol for teleportation is introduced first, then the stochastic Schrödinger equation of the protocol is obtained from quantum trajectory theory. The details of numerical simulation via quantum trajectory theory are explained. Analytical expressions are obtained by working in the Wigner representation, as in Braunstein and Kimble, as well as by solving the stochastic Schrödinger equation. Both expressions are compared and shown to be equivalent.

Chapter 6 presents all the results, both from the simulation and analytic expressions. A few single-shot output states are shown in the Wigner representation. A measure of the quality of teleportation, the fidelity, is introduced and evaluated for various input states. The probability distribution for Alice's measurement results (this statement will become clear in Chapter 6) is also given.

Chapter 7 presents the conclusion and remarks on possible future works.

Finally, some mathematical results as well as the computer codes for numerical simulations are given in the Appendices.

Chapter 2

Introduction to quantum optics

This chapter introduces various tools and concepts in quantum optics, which will be used throughout this thesis. This is not, however, meant to be a complete introduction to quantum optics. We merely state the fundamental concepts without rigorous derivations. For more concrete discussions see Refs. [11, 12, 13].

2.1 Quantized electromagnetic fields

In its most basic form, quantum optics deals with the interaction between electromagnetic fields and atoms. To build a fully quantum mechanical theory, one obviously has to quantize not only the atoms but the electromagnetic fields as well. In this section we briefly look at the formalism of quantized electromagnetic fields.

When the free electromagnetic field is quantized, its Hamiltonian can be written as

$$\hat{H} = \sum_k \hbar\omega_k(\hat{n}_k + \frac{1}{2}), \tag{2.1}$$

where k denotes a mode of the electromagnetic field, ω_k the angular frequency of the mode and $\hat{n}_k$ the photon number operator for the mode. $\hbar$ is the Planck's constant, which makes the units right. The Hamiltonian has the same form as that of a set of harmonic oscillators. Thus, the free electromagnetic field can be formally represented by a set of harmonic oscillators [14]. The $\sum_k 1/2$ gives a, generally infinite, non-zero energy to the ground state, which is due to what is called the vacuum fluctuations. However, because only the change in energy can be measured, the constant term of $\sum_k 1/2$ can be ignored.[1] The vacuum fluctuations are briefly

[1] If the electromagnetic fields exist in different regions with different boundary conditions, the

discussed below Eq. (2.73).

Let us assume that the electromagnetic field is a single-mode field, so that the sum (over k) goes away. The eigenstates (constant energy states) of this Hamiltonian are called number states or Fock states. The Fock state containing n photons is denoted $|n\rangle$. It is assumed that the Fock states form a complete orthonormal basis, that is, any state (ignoring the polarizations) of the electromagnetic field can be represented as a superposition of Fock states, i.e.,

$$|\psi\rangle = \sum_n c_n |n\rangle. \tag{2.2}$$

The completeness of the basis states may be written as

$$\sum |n\rangle\langle n| = \hat{1}, \tag{2.3}$$

where $\hat{1}$ is the unit operator. We can see this by inserting the unit operator in front of an arbitrary state:

$$|\psi\rangle = \hat{1}\ |\psi\rangle = \sum |n\rangle\langle n|\psi\rangle = \sum c_n |n\rangle. \tag{2.4}$$

Note that the coefficient c_n is given by $\langle n|\psi\rangle$.

The number operator can be written as

$$\hat{n} = a^\dagger a, \tag{2.5}$$

where $a^\dagger$ and a are the photon creation and annihilation operators, respectively (the hat on the annihilation and creation operators is omitted). They operate on the Fock states to create and annihilate a photon, i.e.,

$$a^\dagger |n\rangle = \sqrt{n+1}|n+1\rangle, \tag{2.6a}$$

$$a\ |n\rangle = \sqrt{n}|n-1\rangle. \tag{2.6b}$$

Note that $a|0\rangle = 0$. $|0\rangle$, the state with no photons, is called the vacuum state.

Although there are no photons in the vacuum state, the $\hbar\omega/2$ term in Eq. (2.1) – remember, the electromagnetic field is in a single-mode – gives non-zero energy to the state. In terms of mechanical harmonic oscillators, this comes from the perpetual

term cannot be ignored. For example, it could lead to an observable effect called the Casimir effect. See Mandel [15], Section 10.9.3, and Merzbacher [11] p. 574, and the references therein.

jiggling of the particle in a harmonic potential, while in terms of the electromagnetic field, it comes from the vacuum fluctuations mentioned earlier. Since photons are bosons, a and $a^\dagger$ obey the commutation relation given by

$$[a, a^\dagger] = 1. \tag{2.7}$$

A single-mode electric field operator may be represented in terms of the creation and annihilation operators as

$$\hat{E} = i\left(\frac{\hbar\omega}{2\epsilon_0 V}\right)^{\frac{1}{2}}[ae^{i(kx-wt)} - a^\dagger e^{-i(kx-wt)}], \tag{2.8}$$

where V is the volume of the cube the electric field is quantized in. The total electric field inside the cube is a sum over all modes of the electric field obeying periodic boundary conditions. Often, the total electric field is written in terms of its positive and negative frequency parts:

$$\hat{\mathbf{E}}(r,t) = \hat{\mathbf{E}}^{(+)}(r,t) + \hat{\mathbf{E}}^{(-)}(r,t), \tag{2.9}$$

where

$$\hat{\mathbf{E}}^{(+)}(r,t) = i\sum_{\mathbf{k},\lambda}\sqrt{\frac{\hbar\omega_{\mathbf{k}}}{2\epsilon_0 V}}\hat{e}_{\mathbf{k},\lambda}a_{\mathbf{k},\lambda}e^{-i(\omega_k t - \mathbf{k}\cdot r)}, \tag{2.10}$$

$$\hat{\mathbf{E}}^{(-)}(r,t) = \hat{\mathbf{E}}^{(+)}(r,t)^\dagger. \tag{2.11}$$

$\mathbf{k}$ is the wave-vector and $\hat{e}_{\mathbf{k},\lambda}$ is the polarization direction of the electric field, where there are two perpendicular directions of polarization denoted by the subscript λ. A similar expansion exists for a magnetic field operator, but we will not go into it here. The details of expansions of the electric and magnetic field operators can be found in many textbooks; see, for example, Chapter 1 of Scully [12].

2.2 Quadrature operators

Quadrature operators are defined in terms of the creation and annihilation operators as

$$\hat{A}_\theta \equiv \frac{1}{2}\left(ae^{-i\theta} + a^\dagger e^{i\theta}\right), \tag{2.12}$$

where θ is the angle of the quadrature. The quadrature operator is Hermitian and therefore an observable. It can be measured experimentally using the (balanced) homodyne detection [16]. (See Section 2.7.3.) In this thesis, we are mainly interested in the two quadratures defined by $\theta = 0$ and $\theta = \pi/2$. We will call them $\hat{x}$ and $\hat{p}$:

$$\hat{x} \equiv \frac{1}{2}\left(a + a^\dagger\right), \qquad \hat{p} \equiv \frac{1}{2i}\left(a - a^\dagger\right). \tag{2.13}$$

From this equation we obtain

$$a = \hat{x} + i\hat{p}. \tag{2.14}$$

Using the quadrature operators [Eq. (2.13)], we can rewrite Eq. (2.8) as

$$\hat{E} = -\left(\frac{2\hbar\omega}{\epsilon_0 V}\right)^{\frac{1}{2}} [\hat{x}\sin(kx - wt) + \hat{p}\cos(kx - wt)]. \tag{2.15}$$

Looked at in this way, the quadrature operators $\hat{x}$ and $\hat{p}$ are just the amplitude operators of cosinusoidally and sinusoidally varying terms of the electric field, respectively.

From Eq. (2.7), we can derive the commutation relationship between $\hat{x}$ and $\hat{p}$:

$$[\hat{x}, \hat{p}\,] = \frac{i}{2}. \tag{2.16}$$

This commutation relation tells us that the quadrature operators $\hat{x}$ and $\hat{p}$ are canonically conjugate variables, just like the position and momentum operators.[2] It is for this reason that we call the two quadrature operators $\hat{x}$ and $\hat{p}$. Since they are non-commuting observables they obey the Heisenberg Uncertainty Principle (HUP), i.e., they obey

$$\Delta x \Delta p \geq \frac{1}{4}. \tag{2.17}$$

The quadrature operators will be useful later when we look at the Wigner distributions and squeezed light.

[2] $\hbar$ and the factor of 2 are irrelevant, since they can be absorbed into the definition of the $\hat{x}$ and $\hat{p}$. Often the units are chosen such that $\hbar = 1$, in which case we only have to absorb the factor 2.

2.3 Coherent states

It is extremely difficult to generate a Fock state experimentally, and states are generally in a superposition of Fock states as shown in Eq. (2.2). One such state, which is very important in quantum optics, is called the coherent state. It represents, to a good approximation, the state of a laser beam, and is the closest quantum mechanical state to classical light (soon we will see why this is so). Coherent states can be defined as eigenstates of the annihilation operator, i.e.,

$$a|\alpha\rangle = \alpha|\alpha\rangle, \tag{2.18}$$

where $|\alpha\rangle$ is the coherent state. We will not go into details, but the Fock state representation of the coherent states can be found from the relationships

$$\langle n|a|\alpha\rangle = \alpha\langle n|\alpha\rangle, \tag{2.19a}$$

$$\langle n|a|\alpha\rangle = \langle\alpha|a^\dagger|n\rangle^* = \sqrt{n+1}\langle\alpha|n+1\rangle^* = \sqrt{n+1}\langle n+1|\alpha\rangle. \tag{2.19b}$$

and the normalization condition $\langle\alpha|\alpha\rangle = 1$. It is given by

$$|\alpha\rangle = \exp\left(-\frac{|\alpha|^2}{2}\right)\sum_{n=0}^{\infty}\frac{\alpha^n}{\sqrt{n!}}\,|n\rangle. \tag{2.20}$$

It can be proved that the coherent states form a complete set of basis states [13], so they can be used to build up the unit operator, i.e.,

$$\frac{1}{\pi}\int |\alpha\rangle\langle\alpha| d^2\alpha = \hat{1}, \tag{2.21}$$

but they are not orthogonal.[3] In fact, the scalar product of two coherent states is given by

$$\langle\alpha|\beta\rangle = \exp\left[-\frac{1}{2}(|\alpha|^2 + |\beta|^2) + \alpha^*\beta\right] \tag{2.22}$$

Formally, coherent states can be generated using the displacement operator

$$D(\alpha) = \exp\left(\alpha a^\dagger - \alpha^* a\right), \tag{2.23}$$

[3] a is not an observable, it is not Hermitian, so the eigenstates do not have to be orthogonal to each other.

by displacing the vacuum state, i.e.,

$$|\alpha\rangle = D(\alpha)|0\rangle. \tag{2.24}$$

The displacement operators have the following properties:

$$D^\dagger(\alpha) = D^{-1}(\alpha), \tag{2.25a}$$
$$D^\dagger(\alpha) a D(\alpha) = a + \alpha. \tag{2.25b}$$

Incidentally, the coherent states are minimum uncertainty states of the observables $\hat{x}$ and $\hat{p}$. We can see this from a simple calculation:

$$\langle \hat{x} \rangle = \frac{1}{2}\langle \alpha | (a + a^\dagger) | \alpha \rangle = \frac{1}{2}(\alpha + \alpha^*), \tag{2.26}$$

$$\begin{aligned} \langle \hat{x}^2 \rangle &= \frac{1}{4}\langle \alpha | [a^2 + aa^\dagger + a^\dagger a + (a^\dagger)^2] | \alpha \rangle = \frac{1}{4}\langle \alpha | [a^2 + 1 + 2a^\dagger a + (a^\dagger)^2] | \alpha \rangle, \\ &= \frac{1}{4}[\alpha^2 + 1 + 2|\alpha|^2 + (\alpha^*)^2] = \frac{1}{4}(\alpha + \alpha^*)^2 + \frac{1}{4}, \\ &= \langle \hat{x} \rangle^2 + \frac{1}{4}, \\ \Delta x &= \sqrt{\langle \hat{x}^2 \rangle - \langle \hat{x} \rangle} = \frac{1}{2}. \end{aligned} \tag{2.27}$$

Similarly, $\Delta p = \frac{1}{2}$. Thus, for the coherent states, we obtain the uncertainty relation

$$\Delta x \Delta p = \frac{1}{4}. \tag{2.28}$$

Comparing with Eq. (2.17), we immediately see that the coherent states are minimum uncertainty states. In this sense, the coherent states are as close as a quantum state can get to a classical state, i.e., with definite values for both x and p. If the average number of photons for a coherent state is large, the statistical uncertainty in the amplitude of the coherent state becomes negligible and the state approximately describes the field generated by a laser.

2.4 Density operator

So far we have been working only with pure states. Although pure states have a statistical nature guarded by the HUP, it is intrinsically different to the classical uncertainty. For example, the intrinsic statistical nature applies just as well to a

single particle system as it does to an ensemble of such systems. Thus the uncertainty is not from our ignorance about the system.

We now look at the formalism to describe a system which can accommodate our classical ignorance on top of the quantum mechanical uncertainty – the density operator formalism. To motivate the form of density operators, we note that the quantities of importance in quantum mechanical systems are the expectation values, since they are the things that connect the theory to experiments. In bra-ket notation, the expectation value of an operator $\hat{A}$ in a pure state $|\psi\rangle$ is given by

$$\langle\psi|\hat{A}|\psi\rangle. \tag{2.29}$$

Equivalently, it may be written in a trace form:

$$\mathrm{tr}\left[\hat{A}|\psi\rangle\langle\psi|\right] \equiv \sum\langle n|\hat{A}|\psi\rangle\langle\psi|n\rangle, \tag{2.30}$$

where the set of states $|n\rangle$ forms a complete set of basis states (any complete set will do, as the trace is independent of the basis set). We can see the equivalence of Eq. (2.29) and Eq. (2.30) by rearranging the latter:

$$\sum\langle n|\hat{A}|\psi\rangle\langle\psi|n\rangle = \sum\langle\psi|n\rangle\langle n|\hat{A}|\psi\rangle = \langle\psi|\hat{A}|\psi\rangle, \tag{2.31}$$

where, in the second equality we used the completeness of $|n\rangle$.

Now we introduce some classical ignorance. Suppose we have an ensemble of particles which have an observable A such that 20% of them are in a state that gives a_1, 40% give a_2, and 40% give a_3. In classical mechanics, the average value of A of the whole ensemble is given by

$$\langle A\rangle = \frac{1}{5}\,a_1 + \frac{2}{5}\,a_2 + \frac{2}{5}\,a_3, \tag{2.32}$$

where the angled brackets denote the ensemble average. To write the quantum mechanical version of this, we introduce a density operator

$$\hat{\rho} = \frac{1}{5}|a_1\rangle\langle a_1| + \frac{2}{5}|a_2\rangle\langle a_2| + \frac{2}{5}|a_3\rangle\langle a_3|, \tag{2.33}$$

from which we can write the expectation value of $\hat{A}$ as

$$\langle\hat{A}\rangle = \mathrm{tr}\left[\hat{A}\hat{\rho}\right] = \frac{1}{5}\,a_1 + \frac{2}{5}\,a_2 + \frac{2}{5}\,a_3. \tag{2.34}$$

In general, density operators can be written as

$$\hat{\rho} = \sum p_i |i\rangle\langle i|, \tag{2.35}$$

where p_i is the probability to be in the state $|i\rangle$. The expectation value of an arbitrary operator $\hat{A}$ in the ensemble of states described by the density operator $\hat{\rho}$ is given by

$$\langle \hat{A} \rangle = \mathrm{tr}\left[\hat{A}\hat{\rho}\right]. \tag{2.36}$$

2.4.1 Properties of density operators

1. Trace of density operators:

   Because the probabilities add up to one, i.e., $\sum p_i = 1$, we have

   $$\mathrm{tr}\left[\hat{\rho}\right] = 1. \tag{2.37}$$

2. Time evolution of density operators:

   From the Schrödinger equation

   $$i\hbar \frac{d|\psi\rangle}{dt} = \hat{H}|\psi\rangle, \tag{2.38}$$

   we can work out the time evolution of density operators:

   $$\begin{aligned} \frac{d\hat{\rho}}{dt} &= \frac{d|\psi\rangle}{dt}\langle\psi| + |\psi\rangle\frac{d\langle\psi|}{dt} = -\frac{i}{\hbar}\left(\hat{H}|\psi\rangle\langle\psi| - |\psi\rangle\langle\psi|\hat{H}\right), \\ &= -\frac{i}{\hbar}\left[\hat{H}, \hat{\rho}\right]. \end{aligned} \tag{2.39}$$

   This equation (the von Neumann equation) looks like the Heisenberg equation of motion, except for the minus sign, but since we are in the Schrödinger picture and there is no direct connection.

3. Pure states and mixed states:

   A pure state can be represented by a single ket, but a mixed state has to be represented by a density operator. We can find out whether a density

operator is pure or mixed by calculating

$$\mathrm{tr}\left[\hat{\rho}^2\right]. \tag{2.40}$$

If the density operator represents a pure state, $\hat{\rho}^2 = \hat{\rho}$, and thus the trace is equal to one; otherwise, the trace is less than one.

4. The cyclic property:

$$\mathrm{tr}[\hat{A}\hat{B}] = \mathrm{tr}[\hat{B}\hat{A}]. \tag{2.41}$$

It is seen easily from the definition of the trace.

2.5 Wigner distribution

This section introduces what is called a 'phase space representation' of quantum states.[4] There are three commonly used representations, but we will only consider the Wigner representation here. The Wigner distribution[5] was first introduced by Eugen P. Wigner in 1932, and used in working out quantum mechanical corrections to thermal equilibrium [18]. Our main interest, however, is in its ability to provide a visualization of the quantum states. In fact we can 'see' the quantum mechanical fluctuations from the Wigner distribution. We will demonstrate this for the coherent states shortly.

The Wigner distribution is a two-dimensional Fourier transform of a suitably defined characteristic function. For a system represented by a density operator $\hat{\rho}$, it can be written as

$$W(\alpha, \alpha^*) = \frac{1}{\pi^2} \int d^2z \ \mathrm{tr}\left[\hat{\rho} \exp\left(iza + iz^* a^\dagger\right)\right] \exp\left(-i\alpha z - i\alpha^* z^*\right), \tag{2.42}$$

where

$$\chi_s(z, z^*) = \mathrm{tr}\left[\hat{\rho} \exp\left(iza + iz^* a^\dagger\right)\right] \tag{2.43}$$

is the characteristic function. To provide the meaning of α, it is instructive to work

[4] Our discussion on this subject is necessarily very limited. For a more concrete discussion see, for example, Schleich [17].

[5] In the literature, the names Wigner distribution and Wigner function are used synonymously.

out the Wigner distribution for a coherent state. Using the Baker-Hausdorff theorem [19] and $\hat{\rho} = |\beta\rangle\langle\beta|$, we get

$$\begin{aligned} \mathrm{tr}\left[\hat{\rho}\exp\left(iza + iz^*a^\dagger\right)\right] &= \mathrm{tr}\left[\hat{\rho}\exp(iz^*a^\dagger)\exp\left(iza\right)\right]\exp\left(-\frac{1}{2}|z|^2\right), \\ &= \exp(iz^*\beta^*)\exp\left(iz\beta\right)\exp\left(-\frac{1}{2}|z|^2\right). \end{aligned} \tag{2.44}$$

We now put this back into Eq. (2.42) and carry out the integration. To do this, we write the complex variables z and α in terms of real variables, i.e., $z = y+iq$ and $\alpha = x + ip$. Then, $d^2z = dydq$ and the integration can be carried out straightforwardly. The answer we get is

$$W_{|\beta\rangle}(x,p) = \frac{2}{\pi}\exp\left\{-2\left[(x-x_\beta)^2 + (p-p_\beta)^2\right]\right\}, \tag{2.45}$$

where $\beta = x_\beta + ip_\beta$. Figure 2.1 shows the Wigner distribution: a Gaussian distribution centered at $\alpha = \beta$. The coherent state $|\beta\rangle$ is an eigenstate of the annihilation operator $\hat{a} = \hat{x} + i\hat{p}$ with the eigenvalue $x_\beta + ip_\beta$, and since the Wigner distribution of the coherent state is a Gaussian centered at $x = x_\beta$, $p = p_\beta$, we can think of the x and p as the corresponding values of the operators $\hat{x}$ and $\hat{p}$. This interpretation is supported by the fact that the expectation values of $\hat{x}$ and $\hat{p}$ can be worked out by treating the Wigner function as a probability distribution over the x and p representing $\hat{x}$ and $\hat{p}$, respectively. [See Eq. (2.50).]

Figure 2.2 is a schematic representation of a coherent state in the Wigner representation. The center of the circle is placed at the amplitude of the coherent state, and the radius of the circle corresponds to the width of the Gaussian which could be one or two standard deviations. Now imagine that the amplitude of the coherent state is increased. The size of the circle (uncertainty due to the quantum fluctuations) remains the same, but the center moves away from the origin. Therefore the signal to noise ratio decreases. If the average number of photons in a coherent state is very large, the amplitude of the coherent state is also very large ($\langle\alpha|\hat{n}|\alpha\rangle = |\alpha|^2$) and the state behaves like a classical field. The quantum fluctuations can be ignored.

So far we have seen how the Wigner distribution can give a graphical representation of a quantum state. However, this is not all. The Wigner distributions can also act like probability distributions over x and p, although strictly, they are not. We will now see in which sense the Wigner distributions do act like probability distributions and in which sense they do not.

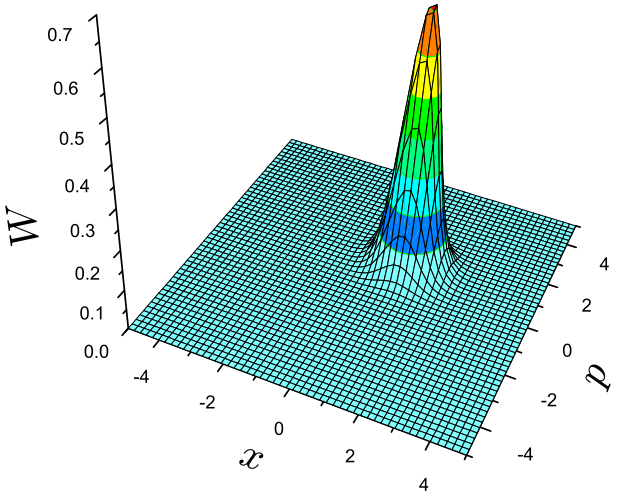

Figure 2.1: Wigner distribution of a coherent state, of amplitude 1 + i.

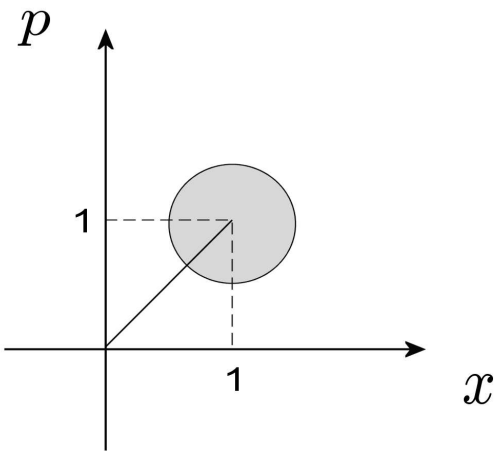

Figure 2.2: Schematic representation of a coherent state, of amplitude 1 + i.

The Wigner distribution can be used to calculate the expectation values of any symmetrically ordered product of annihilation and creation operators, i.e.,

$$\left\langle \left(a^{\dagger n}a^m\right)_s \right\rangle = \int d^2\alpha W(\alpha,\alpha^*)\,\alpha^{*n}\alpha^m, \tag{2.46}$$

where the subscript s denotes the symmetric ordering. In a symmetrically-ordered operator, every possible ordering of a and $a^\dagger$ occurs. For example,

$$\left(a^\dagger a\right)_s = \frac{1}{2}\left(a^\dagger a + aa^\dagger\right), \tag{2.47a}$$

$$\left(a^{\dagger 2}a\right)_s = \frac{1}{3}\left(a^{\dagger 2}a + a^\dagger a a^\dagger + aa^{\dagger 2}\right), \tag{2.47b}$$

$$\left(a^\dagger a^2\right)_s = \frac{1}{3}\left(a^\dagger a^2 + aa^\dagger a + a^2 a^\dagger\right). \tag{2.47c}$$

Eq. (2.46) can be proved in the following way. First, from the definition of the characteristic function [Eq. (2.43)], we get

$$\begin{aligned}\left\langle \left(a^{\dagger n}a^m\right)_s \right\rangle &= \mathrm{tr}\left[\hat\rho\left(a^{\dagger n}a^m\right)_s\right], \\ &= \frac{\partial^{n+m}}{\partial(iz^*)^n\partial(iz)^m}\chi_s(z,z^*)\bigg|_{z=z^*=0}.\end{aligned} \tag{2.48}$$

Then noting that $\chi_s(z,z^*)$ is the inverse Fourier transform of the Wigner distribution, i.e.,

$$\chi_s(z,z^*) = \int d^2\alpha W(\alpha,\alpha^*)\exp(iz^*\alpha^* + iz\alpha), \tag{2.49}$$

after substituting it into Eq. (2.48), we obtain Eq. (2.46).

Since $\hat x^n$ and $\hat p^m$ are symmetrically ordered operators, we can calculate the expectation values of $\hat x^n$ and $\hat p^m$ using the relations

$$\langle \hat x^n\rangle = \int dxdpW(x,p)x^n, \tag{2.50a}$$

$$\langle \hat p^m\rangle = \int dxdpW(x,p)p^m. \tag{2.50b}$$

These equations suggest that the marginal distributions, $\int dxW(x,p)$ and $\int dpW(x,p)$, act as the probability distributions over x and p, respectively. Consequently we can think of $W(x,p)$ as the joint probability distribution, although strictly, it is not a probability density: the expectation value of $\hat x^n\hat p^m$ cannot be

found in the same way as in Eq. (2.50). This is because the two operators do not commute with each other, and what phase space integration finds is, again, the symmetrically ordered operator average, i.e.,

$$\langle (\hat{x}^n \hat{p}^m)_s \rangle = \int dx dp W(x,p) x^n p^m. \tag{2.51}$$

Note that the symmetrically ordered operators are Hermitian, and therefore observables. The ordering issue, however, is a strictly quantum feature. If the quadrature operators $\hat{x}$ and $\hat{p}$ were not operators, ordering would not matter at all. Thus, $W(x,p)$ can still be thought of as a probability distribution which can be used to calculate the (symmetrically ordered) operator averages. The more serious issue is that a Wigner distribution can be negative, and once it is, we can no longer interpret it as a probability distribution. Thus, the Wigner distribution is called a quasi-probability distribution.

2.6 Squeezed light

In the previous section, we have seen the Wigner representation of a coherent state, the minimum uncertainty state with equal uncertainty in all the quadratures. Now we look at a more general kind of minimum uncertainty state; states which have different uncertainty in different quadratures while keeping the product of uncertainties in the orthogonal quadratures to be the minimum. An easy way to see this conceptually, is to look at the schematic diagram of the state in phase space, as shown in Figure 2.2 for the coherent state. Figure 2.3 shows the squeezed version of the coherent state shown in Figure 2.2. Depending on the squeezed 'direction', squeezed states have different names, as captioned in the figure.

We now have some idea of what the squeezed states are; their quadratures have 'squeezed' uncertainty in a certain quadrature or 'direction', at the cost of increased uncertainty in the orthogonal quadrature. Next, we develop a formal approach starting from the squeeze operator.

The squeeze operator is given as [20]

$$S(\varepsilon) = \exp\left(\frac{1}{2}\varepsilon^* a^2 - \frac{1}{2}\varepsilon\, a^{\dagger 2}\right), \tag{2.52}$$

where $\varepsilon = r\mathrm{e}^{2i\phi}$. ϕ determines the angle of the squeezed quadrature and r, the squeezing parameter, determines the amount of squeezing. The squeeze operator is

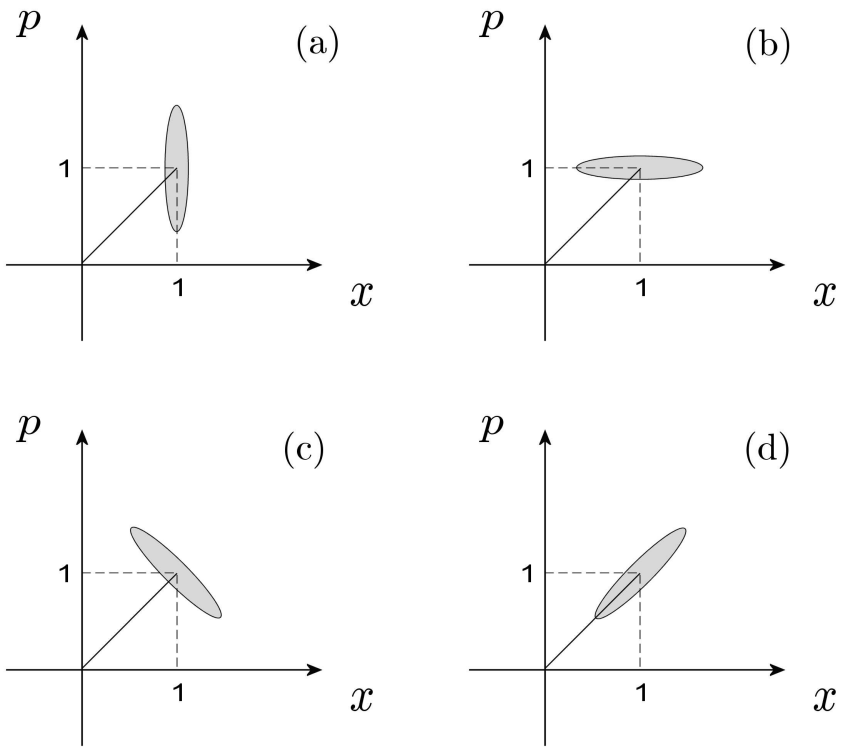

Figure 2.3: Schematic representation of a squeezed coherent state:
(a) squeezed in the x quadrature, (b) squeezed in the p quadrature,
(c) amplitude squeezed, (d) phase squeezed.

unitary:

$$S^\dagger(\varepsilon) = S^{-1}(\varepsilon) = S(-\varepsilon), \tag{2.53}$$

where the last equality follows from the definition. It transforms the annihilation and creation operators as

$$S^\dagger(\varepsilon) a S(\varepsilon) = a\cosh(r) - a^\dagger \mathrm{e}^{+2i\phi}\sinh(r), \tag{2.54a}$$

$$S^\dagger(\varepsilon) a^\dagger S(\varepsilon) = a^\dagger\cosh(r) - a\mathrm{e}^{-2i\phi}\sinh(r). \tag{2.54b}$$

From Eq. (2.54) we can work out the transformation of the quadrature operator

given in Eq. (2.12):

$$S^{\dagger}(\varepsilon)\left(\hat{A}_{\phi}+i\hat{A}_{\phi+\pi/2}\right)S(\varepsilon)=\hat{A}_{\phi}e^{-r}+i\hat{A}_{\phi+\pi/2}e^{r}. \tag{2.55}$$

For example, if $\phi=0$ we get

$$S^{\dagger}(r)\left(\hat{x}+i\hat{p}\right)S(r)=\hat{x}e^{-r}+i\hat{p}e^{r}. \tag{2.56}$$

This explicitly shows that the quadratures are amplified and deamplified. How much they are amplified and deamplified depends on the squeezing parameter r. Squeezed coherent states can be obtained by squeezing the vacuum state and then displacing it:[6]

$$|\alpha,\varepsilon\rangle=D(\alpha)S(\varepsilon)|0\rangle \tag{2.57}$$

For this state, the quadratures have the uncertainties given by

$$\Delta A_{\phi}=\frac{1}{2}e^{-r}, \qquad \Delta A_{\phi+\pi/2}=\frac{1}{2}e^{\,r}. \tag{2.58}$$

Specifically, if $\varepsilon=r$, $|\alpha,r\rangle$ has the uncertainties given by

$$\Delta x=\frac{1}{2}e^{-r}, \qquad \Delta p=\frac{1}{2}e^{\,r}. \tag{2.59}$$

It should be mentioned that the displacement operators do not change the uncertainty of the squeezed states, i.e., the widths of the ellipses in Figure 2.3 do not change. Every squeezed coherent state has the same uncertainty as the squeezed vacuum.

In this section we introduced the quantum mechanical description and phase space representation of squeezed states. Quantum squeezing has received a lot of attention, and found applications, during the past two decades, and now is one of the fundamental resources in the field of quantum information. Reduction of noise in one quadrature has also found use in ultra-sensitive measurements, such as gravitational wave detection. These have all been possible because of the experimental success in generation and detection of squeezed states. For reviews on squeezing see Ref. [21] and Ref. [22].

[6] In some literature the vacuum state is displaced first and then squeezed. There is no fundamental difference between the two approaches, a simple relationship between them exists. See for example Section 2.4 and 2.5 of Walls [13].

2.7 Photoelectric detection

To detect squeezing, people normally use what is called the 'balanced homodyne detection' scheme [23]. In a homodyne detector, the signal field is mixed with a high intensity coherent field (called the local oscillator) and then the mixed field is detected with a photoelectric detector. The local oscillator field introduces a phase in the measurement, and thus the whole detection scheme is phase sensitive. This phase sensitivity is necessary in the detection of squeezing, since squeezing is a phase dependent phenomenon. Balanced homodyne detection is a convenient version of homodyne detection, used often in experiments because it allows unwanted noise to be subtracted.

Our object, in this section, is to introduce the balanced homodyne detection scheme and understand how it can be used to measure the noise reduction in squeezed light. Before we do this, however, we develop the theory of photoelectric detection, since photoelectric detectors are the building blocks of a balanced homodyne detector. The discussion here is essentially that of Carmichael [24].

2.7.1 Semi-classical treatment of photoelectric detection

Suppose we have a beam of light traveling freely across a room. We want to do a photon counting experiment, so we place a photoelectric detector in the path of the beam. When a photon, from the light beam, hits the detector, it ionizes an atom in a photoelectric material; the generated photoelectron subsequently goes through a multiplication process, producing a pulse of current. In photon counting experiments, we simply count the number of these pulses. One of the basic question we might ask is this: what is the probability of measuring n photons in a time interval T? We will try to answer this question.

To describe the photoelectric detection process we need a full quantum mechanical treatment of the light-atom interaction, i.e., quantized electromagnetic fields interacting with quantized atoms. Needless to say, developing the full theory might take some time. So instead, we start with the semi-classical theory of light interacting with atoms. In the semi-classical theory, the atoms are quantized but the electromagnetic field is treated classically. Because of the quantum nature of the interaction between the electromagnetic field and the detector (photoelectric material), we can only talk about the *probabilities* of counting a certain number of photons in a time interval T. Using the semi-classical theory we work out the photon counting distribution $P(n, t, T)$, the probability of counting n photons in a time

interval $(t, t+T)$, which will motivate the form of the fully quantum mechanical expression.

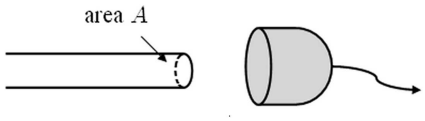

Figure 2.4: Light beam of cycle-averaged intensity $\bar{I}$ and cross-sectional area A incident on a photoelectric detector.

Consider a beam of light with frequency ω incident on a photoelectric detector (Figure 2.4). The light beam has a cross-sectional area A and a constant cycle-averaged intensity $\bar{I}$. In a time interval T, the average number of photons we measure, $\bar{N}$, will be

$$\bar{N} = \frac{A\bar{I}T}{\hbar\omega}, \tag{2.60}$$

where $\hbar\omega$ is the energy of a photon in the beam, whence $A\bar{I}/\hbar\omega$ is the number of photons passing through area A per second. The above equation is true only if all the photons incident on the detector are detected. Otherwise, the detector has a *quantum efficiency* η depending on the details of the light and detector. We will take it as an empirical parameter, a given number between 0 and 1. With a non-unit quantum efficiency η we have

$$\bar{N} = \eta\frac{A\bar{I}T}{\hbar\omega} = \epsilon\bar{I}T. \tag{2.61}$$

Now we divide the time interval T into N subintervals of duration Δt:

$$N = \frac{T}{\Delta t}. \tag{2.62}$$

Then, if $N \gg 1$, $\Delta t \ll 1$ such that $\epsilon\bar{I}\Delta t \ll 1$, the probability for detecting a photon in any subinterval can be approximated as

$$p = \epsilon\bar{I}\Delta t. \tag{2.63}$$

If Δt is small enough, the chance of detecting two photons in a subinterval can be

neglected.

We have only given a heuristic argument here, but Eq. (2.63) can be derived from semi-classical arguments.[7] Note that Eq. (2.63) is valid only as long as $\Delta t \gg 1/\omega$. That is, Δt must be big enough so that only the time averaged intensity $\bar{I}$ is important. We are not interested in the situation where the intensity is so high that the above approximation cannot be true.

Given Eq. (2.63), the probability of having no photodetection in time Δt, which we will call q, is simply given by $1 - p$, i.e.,

$$q = 1 - p = 1 - \epsilon \bar{I} \Delta t. \tag{2.64}$$

Now assume a particular sequence of photoelectric detections (Figure 2.5) in time $N\Delta t$. The probability of having this kind of sequence with n photoelectric detections is given by

$$p^n q^{N-n} = (\epsilon \bar{I} \Delta t)^n (1 - \epsilon \bar{I} \Delta t)^{N-n}. \tag{2.65}$$

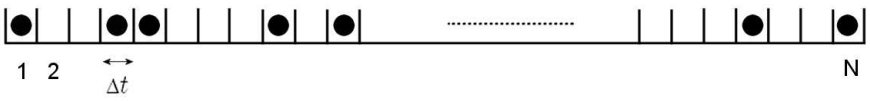

Figure 2.5: Sequence of photoelectric detections. Each cell represents a subinterval of duration Δt. Black dots represent successive photon detections and vacancies represent no detection.

There are $N(N-1)\cdots(N-n+1)/n!$ ways of arranging the n detection events and $N - n$ non-detection events in N intervals. So the probability of having exactly n detection events in N intervals is

$$p(n, t, T) = \frac{N(N-1)\cdots(N-n+1)}{n!} (\epsilon \bar{I} \Delta t)^n (1 - \epsilon \bar{I} \Delta t)^{N-n}. \tag{2.66}$$

[7] Look, for example, in section 9.3 of Mandel and Wolf [15].

In the limit $N \to \infty$, $\Delta t \to 0$, while keeping $N\Delta t = T$ constant, we get

$$p(n,t,T) = \left(1 - \frac{1}{N}\right) \cdots \left(1 - \frac{n-1}{N}\right) \frac{(\epsilon N \bar{I} \Delta t)^n}{n!} (1 - \epsilon \bar{I} \Delta t)^{N-n}$$

$$= \frac{(\epsilon \bar{I} T)^n}{n!} \exp(\epsilon \bar{I} T), \tag{2.67}$$

where we have used

$$(1 - \epsilon \bar{I} \Delta t)^{N-n} \to \exp(-\epsilon \bar{I} T),$$

in the limit given above. The photon counting distribution in Eq. (2.67) is the Poisson distribution. We named it $p(n,t,T)$ but actually it is independent of t; since the intensity is constant, we are free to choose the origin of time. In other words, *when* we start counting does not matter.

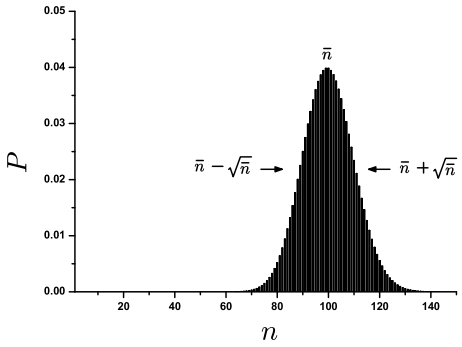

Figure 2.6: The Poisson distribution with $\bar{n} = 100$.

The Poisson distribution has variance $\bar{n}$, where $\bar{n} = \epsilon \bar{I} T$ is the average number of photon counts (Figure 2.6). The signal to noise ratio then is equal to $\sqrt{\bar{n}}/\bar{n} = 1/\sqrt{\bar{n}}$. This noise is normally called the *shot noise*. It arises from the discreteness of the photoelectric pulses – the discreteness due to the nature of light-atom interaction. Note that so far there has been no statistical fluctuations from the light. The intensity was held constant. The noise in the photon counting distribution originated from the quantum mechanical interaction between the classical light and atoms. We will now look at the case of fluctuating intensities.

First consider the case where T is short compared to the correlation time of

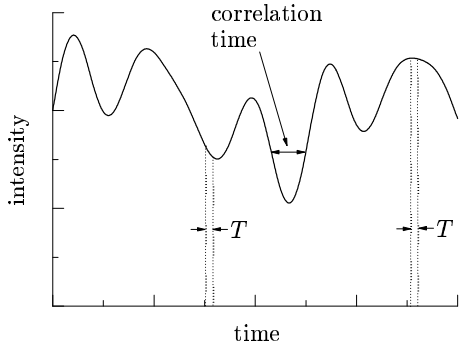

Figure 2.7: Stochastically varying intensity, when the counting time T is short compared with the correlation time.

the intensity. In this case, the intensity over a given counting interval stays almost constant (Figure 2.7). However, the intensity is different for different time intervals due to its fluctuations, and thus the photon counting distribution has to be averaged over the fluctuations, i.e.,

$$\begin{aligned} p(n,t,T) &= \int d\bar{I} P(\bar{I}) \frac{(\epsilon \bar{I} T)^n}{n!} \exp(-\epsilon \bar{I} T), \\ &\equiv \left\langle \frac{(\epsilon \bar{I} T)^n}{n!} \exp(-\epsilon \bar{I} T) \right\rangle . \end{aligned} \tag{2.68}$$

$P(\bar{I})$ is the probability of obtaining a value $\bar{I}$, assumed to be independent of time (the fluctuations are stationary, independent of the time origin).

Generalization to the case where T is not so small is quite straightforward and natural in terms of the result. We simply replace the average number with an integral:[8]

$$\epsilon \bar{I} T \to \epsilon \int_t^{t+T} dt' \bar{I}(t') \equiv \Omega(t, t+T), \tag{2.69}$$

which changes the photon counting distribution to

$$p(n,t,T) = \left\langle \frac{[\Omega(t,t+T)]^n}{n!} \exp[-\Omega(t,t+T)] \right\rangle . \tag{2.70}$$

This is the *semi-classical formula for the photon counting distribution.* $p(n,t,T)$

[8]For derivation of this result, see Loudon [25], pp. 230ff.

now depends on t, since $\bar{I}(t)$ now depends on time. The angled brackets refer to an ensemble average over the different functions $\bar{I}(t)$. This point should be emphasized. There are two averages here: the first is the average in the time integral of intensity $\bar{I}(t)$; the second is the average over all the possible functions $\bar{I}(t)$.

The semi-classical photon counting distribution has a pitfall that we must point out here. We have seen in the constant intensity case that the distribution is Poisson. Then it is not hard to see that, as we add more and more fluctuations in intensity, the distribution should get broader and broader, i.e., the photon counting distribution must be super-Poissonian. Indeed, it can be shown mathematically, that it has to be a super-Poissonian.[9]

This is saying that the Poisson distribution is the narrowest photon counting distribution one could observe. But this looks strange. For example, consider the case where photons come in one after another in a regular time interval, say 0.1 sec interval. In such a case, if we count photons for 1 sec, we are certain to get 10 photons. The lack of this possibility comes from the fact that we have not quantized the electromagnetic field.

2.7.2 Photon counting distribution for quantized optical field

We now seek the generalization of Eq. (2.70) to the case where the electromagnetic field is quantized. We will find that the result looks very similar to Eq. (2.70). Heuristic arguments are used to derive the result, which will then be compared with the fully quantum mechanical formula.

In terms of the positive and negative frequency parts of an electric field operator, introduced in Section 2.1, we can write the intensity operator $\hat{I}$ as

$$\hat{I} = 2\epsilon_0 c \hat{\mathbf{E}}^{(-)}(r,t) \cdot \hat{\mathbf{E}}^{(+)}(r,t), \tag{2.71}$$

where c is the speed of light, ϵ_0 is the permittivity of free space, and the electric field operators are evaluated at the location of the detector. The constant factors are needed to make the unit of intensity right. We can check the validity of this equation by substituting the single-mode electric field operator [Eq. (2.8)] into Eq. (2.71):

$$\hat{I} = \frac{\hbar\omega c}{V} a^\dagger a.$$

Since $a^\dagger a c/V$ is the number of photons that passes through a unit area every second,

[9] See, for example, Carmichael [24], Chapter 5, especially section 5.3.

$\hat{I}$ has the right interpretation of being the energy passing through a unit area every second.

Can we simply put this into Eq. (2.70) to get the answer? Well, almost. There is only one more thing to worry about – operator ordering. The operators usually do not commute with each other and certainly, $\hat{\mathbf{E}}^{(-)}(r,t)$ and $\hat{\mathbf{E}}^{(+)}(r,t)$ do not. Their operator characteristics are in the creation and annihilation operators, and the creation and annihilation operators do not commute. There are many different operator orderings that one can take. In addition to the symmetrical ordering shown in Section 2.5, there are normal and anti-normal orderings as well. In normal ordering we move all the creation operators to the left of the annihilation operators; in anti-normal ordering, as the name suggests, we do the opposite. For example, if we have two creation and two annihilation operators, different orderings give

$$\text{normal ordering} \rightarrow a^\dagger a^\dagger a a,$$
$$\text{anti-normal ordering} \rightarrow a a a^\dagger a^\dagger.$$

It turns out that in a direct photon counting experiment, we have to take normal ordering. Let us see why. For simplicity, we take an idealized photoelectric detector of negligible spatial extension and a frequency-independent photoabsorption probability.[10] Now suppose the detector has clicked. Then an atom must have absorbed a photon and emitted a photoelectron. This implies that the photon has been destroyed. Photoelectric detectors work by annihilating the photons they detect. To see how the ordering occurs, suppose the detector is initially in a ground state, and denote the state of the detector plus field as $|i\rangle$. After the detector absorbs a photon, the total state jumps to a final state $|f\rangle$, where now the detector is in an excited state. Then the probability amplitude of this event happening is proportional to the matrix element

$$\langle f|\hat{E}_\lambda^{(+)}(\mathbf{r},t)|i\rangle, \tag{2.72}$$

since $\hat{E}_\lambda^{(+)}(\mathbf{r},t)$ is the negative frequency part (which contains the photon annihilation operator, see Section 2.1) of the electric field operator. $\hat{E}_\lambda^{(+)}(\mathbf{r},t)$ is a particular frequency component – the frequency of the photon that was absorbed – of the total

[10] Our argument follows closely that of Glauber [26]. The assumption of frequency independence makes the sum over the final states independent of frequency, hence making the probability independent of final states. For this point see Gardiner and Zoller [27], Section 8.2.

electric field operator, which has a polarization specified by λ. Now the total probability of there being a photon absorption in a time interval $(t, t+dt]$ is proportional to the sum over the final states of the transition probabilities, i.e., it is proportional to

$$\sum_f |\langle f|\hat{E}_\lambda^{(+)}(\mathbf{r},t)|i\rangle|^2 dt = \sum_f \langle i|\hat{E}_\lambda^{(-)}(\mathbf{r},t)|f\rangle\langle f|\hat{E}_\lambda^{(+)}(\mathbf{r},t)|i\rangle dt,$$
$$= \langle i|\hat{E}_\lambda^{(-)}(\mathbf{r},t)\hat{E}_\lambda^{(+)}(\mathbf{r},t)|i\rangle dt. \tag{2.73}$$

One immediate consequence of this is that the probability for the detector to click vanishes for the vacuum field. Classically, this is very trivial. There is nothing in the vacuum, so there is nothing to make the detector click. Remember, however, that in the quantum world the vacuum fluctuates, i.e., the fluctuations of electric field in the vacuum is non-zero:

$$\langle 0|\hat{E}_\lambda^2(\mathbf{r},t)|0\rangle > 0. \tag{2.74}$$

Nevertheless, according to Eq. (2.73), this vacuum will not make the detector go click, which means we cannot think of the vacuum fluctuations as being real fluctuations of the electromagnetic field.[11]

Going back to finding the expression for the photon absorption probability, we now imagine a situation where two photons are absorbed, at different time intervals $(t, t+dt]$ and $(t', t'+dt']$. The matrix element for this situation is given by

$$\langle f|\hat{E}_\lambda^{(+)}(\mathbf{r},t')\hat{E}_\lambda^{(+)}(\mathbf{r},t)|i\rangle, \tag{2.75}$$

and the probability is proportional to

$$\langle i|\hat{E}_\lambda^{(-)}(\mathbf{r},t)\hat{E}_\lambda^{(-)}(\mathbf{r},t')\hat{E}_\lambda^{(+)}(\mathbf{r},t')\hat{E}_\lambda^{(+)}(\mathbf{r},t)|i\rangle dt dt'. \tag{2.76}$$

Note the normal ordering of the operators. The creation operators to the left of the annihilation operators. Also the operators are time-ordered. Operators at earlier times lie 'outside', closer to the kets and bras, of the operators at later times. Generalization to the case of a larger number of detections at different times gives us the normal and time ordering of the operators.

We have seen that the detection of photons by photoelectric detectors results in

[11] This does not mean that the vacuum fluctuations do not exist, though. The vacuum fluctuation can yield the Casimir effect mentioned in Section 2.1.

the normal ordering of the creation and annihilation operators. Combining this fact with Eq. (2.71) and Eq. (2.70) our guess to the correct form of the photon counting distribution is

$$p(n,t,T) = \left\langle : \frac{[\hat{\Omega}(t,t+T)]^n}{n!} \exp[-\hat{\Omega}(t,t+T)] : \right\rangle, \tag{2.77}$$

where

$$\hat{\Omega}(t,t+T) = \xi \int_t^{t+T} dt' \hat{E}^{(-)}(\mathbf{r},t')\hat{E}^{(+)}(\mathbf{r},t'),$$

$$\xi \equiv \eta A \frac{2\epsilon_0 c}{\hbar\omega}.$$

The notation : : indicates the normal and time ordering of the operators, and the angled brackets now stand for the expectation value with respect to the initial state $|i\rangle$. The fully quantum mechanical derivation (with fields quantized) of the photon counting distribution, using perturbation theory with appropriate approximations, is given by Kelley and Kleiner [28]. Their result agrees with Eq. (2.77). We will not go into the detail here, but this formula, as expected, allows sub-Poissonian photon counting distributions, i.e., it tells us that photons can come in regular intervals.

2.7.3 Balanced homodyne detection

We are now ready to talk about the balanced homodyne detection scheme mentioned earlier in relation to the detection of squeezing. Before we can talk about the detection of squeezing, however, we must first know the trait we are looking for. The central feature of squeezed light is its phase dependent noise reduction. As we have seen in section 2.6, a squeezed state has its noise reduced below the vacuum fluctuation limit, possibly for a range of quadratures. Thus, what we are looking for experimentally is a reduction of noise below a threshold; the threshold is set by the noise of the vacuum fluctuations.[12] The threshold is called the shot noise limit, related to the shot noise in photon counting experiments. In fact, what we are doing is carrying out a phase-dependent photon counting experiment and obtaining sub-Poissonian statistics for the squeezed quadrature.

The homodyne detection scheme is shown in Figure 2.8. LO denotes the local

[12] Although the vacuum fluctuations cannot be measured directly (since the vacuum does not fire the detectors), they can, in effect, be measured indirectly by mixing a known field with the vacuum (via a beam splitter) and detecting the mixed field.

oscillator field: experimentally it is the field out of a laser, theoretically it is a coherent state with large amplitude. The local oscillator field has to be mode-matched to the input field, meaning that they must overlap completely in space and time. To achieve this it has to have the same frequency, or central frequency, as the input light. The field to be homodyned is mixed with the local oscillator by passing both field through a 50/50 beam splitter, then the two outputs are detected by the photoelectric detectors. In the balanced homodyne detection scheme, the two photocurrents coming out of the photoelectric detectors are then subtracted [23] yielding the output dQ (shown in the figure). The subtraction creates a desirable effect of cancelling the local oscillator amplitude terms.

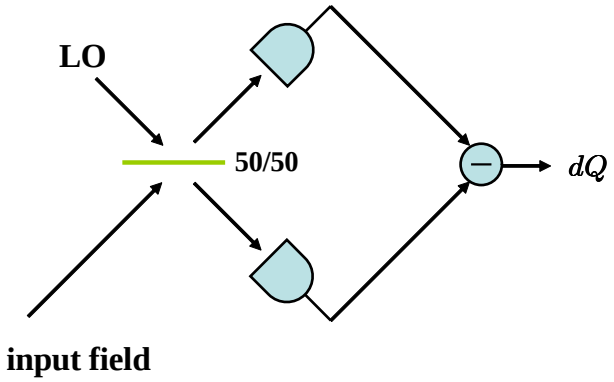

Figure 2.8: Schematic representation of the balanced homodyne detection scheme.

The balanced homodyne detector can be used to detect a quadrature of the input field, and hence its fluctuations. The angle of the quadrature is specified by the phase of the local oscillator. We now analyze the scheme mathematically. Assume the input and the local oscillator fields are single-modes, to which we give the annihilation operators a and b, respectively. The state of the local oscillator field is that of a laser, which can be described by a coherent state, say $|\beta\rangle$, where $\beta = |\beta| \exp(i\phi)$. The effect of the beam splitter is to produce two output fields with the mode annihilation operators c and d. The output annihilation operators can be written in terms of the input annihilation operators as

$$c = \frac{1}{\sqrt{2}}(a + b), \tag{2.78a}$$

$$d = \frac{1}{\sqrt{2}}(a - b). \tag{2.78b}$$

The output of the photodetectors is proportional to the intensities of the two output fields, i.e.,

$$I_+ \propto \langle c^\dagger c\rangle = \frac{1}{2}\langle a^\dagger a + b^\dagger b + a^\dagger b + b^\dagger a\rangle, \tag{2.79}$$

$$I_- \propto \langle d^\dagger d\rangle = \frac{1}{2}\langle a^\dagger a + b^\dagger b - a^\dagger b - b^\dagger a\rangle, \tag{2.80}$$

where $\langle\cdot\rangle$ denotes the expectation value with respect to the state $|\text{in}\rangle \otimes |\beta\rangle$. Thus,

$$\begin{aligned}\overline{dQ} \propto I_+ - I_- &\propto \langle a^\dagger b + b^\dagger a\rangle, \\ &= |\beta|(\exp(i\phi)a^\dagger + \exp(-i\phi)a),\end{aligned} \tag{2.81}$$

where $\overline{dQ}$ is the average value of charge deposited in time dt. We have used the fact that $\langle\beta|b|\beta\rangle = |\beta|\exp(i\phi)$ and $\langle\beta|b^\dagger|\beta\rangle = |\beta|\exp(-i\phi)$ to obtain the second line. Then, from the definition of quadrature operator, Eq. (2.12), we obtain

$$\overline{dQ} \propto \langle \hat{A}_\phi\rangle. \tag{2.82}$$

We can also obtain the shot noise by calculating the intensity fluctuations in the output photocurrent. To make things simple, assume the input state is the squeezed vacuum so the mean value of the quadrature operator is zero. In this case, variance of the input field is given by

$$\begin{aligned}\langle(c^\dagger c - d^\dagger d)^2\rangle &= \langle a^{\dagger 2}b^2 + b^{\dagger 2}a^2 + a^\dagger a b b^\dagger + a a^\dagger b^\dagger b\rangle, \\ &= \langle a^{\dagger 2}b^2 + b^{\dagger 2}a^2 + 2a^\dagger a b^\dagger b + a^\dagger a + b^\dagger b\rangle, \\ &= |\beta|^2\langle a^{\dagger 2}\exp(2i\phi) + a^2\exp(-2i\phi) + 2a^\dagger a\rangle + \langle a^\dagger a\rangle + |\beta|^2.\end{aligned} \tag{2.83}$$

The last two terms constitute the shot noise. Note how the shot noise terms appear, they appear from the commutation relations $[a, a^\dagger] = 1$ and $[b, b^\dagger] = 1$. Thus, we can think of the shot noise as coming from the vacuum fluctuations of the input and the local oscillator field. In most cases, the local oscillator field dominates the fluctuation and the $\langle a^\dagger a\rangle$ term can be neglected. Then, the $|\beta|^2$ term acts like a noise threshold, independent of the input field. If the squeezed quadrature of the squeezed state is measured, the other terms in Eq. (2.83) can take a negative value and the variance goes below the shot noise.

Chapter 3

Quantum trajectory theory

Most quantum optical experiments employ a scattering-type scenario: light (typically from a laser) comes into the region of interest, interacts with the system (a non-linear crystal, for example), then leaves the region of interest. When we perform a measurement it is usually the output light we detect, and usually with photoelectric detectors.

Master equations, the equations describing the evolution of density operators, are the standard tool used in quantum optics to describe the system dynamics. In a scattering-type scenario, a system is interacting with a reservoir that carries the output field. The master equation only describes the evolution of the system states; the reservoir states are traced out, i.e., the reservoir is ignored.

Quantum trajectory theory seeks a different way to analyze the evolution of the system; the reservoir states are not traced out, but disentangled. By creating our own reservoir, or environment, with detecting equipment, we select out a particular reservoir state from the measurement records. This in turn selects out a particular state of the system, one which we *infer* from the measurement records. These points will become clearer when we use the theory to analyze some simple examples later in this chapter. Quantum trajectory theory will be developed by unravelling the master equation, then applied to two examples: photoelectric counting and balanced homodyne detection of an optical field in a damped (or leaky) cavity.

We start off with an introduction to the master equation, applying it to a dissipative system. Then a general unravelling of the master equation is introduced using a superoperator notation, followed by examples that will make the use of the unravelling and the interpretation of quantum trajectory theory clear.

3.1 Dissipation in quantum mechanics and master equations

Dissipation, or damping, plays an important role in quantum optics: the simplest example is spontaneous emission, random emission of photons to the environment. Another example, which shows the typical feature of quantum optical experiments, is a laser; there is a medium (lasing medium) in a cavity, and the laser beam is the output from the cavity. Obviously, the cavity has to be leaky if there is to be any output, i.e., a laser beam. In the case of spontaneous emission, atoms are coupled to infinitely many modes of the electromagnetic field in their environment; there are an infinity of vacuum modes, which any atom can spontaneously emit a photon to. In the case of a laser, the intracavity field is coupled to infinitely many modes of the field outside the cavity, which, again, is the environment.

Now, the origin of dissipation is clear. It comes from the coupling of the system to its environment. If you look at the whole system, system plus reservoir, there is no dissipation; photons from the system have merely migrated to the reservoir. But if we take the system's point of view, it has lost the photons; lost them forever, since the photons travel away at the speed of light. Thus, the dissipation occurs from ignoring the states of the reservoir. The system and reservoir way of treating dissipation in quantum systems was pioneered by Senitzky [29, 30].

3.1.1 Master equations

We seek to find the equation of motion for the density operator of a system. We use a density operator because it provides a straightforward way to ignore the reservoir states, namely tracing over the reservoir states. Our derivation follows that of Carmichael [19] (Chapter 1).

Let $\chi(t)$ be the density operator for the total system, and let us write the total Hamiltonian as

$$H = H_S + H_R + H_{SR}, \tag{3.1}$$

where H_S is the Hamiltonian of the system alone, H_R is the Hamiltonian for the reservoir, and H_{SR} is an interaction Hamiltonian. We introduce the reduced density

operator $\rho(t)$, where

$$\rho(t) = \mathrm{tr}_R[\chi(t)] \tag{3.2}$$

is the density operator of the system alone, since the reservoir states have been traced over. All the expectation values of system operators can be worked out from $\rho(t)$; for a system operator $\hat{O}$, the expectation value is give by

$$\left\langle \hat{O} \right\rangle = \mathrm{tr}_{S\oplus R}\left[\hat{O}\chi(t)\right] = \mathrm{tr}_S\left\{\hat{O}\,\mathrm{tr}_R[\chi(t)]\right\} = \mathrm{tr}_S\left[\hat{O}\rho(t)\right]. \tag{3.3}$$

Our objective now is to find the equation that governs the evolution of $\rho(t)$. As shown in Section 2.4, the Schrödinger equation for $\chi(t)$ is given by

$$\dot{\chi}(t) = \frac{1}{i\hbar}\left[H, \chi(t)\right], \tag{3.4}$$

where the dot above χ stands for the time derivative. The above equation is very hard to solve, so we need to make some approximations. For this purpose, it is best to change to the interaction picture as follows:

$$\chi(t) \to \tilde{\chi}(t) = \exp\left[\frac{i}{\hbar}(H_S + H_R)t\right]\chi(t)\exp\left[-\frac{i}{\hbar}(H_S + H_R)t\right]. \tag{3.5}$$

Then, Eq. (3.4) becomes

$$\dot{\tilde{\chi}}(t) = \frac{1}{i\hbar}\left[\tilde{H}_{SR}(t), \tilde{\chi}(t)\right], \tag{3.6}$$

where the interaction Hamiltonian,

$$\tilde{H}_{SR}(t) = \exp\left[\frac{i}{\hbar}(H_S + H_R)t\right]H_{SR}\exp\left[-\frac{i}{\hbar}(H_S + H_R)t\right], \tag{3.7}$$

is now explicitly time dependent. The formal solution to Eq. (3.6) can be written as

$$\tilde{\chi}(t) = \tilde{\chi}(0) + \frac{1}{i\hbar}\int_0^t dt'\left[\tilde{H}_{SR}(t'), \tilde{\chi}(t')\right]. \tag{3.8}$$

Substituting this equation back into Eq. (3.6) we obtain

$$\dot{\tilde{\chi}}(t) = \frac{1}{i\hbar}\left[\tilde{H}_{SR}(t), \tilde{\chi}(0)\right] - \frac{1}{\hbar^2}\int_0^t dt'\left[\tilde{H}_{SR}(t), \left[\tilde{H}_{SR}(t'), \tilde{\chi}(t')\right]\right]. \tag{3.9}$$

Eq. (3.6) and Eq. (3.9) are completely equivalent; the reason we put it in the latter form is to make subsequent approximations easier. Assume the interaction is turned on at $t = 0$, and assume there is no correlation between the system and the reservoir at $t = 0$.[1] Then $\tilde{\chi}(0) = \chi(0)$ can be factorized as

$$\chi(0) = \rho(0)R_0, \tag{3.10}$$

where R_0 is the reservoir density operator at $t = 0$. We now take the trace of Eq. (3.9) over the reservoir. Note that[2]

$$\mathrm{tr}_R\left[\tilde{\chi}(t)\right] = \exp\left(\frac{i}{\hbar}H_S t\right)\rho(t)\exp\left(-\frac{i}{\hbar}H_S t\right) \equiv \tilde{\rho}(t). \tag{3.11}$$

Using Eq. (3.11), Eq. (3.9) becomes

$$\dot{\tilde{\rho}}(t) = -\frac{1}{\hbar^2}\int_0^t dt' \mathrm{tr}\left\{\left[\tilde{H}_{SR}(t), \left[\tilde{H}_{SR}(t'), \tilde{\chi}(t')\right]\right]\right\}, \tag{3.12}$$

where, for simplicity, the trace over the first term has been set to zero, i.e., $\mathrm{tr}_R\left\{\left[\tilde{H}_{SR}(t), \tilde{\chi}(0)\right]\right\} = 0$. This is true if $\mathrm{tr}_R\left[\tilde{H}_{SR}R_0\right] = 0$, that is, if the reservoir operator in $\tilde{H}_{SR}$ has a mean value of zero. Even if this is not the case, we can always move the mean value to H_S, making Eq. (3.12) true.

We now make two major approximations that assume a reasonable behaviour of system and reservoir. The first one is called the *Born approximation*. This approximation can be stated as

$$\tilde{\chi}(t) \approx \tilde{\rho}(t)R_0. \tag{3.13}$$

It is saying that the reservoir is a huge system, making the effect of the interaction on it negligible, whereas the effect of the interaction on the system is large; the system is expected to change significantly from the interaction. Furthermore, this approximation states that an initially uncorrelated system and reservoir remain uncorrelated. This is possible when the interaction is sufficiently weak.

In summary, the Born approximation is saying that the interaction strength

[1] The assumption that the interaction can be turned on abruptly (leaving the system and reservoir initially uncorrelated) can only be made on high frequency systems such as the optical systems we are dealing with.

[2] To see why, just take the trace with energy eigenstates; H_R and H_S commute, so the $\exp(\pm i/\hbar H_R)$ factors become ordinary numbers and cancel out, leaving the trace of $\exp\left(\frac{i}{\hbar}H_S\right)\chi(t)\exp\left(-\frac{i}{\hbar}H_S\right)$ over the reservoir states.

is feeble, leaving the reservoir essentially undisturbed, although the system *is* significantly disturbed by this interaction. With the Born approximation Eq. (3.12) becomes

$$\dot{\tilde{\rho}}(t) = -\frac{1}{\hbar^2}\int_0^t dt' \mathrm{tr}_R \left\{ \left[\tilde{H}_{SR}(t), \left[\tilde{H}_{SR}(t'), \tilde{\rho}(t')R_0 \right] \right] \right\}. \tag{3.14}$$

This equation is correct up to second order in H_{SR}, higher order terms are ignored by virtue of the approximation.

Eq. (3.14) is still very hard to solve, because the future evolution of the system depends on the past history of itself, i.e., the system is non-Markovian. We now introduce our second major approximation, the *Markov approximation* – we simply change $\tilde{\rho}(t')$ into $\tilde{\rho}(t)$. Then, Eq. (3.14) becomes

$$\dot{\tilde{\rho}}(t) = -\frac{1}{\hbar^2}\int_0^t dt' \mathrm{tr}_R \left\{ \left[\tilde{H}_{SR}(t), \left[\tilde{H}_{SR}(t'), \tilde{\rho}(t)R_0 \right] \right] \right\}. \tag{3.15}$$

This is our final result, the *master equation in the Born-Markov approximation*.

Let us examine the validity of the Markov approximation. It states that future evolution of the system depends only on the current state of the system; that is, there is no memory about the past history in the whole system. In theory, the reservoir does obtain some information about the state of the system through their interaction, and it can 'remember' this information. This way the future evolution could depend on the past history. In practice, the reservoir is usually in thermal equilibrium and its memory is very short-lived; it will re-equilibrate very fast compared with the system dynamics. In such a case, the Markovian approximation is a good assumption. So the question boils down to this: is the typical time scale of reservoir dynamics short enough compared with the typical time scale of the system dynamics? The answer must be 'Yes' if one is to use the master equation.

3.1.2 Example: damped harmonic oscillator

We now consider a specific example: a damped harmonic oscillator. This is a model for describing the electromagnetic field in an optical cavity, coupled to the field outside the cavity through the cavity's non-zero transmissivity. The damped harmonic oscillator is one of the simplest examples of a damped system, but is still quite interesting as it captures the essence of the physics for a variety of systems.

Let us restrict our system to a single-mode of the optical field, in a cavity, with

frequency ω_0. The reservoir comprises harmonic oscillators, or photon modes, in the vacuum states. We will call it the vacuum reservoir. For this system, the Hamiltonian can be written as (see Chapter 6 of Louisell [31])

$$H_S = \hbar\omega_0 a^\dagger a, \tag{3.16a}$$

$$H_R = \sum_j \hbar\omega_j r_j^\dagger r_j, \tag{3.16b}$$

$$H_{SR} = \kappa \sum_j \hbar \left(a r_j^\dagger + a^\dagger r_j \right), \tag{3.16c}$$

where r_j and $r_j^\dagger$ are the annihilation and creation operators for the jth harmonic oscillator of the reservoir, and ω_j is the frequency for the jth harmonic oscillator. For simplicity we have taken the interaction parameter κ to be real and frequency independent; in general it could be complex and frequency dependent.

We now explicitly calculate the commutators in Eq. (3.15) to obtain the master equation for this damped harmonic oscillator. Changing to the interaction picture, we write

$$\begin{aligned}\tilde{H}_{SR} &= \kappa \sum_j \hbar \left[(a e^{-i\omega_0 t})(r_j^\dagger e^{i\omega_j t}) + (a^\dagger e^{i\omega_0 t})(r_j e^{-i\omega_j t}) \right], \\ &= \kappa \sum_j \hbar \left[a(t) r_j^\dagger(t) + a^\dagger(t) r_j(t) \right].\end{aligned} \tag{3.17}$$

Substituting this interaction Hamiltonian into Eq. (3.15), we obtain

$$\begin{aligned}\dot{\tilde{\rho}}(t) = -\kappa^2 \int_0^t dt' \mathrm{tr}_R &\left[\sum_{k,j} r_k^\dagger(t) r_j^\dagger(t') R_0 \right] \left[a(t) a(t') \tilde{\rho}(t) - a(t') \tilde{\rho}(t) a(t) \right] + h.c. \\ &+ \mathrm{tr}_R \left[\sum_{k,j} r_k^\dagger(t') r_j^\dagger(t) R_0 \right] \left[\tilde{\rho}(t) a(t') a(t) - a(t) \tilde{\rho}(t) a(t') \right] + h.c. \\ &+ \mathrm{tr}_R \left[\sum_{k,j} r_k(t) r_j^\dagger(t') R_0 \right] \left[a^\dagger(t) a(t') \tilde{\rho}(t) - a(t') \tilde{\rho}(t) a^\dagger(t) \right] + h.c. \\ &+ \mathrm{tr}_R \left[\sum_{k,j} r_k^\dagger(t') r_j(t) R_0 \right] \left[\tilde{\rho}(t) a(t') a^\dagger(t) - a^\dagger(t) \tilde{\rho}(t) a(t') \right] + h.c.,\end{aligned} \tag{3.18}$$

where the *h.c.* stands for Hermitian conjugate. Because the reservoir is in the vacuum

state, the first, second and fourth traces are zero, but the third one is not. Let us write the trace in the third line explicitly:

$$\mathrm{tr}_R\left[\sum_{k,j} r_k(t) r_j^\dagger(t') R_0\right] = \sum_{k,j} \exp(-i\omega_k t + i\omega_j t')\langle 0|r_k r_j^\dagger|0\rangle. \tag{3.19}$$

It is equal to zero unless $k = j$; in the case $k = j$ we get

$$\begin{aligned}\mathrm{tr}_R\left[\sum_{k,j} r_k(t) r_j^\dagger(t') R_0\right] &= \sum_j \exp[-i\omega_j(t-t')]\langle 0|r_j r_j^\dagger|0\rangle, \\ &= \sum_j \exp[-i\omega_j(t-t')]\langle 0|r_j^\dagger r_j + 1|0\rangle, \\ &= \sum_j \exp[-i\omega_j(t-t')]. \end{aligned}\tag{3.20}$$

Putting this equation back into Eq. (3.18), we obtain

$$\begin{aligned}\dot{\tilde{\rho}}(t) = -\kappa^2 \int_0^t dt' \sum_j \exp[-i\omega_j(t-t')] \left[a^\dagger(t)a(t')\tilde{\rho}(t) - a(t')\tilde{\rho}(t)a^\dagger(t)\right] \\ + \sum_j \exp[+i\omega_j(t-t')] \left[\tilde{\rho}(t)a^\dagger(t')a(t) - a(t)\tilde{\rho}(t)a^\dagger(t')\right]. \end{aligned}\tag{3.21}$$

Changing the variable t' into $\tau = t - t'$ and pulling out the time dependence of $a(t)$ and $a^\dagger(t)$ we get

$$\begin{aligned}\dot{\tilde{\rho}}(t) = -\kappa^2 \int_0^t d\tau \sum_j \exp[-i(\omega_j - \omega_0)\tau] \left[a^\dagger a\tilde{\rho}(t) - a\tilde{\rho}(t)a^\dagger\right] \\ + \sum_j \exp[-i(\omega_0 - \omega_j)\tau] \left[\tilde{\rho}(t)a^\dagger a - a\tilde{\rho}(t)a^\dagger\right]. \end{aligned}\tag{3.22}$$

The next step is to change the summation to an integration by introducing a density of states $g(\omega)$, where $g(\omega)d\omega$ is the number of oscillators in the frequency range ω to $\omega + d\omega$, i.e., we make a substitution

$$\sum_j \to \int_0^\infty d\omega g(\omega). \tag{3.23}$$

Making this change in Eq. (3.22) gives us

$$\dot{\tilde{\rho}}(t) = -\kappa^2 \int_0^t d\tau \int_0^\infty d\omega g(\omega) \Big\{ \exp[-i(\omega-\omega_0)\tau] \left[a^\dagger a \tilde{\rho}(t) - a\tilde{\rho}(t)a^\dagger \right] + \exp[-i(\omega_0-\omega)\tau] \left[\tilde{\rho}(t)a^\dagger a - a\tilde{\rho}(t)a^\dagger \right] \Big\}. \quad (3.24)$$

When τ is large, the frequency integral will quickly converge to zero, due to the rapidly oscillating exponential term; $g(\omega)$ is usually a slowly varying function of ω. Since the frequency integral is small for large τ, we can increase the limit of the time integral to infinity, i.e., we can write

$$\int_0^t d\tau \int_0^\infty d\omega g(\omega) \exp[-i(\omega-\omega_0)\tau] \rightarrow \int_0^\infty d\tau \int_0^\infty d\omega g(\omega) \exp[-i(\omega-\omega_0)\tau] \quad (3.25)$$

To solve Eq. (3.24) we evaluate the time integral first. We use

$$\int_0^\infty d\tau \exp[-i(\omega-\omega_0)\tau] = \pi\delta(\omega-\omega_0) + i\frac{P}{\omega_0-\omega}, \quad (3.26)$$

where P denotes the Cauchy principal value, to get

$$\dot{\tilde{\rho}}(t) = (\pi\kappa^2 g(\omega_0) + i\Delta) \left(a\tilde{\rho}(t)a^\dagger - a^\dagger a\tilde{\rho}(t) \right) + h.c., \quad (3.27)$$

where

$$\Delta = P\int_0^\infty d\omega \frac{g(\omega)\kappa^2}{\omega_0-\omega}. \quad (3.28)$$

A short derivation of Eq. (3.26) is given in Appendix A.

Note that Eq. (3.27) is in the interaction picture. We now convert back to the Schrödinger picture using

$$\dot{\rho}(t) = \frac{1}{i\hbar}[H_S, \rho] + \exp\left(-\frac{i}{\hbar}H_S t\right) \dot{\tilde{\rho}}(t) \exp\left(\frac{i}{\hbar}H_S t\right), \quad (3.29)$$

which is obtained from Eq. (3.11). Substituting $H_S = \hbar\omega_0 a^\dagger a$ and Eq. (3.27) into

this equation, and using

$$\begin{aligned}
&\exp\left(-i\omega_0 a^\dagger a t\right) a\tilde{\rho}(t)a^\dagger \exp\left(i\omega_0 a^\dagger a t\right) \\
&= \exp\left(-i\omega_0 a^\dagger a t\right) a \exp\left(i\omega_0 a^\dagger a t\right) \rho(t) \exp\left(-i\omega_0 a^\dagger a t\right) a^\dagger \exp\left(i\omega_0 a^\dagger a t\right), \\
&= a\exp\left(-i\omega_0 t\right)\rho(t)a^\dagger \exp\left(i\omega_0 t\right), \\
&= a\rho(t)a^\dagger, \qquad (3.30)
\end{aligned}$$

and similar terms, we obtain

$$\dot{\rho}(t) = -i\omega_0'[a^\dagger a, \rho(t)] + \frac{\gamma}{2}\left(2a\rho(t)a^\dagger - a^\dagger a\rho(t) - \rho(t)a^\dagger a\right), \qquad (3.31)$$

where $\omega_0' = \omega_0 + \Delta$ and $\gamma = 2\pi\kappa^2 g(\omega_0)$. This is the *master equation for a damped harmonic oscillator in a vacuum reservoir.*

Instead of a vacuum reservoir we could have used a thermal reservoir (thermal bath), which is often a better approximation to real systems. In this case the master equation becomes

$$\begin{aligned}
\dot{\rho}(t) = -i\omega_0'[a^\dagger a, \rho(t)] &+ \frac{\gamma}{2}(\bar{n}+1)\left(2a\tilde{\rho}(t)a^\dagger - a^\dagger a\rho(t) - \rho(t)a^\dagger a\right) \\
&+ \frac{\gamma}{2}\bar{n}\left(2a^\dagger\tilde{\rho}(t)a - aa^\dagger\rho(t) - \rho(t)aa^\dagger\right), \qquad (3.32)
\end{aligned}$$

where $\bar{n}$ is the average number of quanta in a reservoir mode of frequency ω_0. This type of master equation is said to be in Lindblad form, named after G. Lindblad who studied it extensively [32].[3] Note that when $\bar{n} = 0$, the result becomes the same as the vacuum reservoir case, which is obvious, since a thermal reservoir with no photons is a vacuum reservoir. The treatment of the thermal reservoir is given in Chapter 1 of Carmichael [19], amongst many other references.

3.2 Quantum trajectories

We are now ready to investigate quantum trajectory theory, the main theme of this chapter and an integral part of this thesis. There is an analogy to the relationship between the master equation approach and the quantum trajectory approach. This analogy is as follows. In classical statistical mechanics there are largely two ways of describing the dynamics of a system. The first way is to look at a probabil-

[3] Lindblad form is required for exact conservation of probability.

ity distribution of the states of the system, where the probability is governed by a Fokker-Planck equation. The second way is to follow the dynamics of a single state going through a trajectory in a phase space, by using a stochastic differential equation. An ensemble average over the trajectories lead to the same result as that obtained from the Fokker-Planck equation method.

The master equation way of looking at the dynamics is analogous to the F-P equation method, the density operator being the quantum mechanical probability density. The quantum trajectory theory approach is analogous to the stochastic trajectories method. There are two ways to work out trajectories. One is working out a quantum Langevin equation, by working out the operator evolutions in the Heisenberg picture [33, 27]. The second way, the quantum trajectory method, is essentially in the Schrödinger picture. It describes a stochastic evolution of a state.

The stochastic nature of the evolution is inevitable; in classical systems the stochastic nature arises from our incomplete knowledge about the system – for example consider Brownian motion: the intractable number of molecules colliding with a grain of pollen means that we cannot possibly follow them all. Instead we treat them as if their motion is completely random or stochastic. In quantum mechanics, we have to resort to stochastic equations even if we have a comparatively simple system (such as a damped cavity). The reason is, of course, the intrinsically probabilistic nature of quantum mechanics; quantum processes are necessarily stochastic.

3.2.1 Exclusive photon counting distribution

Quantum trajectory theory relies heavily on what is called the exclusive photon counting distribution, which we will introduce now. We have derived in Chapter 2 the photon counting distribution given by Eq. (2.77):

$$p(n,t,T) = \left\langle : \frac{[\hat{\Omega}(t,t+T)]^n}{n!} \exp[-\hat{\Omega}(t,t+T)] : \right\rangle . \tag{3.33}$$

This probability distribution describes the likelihood of detecting n photons in a time interval T. It can be expressed in terms of exclusive photon counting densities:

$$p(n,t,T) = \int_t^{t+T} dt_n \int_{t_{n-1}}^{t_n} dt_{n-1} \cdots \int_{t_1}^{t_2} dt_1 \wp_n(t_1,t_2,...,t_n;(t,t+T]) \tag{3.34}$$

where $\wp_n(t_1,t_2,...,t_n;(t,t+T])$ is the exclusive photon counting probability density. $\wp_n(t_1,t_2,...,t_n;(t,t+T])\Delta t_1 \Delta t_2 ... \Delta t_n$ is the probability of detecting n photons in

time intervals $(t_1, t_1+\Delta t_1), [t_2, t_2+\Delta t_2), ..., [t_n, t_n+\Delta t_n]$ and only at these intervals. The time intervals do not overlap and they fall inside $(t, t+T]$. It is called *exclusive* because no other photons are detected apart from the n photons. In the *non-exclusive* probability distribution, it does not matter whether there are more photons detected or not. The above equation is telling us that the probability of counting n photons in the time interval $(t, t+T]$ is a sum over all possible ways the photon countings are distributed in time.

It can be shown from Eq. (3.33) and Eq. (3.34) that the exclusive photon counting probability densities take the form:[4]

$$\wp_n(t_1, t_2, ..., t_n; (t, t+T]) = \left\langle : e^{-\hat{\Omega}(t+T,t_n)} \hat{I}(t_n) \cdots \hat{I}(t_2) e^{-\hat{\Omega}(t_2,t_1)} \hat{I}(t_1) e^{-\hat{\Omega}(t_1,t)} : \right\rangle, \tag{3.35}$$

where $\hat{I}(t_i) = \epsilon \hat{E}^{(-)}(t_i)\hat{E}^{(+)}(t_i)$ and

$$\hat{\Omega}(t_j, t_i) = \int_{t_i}^{t_j} dt' \hat{I}(t').$$

Eq. (3.35) has a straightforward interpretation if the fields are treated classically. $\hat{I}(t_i)$ corresponds to the probability of detection, which is proportional to the intensity, and $e^{-\hat{\Omega}(t_j,t_i)}$ is the probability of there being no detection in time interval $(t_i, t_j]$. The quantum mechanical expression Eq. (3.35) can be obtained from the classical expression by going through the same steps we went through in going from Eq. (2.70) to Eq. (2.77).

Our objective now is to build a bridge between the exclusive photon counting distribution and the master equation by unravelling the master equation.

3.2.2 Unravelling the master equation

At this point it is convenient to introduce a superoperator notation. Superoperators operate on operators rather than states. Using the superoperator notation we can write:

$$\dot{\rho}(t) = \mathcal{L}\rho(t). \tag{3.36}$$

[4] Actually, one starts from the non-exclusive probability density, which can be derived from Eq. (3.33) (or the Kelley-Kleiner formula, which is obtained while deriving Eq. (3.33)), and uses a relationship between the exclusive and non-exclusive probability densities to get to this result. Discussion of this is given by Carmichael [24] and references therein.

For example, the master equation could be Eq. (3.32), in which case $\mathcal{L}$ contains all the details in Eq. (3.32). We can write down the formal solution to Eq. (3.36) as

$$\rho(t) = e^{\mathcal{L}t}\rho(0). \tag{3.37}$$

Now, we make a formal substitution $\mathcal{L} = (\mathcal{L} - \mathcal{S}) + \mathcal{S}$, and then expand the master equation as a Dyson series, treating $\mathcal{S}$ as an interaction term:

$$\begin{aligned}\rho(t) &= e^{[(\mathcal{L}-\mathcal{S})+\mathcal{S}]t}\rho(0) \\ &= \sum_{n=0}^{\infty}\int_0^t dt_n \int_0^{t_n} dt_{n-1}\cdots\int_0^{t_2} dt_1 e^{(\mathcal{L}-\mathcal{S})(t-t_n)}\mathcal{S} \\ &\qquad \times e^{(\mathcal{L}-\mathcal{S})(t_n-t_{n-1})}\mathcal{S}\cdots\mathcal{S}e^{(\mathcal{L}-\mathcal{S})t_1}\rho(0). \end{aligned} \tag{3.38}$$

So far, this expression does not tell us anything useful, but we will soon make it useful by providing a link between this unravelling and the exclusive photon counting distribution. To make the understanding easier, we will work with a specific example: a damped cavity in a vacuum reservoir.

3.2.3 Connection between the exclusive counting probability and the master equation

We want to put the exclusive photon counting distribution, Eq. (3.35), into the form that is convenient to compare with Eq. (3.38). For concreteness, we work with a specific case. The system consists of a field in a cavity. The cavity is coupled to a vacuum reservoir through one mirror only; the other mirror is assumed to be perfectly reflecting. For this system our master equation is

$$\dot{\rho}(t) = -i\omega_0'[a^\dagger a, \rho(t)] + \frac{\gamma}{2}\left(2a\tilde{\rho}(t)a^\dagger - a^\dagger a\rho(t) - \rho(t)a^\dagger a\right), \tag{3.39}$$

as derived earlier.

Expansion of the exclusive counting probability

Let us now look at the exclusive photon counting probability. We first give a redefinition: $\wp_n(t_1, t_2, ..., t_n; (t, t+T]) \equiv P_{(\mathrm{REC})}$, specifying that it is the probability

density for a particular measurement record.

$$P_{(\mathrm{REC})} = \left\langle : e^{-\hat{\Omega}(t+T,t_n)} \hat{I}(t_n) \cdots \hat{I}(t_2) e^{-\hat{\Omega}(t_2,t_1)} \hat{I}(t_1) e^{-\hat{\Omega}(t_1,t)} : \right\rangle. \tag{3.40}$$

We introduce a new operator, such that the intensity operator can be written as

$$\hat{I}(t) = \hat{\mathcal{E}}^{(-)}(t)\hat{\mathcal{E}}^{(+)}(t). \tag{3.41}$$

$\hat{\mathcal{E}}$ is just a rescaled version of $\hat{E}$, to simplify the equation. We now expand the exponentials in $P_{(\mathrm{REC})}$. First let us look at

$$\begin{aligned}
&\left\langle : \hat{I}(t_1) e^{-\hat{\Omega}(t_1,t)} : \right\rangle \\
&\quad = \sum_{m=0}^{\infty} (-1)^m \int_0^{t_1} dt'_m \int_0^{t'_m} dt'_{m-1} \cdots \int_0^{t'_2} dt'_1 \mathrm{tr} \Big[\hat{\mathcal{E}}^{(-)}(t'_1) \cdots \hat{\mathcal{E}}^{(-)}(t'_{m-1}) \\
&\qquad \times \hat{\mathcal{E}}^{(-)}(t'_m) \hat{\mathcal{E}}^{(-)}(t_1) \hat{\mathcal{E}}^{(+)}(t_1) \hat{\mathcal{E}}^{(+)}(t'_m) \hat{\mathcal{E}}^{(+)}(t'_{m-1}) \cdots \hat{\mathcal{E}}^{(+)}(t'_1) \chi(0) \Big],
\end{aligned} \tag{3.42}$$

where the expectation value is now taken by the trace. $\chi(0)$ is the total density matrix of the system and the reservoir at time $t = 0$.

$\hat{\mathcal{E}}$ consists of the source term, from the cavity, and the free field term, which always exists outside the cavity: when we detect the light coming out of a cavity the free field term is invariably added [33]. For a vacuum reservoir, however, the free field does not contribute to the photon counts, i.e., the vacuum cannot make the detector click. For this reason, the free field terms contribute nothing to Eq. (3.42) in the case of a vacuum reservoir. We can see this explicitly by substituting

$$\hat{\mathcal{E}} = \hat{\mathcal{E}}_S + \hat{\mathcal{E}}_R, \tag{3.43}$$

into

$$\begin{aligned}
&\left\langle : \hat{I}(t_1) e^{-\hat{\Omega}(t_1,t)} : \right\rangle \\
&= \sum_{m=0}^{\infty} (-1)^m \int_0^{t_1} dt'_m \int_0^{t'_m} dt'_{m-1} \cdots \int_0^{t'_2} dt'_1 \mathrm{tr} \Big[\hat{\mathcal{E}}^{(-)}(t_1) \hat{\mathcal{E}}^{(-)}(t'_m) \hat{\mathcal{E}}^{(-)}(t'_{m-1}) \\
&\qquad \times \cdots \hat{\mathcal{E}}^{(-)}(t'_1) \chi(0) \hat{\mathcal{E}}^{(+)}(t'_1) \cdots \hat{\mathcal{E}}^{(+)}(t'_{m-1}) \hat{\mathcal{E}}^{(+)}(t'_m) \hat{\mathcal{E}}^{(+)}(t_1) \Big],
\end{aligned} \tag{3.44}$$

which is a rearranged version of Eq. (3.42). Note the operators are already normal ordered. Then, because the operators are time ordered, i.e., $t'_1 < t'_2 < \cdots < t'_m$, and

because free-field operators ($\hat{\mathcal{E}}_R$) commute with the source field operators ($\hat{\mathcal{E}}_S$) at earlier times [33], we can move all the free field terms to the immediate left (creation operators) and right (annihilation operators) of the density operator $\chi(0)$. Thus, when acting on the vacuum reservoir, their contribution to Eq. (3.44) is zero.

This means that we can make the substitution

$$\hat{\mathcal{E}} \to \hat{\mathcal{E}}_S, \tag{3.45}$$

in Eq. (3.44) to get

$$\begin{aligned}
&\left\langle : \hat{I}(t_1) e^{-\hat{\Omega}(t_1,t)} : \right\rangle \\
&= \sum_{m=0}^{\infty} (-1)^m \int_0^{t_1} dt'_m \int_0^{t'_m} dt'_{m-1} \cdots \int_0^{t'_2} dt'_1 \mathrm{tr}\left[\hat{\mathcal{E}}_S^{(-)}(t_1)\hat{\mathcal{E}}_S^{(-)}(t'_m)\hat{\mathcal{E}}_S^{(-)}(t'_{m-1})\right. \\
&\qquad \left. \times \cdots \hat{\mathcal{E}}_S^{(-)}(t'_1)\chi(0)\hat{\mathcal{E}}_S^{(+)}(t'_1)\cdots\hat{\mathcal{E}}_S^{(+)}(t'_{m-1})\hat{\mathcal{E}}_S^{(+)}(t'_m)\hat{\mathcal{E}}_S^{(+)}(t_1)\right],
\end{aligned} \tag{3.46}$$

Note that we still have $\chi(0)$ rather than $\rho(0)$ even though all the operators inside the trace are system operators. This is because, due to the interaction between system and reservoir, the system operator at time t depends on the reservoir operator at earlier times.

Superoperator notation; re-summation of exclusive counting probability

Now, we use superoperator notation to recast Eq. (3.46) into a form that is easier to apply the Born-Markov approximation to. First, we introduce $\mathcal{S}$ such that

$$\mathcal{S}\hat{O} = \hat{\mathcal{E}}_S^{(-)}(0)\hat{O}\hat{\mathcal{E}}_S^{(+)}(0), \tag{3.47}$$

and L, where

$$L\hat{O} = \frac{1}{i\hbar}[H, \hat{O}]. \tag{3.48}$$

Whence, we can write

$$\dot{\hat{\mathcal{E}}}_S(t) = L\hat{\mathcal{E}}_S(t), \tag{3.49}$$

from which we obtain the formal solution

$$\hat{\mathcal{E}}_S(t) = e^{Lt}\hat{\mathcal{E}}_S(0). \tag{3.50}$$

Equation (3.46) is in the Heisenberg picture – the time dependence is in the operators. We want to convert to the Schrödinger picture, so that we can describe the evolution of the state. Using Eq. (3.47) and Eq. (3.50), the Schrödinger picture version of Eq. (3.46) is written as

$$\begin{aligned}\left\langle : \hat{I}(t_1)e^{-\hat{\Omega}(t_1,t)} : \right\rangle \\ = \sum_{m=0}^{\infty}(-1)^m \int_0^{t_1} dt'_m \int_0^{t'_m} dt'_{m-1} \cdots \int_0^{t'_2} dt'_1 \mathrm{tr}\left[\mathcal{S}e^{L(t_1-t'_m)}\mathcal{S}e^{L(t'_m-t'_{m-1})}\cdots \right. \\ \left. \cdots \mathcal{S}e^{L(t'_2-t'_1)}\mathcal{S}e^{Lt'_1}\chi(0)\right]. \end{aligned} \tag{3.51}$$

We now make the Born-Markov approximation, as we did when we derived the master equation; this makes a change $L \to \mathcal{L}$, which allows us to take the trace over the reservoir, and replace the density operator $\chi(0)$ with $\rho(0)$. After making the replacements, we re-sum the expansion.[5] Doing the summation we obtain an expression

$$\left\langle : \hat{I}(t_1)e^{-\hat{\Omega}(t_1,t)} : \right\rangle = \mathrm{tr}_S\left[\mathcal{S}e^{(\mathcal{L}-\mathcal{S})t_1}\rho(0)\right]. \tag{3.52}$$

Note that the trace is only over the system variables now.

So far, we have concentrated on a small part of Eq. (3.40), we now state the result for the full expression. The answer is, not surprisingly,

$$\begin{aligned} P_{(\mathrm{REC})} &= \mathrm{tr}_S\left[e^{(\mathcal{L}-\mathcal{S})(t-t_n)}\mathcal{S}\cdots\mathcal{S}e^{(\mathcal{L}-\mathcal{S})(t_2-t_1)}\mathcal{S}e^{(\mathcal{L}-\mathcal{S})t_1}\rho(0)\right], \\ &\equiv \mathrm{tr}_S\left[\mathcal{K}_{\mathrm{REC}}(t)\rho(0)\right]. \end{aligned} \tag{3.53}$$

Interpretation of the master equation in terms of quantum trajectories

Comparing Eq. (3.53) with Eq. (3.38), we can immediately recognize the similarity. In fact, we can rewrite Eq. (3.38), in the right definition of $\mathcal{S}$, as

$$\rho(t) = \sum_{n=0}^{\infty}\int_0^t dt_n \int_0^{t_n} dt_{n-1}\cdots\int_0^{t_2} dt_1 \mathcal{K}_{\mathrm{REC}}(t)\rho(0). \tag{3.54}$$

[5] To do the summation we only have to recognize that this is a Dyson series - cf. Eq. (3.38).

Note, for the moment, that this equation takes the form of a sum over all measurement records. For example, if the initial state was an n-photon Fock state, it gives a sum over all the different ways n photons, and only n photons, are detected in the time interval $(0, t]$.

To simplify things a bit, we now convert to the interaction picture. Instead of $\mathcal{L}$ we have $\tilde{\mathcal{L}}$, giving

$$\dot{\tilde{\rho}}(t) = \tilde{\mathcal{L}}\tilde{\rho} = \frac{\gamma}{2}\left(2a\tilde{\rho}(t)a^\dagger - a^\dagger a\tilde{\rho}(t) - \tilde{\rho}(t)a^\dagger a\right). \tag{3.55}$$

There is one thing we have ignored so far – the finite speed of photons. To take it into account, we have to shift the time origin: if a photon enters the detector at time t, it must have left the cavity at some earlier time $t - \tau$, where τ is the time that light takes to travel from the cavity (mirror) to the detector. Thus, making the change $t \to t' = t - \tau$, we get

$$\tilde{\rho}(t') = \sum_{n=0}^{\infty} \int_{-\tau}^{t'} dt'_n \int_{-\tau}^{t'_n} dt'_{n-1} \cdots \int_{-\tau}^{t'_2} dt'_1 \tilde{\mathcal{K}}_{\mathrm{REC}}(t)\tilde{\rho}(-\tau), \tag{3.56}$$

with

$$\tilde{\mathcal{K}}_{\mathrm{REC}}(t') = e^{(\tilde{\mathcal{L}}-\mathcal{S})(t'-t'_n)}\mathcal{S}\cdots\mathcal{S}e^{(\tilde{\mathcal{L}}-\mathcal{S})(t'_2-t'_1)}\mathcal{S}e^{(\tilde{\mathcal{L}}-\mathcal{S})t'_1}. \tag{3.57}$$

We interpret $\tilde{\mathcal{K}}_{\mathrm{REC}}(t')\tilde{\rho}(-\tau)$ as the unnormalized conditional density operator, conditioned on the measurement records described by $\tilde{\mathcal{K}}_{\mathrm{REC}}(t')$. Then Eq. (3.56) takes the form of a sum over the conditional density operator

$$\begin{aligned}\tilde{\rho}(t') &= \sum_{\mathrm{REC}} \mathrm{tr}[\tilde{\tilde{\rho}}_c(t')]\frac{\tilde{\tilde{\rho}}_c(t')}{\mathrm{tr}[\tilde{\tilde{\rho}}_c(t')]}, \\ &= \sum_{\mathrm{REC}} P_{(\mathrm{REC})}\tilde{\rho}_c(t'),\end{aligned} \tag{3.58}$$

where $\tilde{\tilde{\rho}}_c(t') = \tilde{\mathcal{K}}_{\mathrm{REC}}(t')\tilde{\rho}(-\tau)$ is the unnormalized conditional density operator, and $P_{(\mathrm{REC})} = \mathrm{tr}[\tilde{\tilde{\rho}}_c(t')]$ is the probability density of obtaining the particular measurement record, as shown earlier in Eq. (3.53).

In this section we have shown that the master equation, in the Born-Markov approximation, is equivalent to Eq. (3.58), which is interpreted as a sum, over all possible measurement records, of the conditional density operator. This is the basis of quantum trajectory theory. We will see a way to numerically create measurement

records through Monte-Carlo simulation, evolving the state as we go along. But first, we will show that for a large class of master equations, taking the Lindblad form, the evolution preserves the pureness of the state. That is, if the initial state is pure the state remains pure throughout its entire evolution. However, it should be mentioned that this feature is not generally true, even for the Lindblad form. If the detection is not perfect – so we lose some photons that are emitted – the pure state evolves into a mixed state, reflecting our ignorance of the exact state, due to information loss.

Pure state evolution

For the field in a damped cavity described by the annihilation operator a, the output field impinging on the detector is given by $\sqrt{\gamma}(\hat{\mathcal{E}}_S+\hat{\mathcal{E}}_R)$. Correspondingly, $\mathcal{S}$ changes into

$$\mathcal{S}\hat{O} = \sqrt{\gamma}a\hat{O}\sqrt{\gamma}a^\dagger. \tag{3.59}$$

From this and Eq. (3.55) we can see that

$$(\tilde{\mathcal{L}} - \mathcal{S})\hat{O} = -\frac{\gamma}{2}[a^\dagger a, \hat{O}]_+, \tag{3.60}$$

where $[,]_+$ denotes the anticommutator. This implies

$$e^{(\tilde{\mathcal{L}}-\mathcal{S})t}\hat{O} = e^{-\frac{\gamma}{2}a^\dagger at}\hat{O}e^{-\frac{\gamma}{2}a^\dagger at}. \tag{3.61}$$

We now introduce a *non-Hermitian Hamiltonian*

$$\tilde{H}_B = -i\hbar\frac{\gamma}{2}a^\dagger a, \tag{3.62}$$

with which Eq. (3.61) is turned into

$$e^{(\tilde{\mathcal{L}}-\mathcal{S})t}\hat{O} = e^{-\frac{i}{\hbar}\tilde{H}_B t}\hat{O}e^{\frac{i}{\hbar}\tilde{H}_B t} \equiv \tilde{B}(t)\hat{O}\tilde{B}^\dagger(t). \tag{3.63}$$

Using Eq. (3.59) and Eq. (3.63), we can rewrite Eq. (3.57) as

$$\tilde{\mathcal{K}}_{\mathrm{REC}}(t')\hat{O} = \tilde{K}_{\mathrm{REC}}(t')\hat{O}\tilde{K}^\dagger_{\mathrm{REC}}(t'), \tag{3.64}$$

where

$$\tilde{K}_{\rm REC}(t') = \tilde{B}(t' - t'_n)J\tilde{B}(t'_n - t'_{n-1})\cdots J\tilde{B}(t'_2 - t'_1)J\tilde{B}(t'_1), \tag{3.65}$$

with $J = \sqrt{\gamma}a$. The reason we have introduced $\tilde{H}_B$, $\tilde{B}(t')$, and J is that we can give a straightforward interpretation of Eq. (3.65): $\tilde{B}(t_j - t_i)$ describes the evolution of the system from time t_i to t_j; the form of $\tilde{B}(t_j - t_i)$ is that of the evolution operator introduced in undergraduate quantum mechanics courses, the only difference being that the Hamiltonian is non-unitary. The non-unitarity arises from the fact that our system is an open system and does not change the fact that $\tilde{B}$ is a time evolution operator. J describes the jump or collapse of the state when the photon gets absorbed in the detector; we call it the jump operator. With these interpretations of $\tilde{B}$ and J, Eq. (3.65) describes a process where there are no photons emitted up to time t'_1, then a click in the detector (corresponding to an emitted photon from the cavity), no photons up to time t'_2, then another click ...etc... until time t'.

Now assume that the initial state of the field in the cavity is pure, i.e., $\tilde{\rho}(-\tau) = \rho(-\tau) = |\psi\rangle\langle\psi|$. In this case, the unnormalized conditional density operator $\tilde{\tilde{\rho}}_c(t')$ takes the form

$$\tilde{\tilde{\rho}}_c(t') = |\tilde{\tilde{\psi}}_{\rm (REC)}(t')\rangle\langle\tilde{\tilde{\psi}}_{\rm (REC)}(t')|, \tag{3.66}$$

where

$$|\tilde{\tilde{\psi}}_{\rm (REC)}(t')\rangle = \tilde{K}_{\rm REC}(t')|\tilde{\tilde{\psi}}(-\tau)\rangle \tag{3.67}$$

is the unnormalized conditional state. The probability of a measurement record is given by

$$P_{\rm (REC)} = \langle\tilde{\tilde{\psi}}_{\rm (REC)}(t')|\tilde{\tilde{\psi}}_{\rm (REC)}(t')\rangle. \tag{3.68}$$

3.2.4 Photoelectric detection of a Fock state in a cavity

In this section, we will see how we can generate the measurement records numerically for the photoelectric detection scheme; we then apply the method to the case of a Fock state in a cavity.[6]

[6]This may not seem to fit a scattering type scenario, but the scattering picture is recovered when we think about how the photons got into the cavity in the first place, i.e., there was a non-vacuum input some time in the past.

Note that the photon counting record is described by probabilities, implying the process of emission and detection are random. In a computer simulation, we will have to deal with random numbers to take this into account. From the formalism we have developed so far, we can work out the probability that an emission occurs in a time interval $[t, t+\Delta t)$, given a particular measurement history. We start with the joint probability of the measurement history plus emission, given by

$$P_{(\text{REC+emission})} = \langle \tilde{\tilde{\psi}}_{(\text{REC})}(t)|J^\dagger J|\tilde{\tilde{\psi}}_{(\text{REC})}(t)\rangle \Delta t. \tag{3.69}$$

The conditioned probability is the probability of the emission occurring given a particular measurement history. It can be calculated by dividing the joint probability by the probability of getting the particular record, i.e.,

$$\begin{aligned} P_{(\text{emission|REC})} &= \frac{P_{(\text{REC+emission})}}{P_{(\text{REC})}}, \\ &= \frac{\langle \tilde{\tilde{\psi}}_{(\text{REC})}(t)|J^\dagger J|\tilde{\tilde{\psi}}_{(\text{REC})}(t)\rangle \Delta t}{\langle \tilde{\tilde{\psi}}_{(\text{REC})}(t)|\tilde{\tilde{\psi}}_{(\text{REC})}(t)\rangle}, \\ &= \langle \tilde{\psi}_{(\text{REC})}(t)|J^\dagger J|\tilde{\psi}_{(\text{REC})}(t)\rangle \Delta t. \end{aligned} \tag{3.70}$$

We can now specify the procedure to solve for $|\tilde{\psi}_{(\text{REC})}(t)\rangle$ by numerical simulation. Our problem is this: given an unnormalized conditional state $|\tilde{\tilde{\psi}}_{(REC)}(t)\rangle$ at time t, what is the unnormalized conditional state $|\tilde{\tilde{\psi}}_{(REC)}(t+\Delta t)\rangle$ at time $t+\Delta t$? The following procedure allows us to answer this question:

1. Specify a small time step Δt[7] and compute the conditioned probability $P_{(\text{emission|REC})} = \langle \tilde{\psi}(t)|J^\dagger J|\tilde{\psi}(t)\rangle \Delta t$ by normalizing the conditional state.

2. Generate a uniform random number r between 0 and 1.

3. If $r < \langle \tilde{\psi}(t)|J^\dagger J|\tilde{\psi}(t)\rangle \Delta t$, apply J to the state, i.e., collapse it.

$$|\tilde{\tilde{\psi}}(t+\Delta t)\rangle = J|\tilde{\tilde{\psi}}_{(\text{REC})}(t)\rangle = \sqrt{\gamma}a|\tilde{\tilde{\psi}}_{(\text{REC})}(t)\rangle. \tag{3.71}$$

4. If $r > \langle \tilde{\psi}(t)|J^\dagger J|\tilde{\psi}(t)\rangle \Delta t$, evolve the state with the non-Hermitian evolution operator, $\tilde{B}(t') = e^{-\frac{\gamma}{2}a^\dagger a \Delta t}$, for a short time step Δt, i.e., compute

$$|\tilde{\tilde{\psi}}(t+\Delta t)\rangle = \left(1 - \frac{\gamma}{2}a^\dagger a \Delta t\right)|\tilde{\tilde{\psi}}(t)\rangle. \tag{3.72}$$

[7] Δt has to be small enough, such that $P_{(\text{emission|REC})} \ll 1$.

Starting from an initial state $|\psi(0)\rangle = |n\rangle$, we can iterate this procedure to find the conditional state at time t, as well as the probability of obtaining a particular measurement record. These *paths* the conditional state is going through are called the *quantum trajectories*, the term coined by Carmichael [24]. Note that we did not worry about the retardation time. However, this does not cause a significant problem; all we have to do is remember that when a photon enters a detector at time t, we *infer* that the collapse *had happened* already at time $t - \tau$. All it does is change the time origin, so let us ignore the problem altogether.

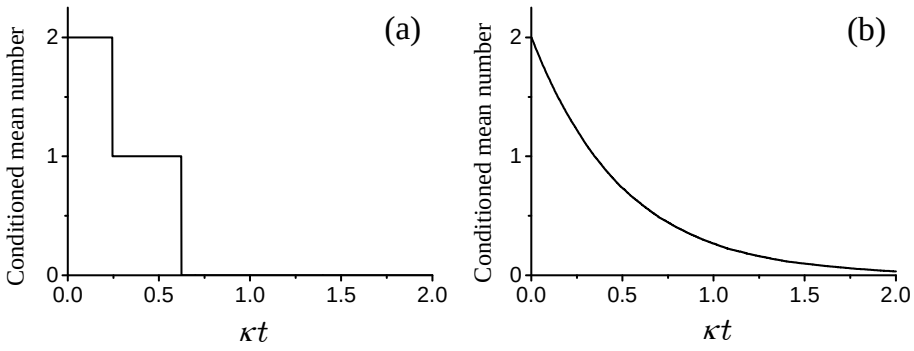

Figure 3.1: Conditioned mean photon number for a damped cavity initially containing a two-photon Fock state. (a) Single trajectory. (b) Average of 10,000 trajectories.

Figure 3.1 shows an example of a quantum trajectory. On the y-axis we have the conditioned mean number of photons inside the cavity; the x-axis is a scaled time variable. We start with a two-photon Fock state in the cavity and iterate according to our procedure, calculating the average number with respect to the conditioned state at each time step. Let us look at Figure 3.1(a). The conditioned mean number starts at 2 and remains at 2 until it drops down to 1 near $\kappa t = 0.25$. From then on, the conditioned number stays at 1, until it drops down to zero around $\kappa t = 0.7$. The interpretation from quantum trajectory theory is this. Until $\kappa t \approx 0.25$, the conditioned mean number is 2 since we know we started with 2 photons in the cavity. Then around $\kappa t = 0.25$ the photoelectric detector has clicked, indicating that a photon has left the cavity. Then, our knowledge about the intracavity field has changed: we know it has one photon now. This change of knowledge is indicated by an abrupt change of the conditioned mean number from 2 to 1. The same thing happens around $\kappa t = 0.7$, except that this time there is no photon left in the cavity; there will be no more detections.

Note the interpretation we make: the conditioned state is the state we *infer* from the measurement. Consequently, whatever average we take from it is the inferred quantity. This procedure and interpretation is very appealing because it is just what our intuition tells us.

The quantum trajectory approach is equivalent to the master equation approach as far as it is averaged over many trajectories; but what about the single trajectories? We have created an artificial, and ideal, environment which detects everything out of a system allowing us to infer the state perfectly. The quantum trajectory theory puts together the artificial environment, quantum theory and Born-Markov approximation. As far as the three ingredients are correct, the quantum trajectory theory yields the correct answer. Experimentally, these ideal conditions, especially the ideal environment, can never be reached, but we can extract some useful information from these idealized numerical experiments.

3.2.5 Balanced homodyne detection

This section develops the quantum trajectory theory of balanced homodyne detection, following the work of Carmichael [24, 34].

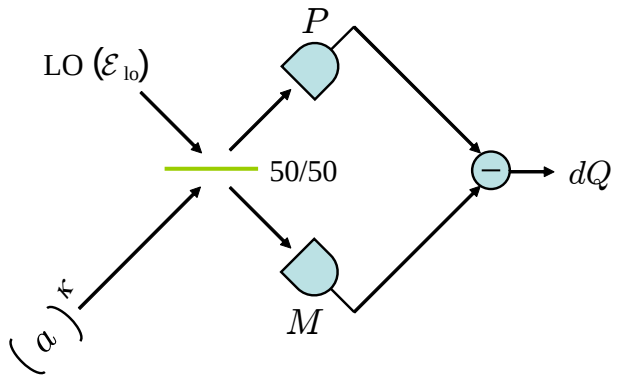

Figure 3.2: Model of the balanced homodyne detection scheme.

Figure 3.2 shows the balanced homodyne detection scheme. Again, we have a Fock state $|2\rangle$ in a cavity of damping rate $\kappa \equiv \gamma/2$. The intracavity field is a single-mode field with the mode annihilation operator a and frequency ω_0. The leaked field is the input to the balanced homodyne detector. The local oscillator field $\mathcal{E}_{\rm lo}\exp(-i\omega_0 t)$ is treated as a classical field, so $\mathcal{E}_{\rm lo}$ is an ordinary complex number. If we wanted to be more rigorous, we could use a coherent state for the

local oscillator field, but since we work with normal-ordered operators the answer will not be affected.

When the field inside the cavity leaks out it is superposed with the local oscillator field using a 50/50 beam splitter. The two superposed fields are measured by separate photoelectric detectors, denoted by P and M. The fields entering P and M are composed of the local oscillator field and the input field. These fields, which will be described by the annihilation operators b and c, can be written as

$$b = \frac{1}{\sqrt{2}}(\mathcal{E}_{\rm lo} + \sqrt{2\kappa}a), \tag{3.73a}$$

$$c = \frac{1}{\sqrt{2}}(\mathcal{E}_{\rm lo} - \sqrt{2\kappa}a), \tag{3.73b}$$

as we have already seen in Chapter 2. Consequently, the jump operators are

$$J_P = \frac{1}{\sqrt{2}}(\mathcal{E}_{\rm lo} + \sqrt{2\kappa}a), \tag{3.74a}$$

$$J_M = \frac{1}{\sqrt{2}}(\mathcal{E}_{\rm lo} - \sqrt{2\kappa}a). \tag{3.74b}$$

This changes the superoperator $\mathcal{S}$. In fact, we now have two of them, $\mathcal{S}_P$ and $\mathcal{S}_M$

$$\mathcal{S}_P \equiv J_P \cdot J_P^\dagger, \tag{3.75a}$$

$$\mathcal{S}_M \equiv J_M \cdot J_M^\dagger. \tag{3.75b}$$

When we have more than one jump operator, or jump superoperator, $\tilde{\mathcal{K}}_{\rm REC}(t)$ changes to something like

$$\tilde{\mathcal{K}}_{\rm REC}(t) = e^{(\tilde{\mathcal{L}}-\mathcal{S})(t-t_n)}\mathcal{S}_P \cdots \mathcal{S}_M e^{(\tilde{\mathcal{L}}-\mathcal{S})(t_2-t_1)}\mathcal{S}_M e^{(\tilde{\mathcal{L}}-\mathcal{S})t_1}, \tag{3.76}$$

where the arrangement of S_P and S_M changes for different measurement records. Obviously, $\tilde{\mathcal{L}} - \mathcal{S}$ is changed also, resulting in a change to $\tilde{H}_B$:

$$\tilde{H}_B \to \tilde{H}_B - i\hbar\frac{1}{2}|\mathcal{E}_{\rm lo}|^2 = -i\hbar(\kappa a^\dagger a + \frac{1}{2}|\mathcal{E}_{\rm lo}|^2). \tag{3.77}$$

Suppose there are n photons counted in time interval $(0, t]$. For a given record, we have a propagator

$$\tilde{K}_{\rm REC}(t) = \tilde{B}(t-t_n)J_n\tilde{B}(t_n-t_{n-1})\cdots J_2\tilde{B}(t_2-t_1)J_1\tilde{B}(t_1), \tag{3.78}$$

where $J_i \in J_M, J_P$ corresponds to the ith jump. We can now apply the procedure of the previous section to evolve the conditional state, but there is a slight complication. There are now two types of jumps, hence different probabilities for each type of jump, corresponding to the detection in P or M. The two probabilities P_P and P_M are given by

$$P_P = \langle\tilde{\psi}_{(\mathrm{REC})}(t')|J_P^\dagger J_P|\tilde{\psi}_{(\mathrm{REC})}(t')\rangle\Delta t, \tag{3.79a}$$

$$P_M = \langle\tilde{\psi}_{(\mathrm{REC})}(t')|J_M^\dagger J_M|\tilde{\psi}_{(\mathrm{REC})}(t')\rangle\Delta t, \tag{3.79b}$$

where P_P is the probability of there being a detection in $[t', t'+\Delta t)$ at the detector P, and similar for P_M. Now the procedure is modified as follows. When we generate a random number to decide whether there will be a jump or not, we compare the random number r with $P = P_P + P_M$. If $r > P$ there is a free evolution to next time step, if $r < P$ we have two choices: if $r < P_P$, we make the jump J_P; if $P_P < r < P_P + P_M$, we make the jump J_M. (Exchanging the subscripts P and M gives the same results.)

Having described the procedure, we are not actually going to use it exactly as described. The problem is, in experiments, the local oscillators are lasers – because they provide good monochromaticity and phase – and lasers have high intensities, whereas the input fields are weak. Since the $\mathcal{E}_{\mathrm{lo}}$ part of the jump operator does not change the conditional state, the conditional state only suffers a little change at each jump. We have many collapses, due to large $\mathcal{E}_{\mathrm{lo}}$, but with a little changes at each one. Obviously, this is very undesirable in simulations.

We will overcome this problem by coarse graining over time: we choose our time step Δt to be sufficiently large that many jumps occur, but small compared with the timescale on which the state of the source, or input, changes appreciably. Essentially we are choosing a time step which is small enough to take the change in conditional state as infinitesimal, but not any smaller.[8] Note that in such a time interval Δt, we have a lot of jumps at the detectors P and M; denoting the number of jumps q_P and q_M, we have $q_P \approx q_M \approx (1/2)|\mathcal{E}_{\mathrm{lo}}|^2\Delta t \gg 1$. We take the limits $\Delta t \to 0$ and $|\mathcal{E}_{\mathrm{lo}}| \to \infty$ such that $|\mathcal{E}_{\mathrm{lo}}|^2\Delta t \gg 1$ and expand the propagator

$$\begin{aligned}\tilde{K}_{\mathrm{REC}}(\Delta t) = \tilde{B}(\Delta t - t_{q_P+q_M})J_{q_P+q_M}\tilde{B}(t_{q_P+q_M} - t_{q_P+q_M-1})\cdots \\ \cdots J_2\tilde{B}(t_2 - t_1)J_1\tilde{B}(t_1),\end{aligned} \tag{3.80}$$

[8] $\Delta t/|\mathcal{E}_{\mathrm{lo}}|$ is infinitesimal but Δt is not.

where

$$\tilde{B}(t_i - t_j) = e^{-(\kappa a^\dagger a + \frac{1}{2}|\mathcal{E}_{\rm lo}|^2)(t_i - t_j)}, \tag{3.81a}$$

$$J_i \in \{J_P, J_M\}. \tag{3.81b}$$

Our limit is such that we discard all the terms with $(\Delta t)^n$ for $n > 1$, apart from any multiples of $|\mathcal{E}_{\rm lo}|^2 \Delta t$. Rewriting J_P and J_M as

$$\frac{\mathcal{E}_{\rm lo}}{\sqrt{2}}(1 \pm J), \tag{3.82}$$

where $J = \sqrt{2\kappa}a/\mathcal{E}_{\rm lo}$, we can write

$$\begin{aligned}\tilde{K}_{\rm REC}(\Delta t) = \exp\left(-\frac{1}{2}|\mathcal{E}_{\rm lo}|^2 \Delta t\right)\left(\frac{\mathcal{E}_{\rm lo}}{\sqrt{2}}\right)^{q_P + q_M} \\ \times \left[e^{-\kappa a^\dagger a(\Delta t - t_{q_P+q_M})}(1 \pm J)\cdots(1 \pm J)e^{-\kappa a^\dagger a t_1}\right].\end{aligned} \tag{3.83}$$

There are $q_P + q_M$ terms of $(1 \pm J)$ altogether, q_P with $+J$ and q_M with $-J$, and $q_P(1-q_P)/2 + q_M(1-q_M)/2 - q_P q_M = (q_P - q_M)^2 - (q_P + q_M)$ quadratic terms J^2. Higher orders of Js vanish in the limit of infinite oscillator strength we are taking. So we have

$$\begin{aligned}&e^{-\kappa a^\dagger a(\Delta t - t_{q_P+q_M})}(1 \pm J)\cdots(1 \pm J)e^{-\kappa a^\dagger a t_1} \\ &= 1 - \kappa a^\dagger a \Delta t + \frac{q_P - q_M}{\mathcal{E}_{\rm lo}}\sqrt{2\kappa}a + \frac{1}{2}\frac{(q_P - q_M)^2 - (q_P + q_M)}{\mathcal{E}_{\rm lo}^2}a^2.\end{aligned} \tag{3.84}$$

The next step is to write q_P and q_M as the sum of a mean and a fluctuation:

$$q_P = \frac{1}{2}\left\langle(\mathcal{E}_{\rm lo}^* + \sqrt{2\kappa}a^\dagger)(\mathcal{E}_{\rm lo} + \sqrt{2\kappa}a)\right\rangle_{REC}\Delta t + \frac{1}{\sqrt{2}}|\mathcal{E}_{\rm lo}|\Delta W_P, \tag{3.85a}$$

$$q_M = \frac{1}{2}\left\langle(\mathcal{E}_{\rm lo}^* - \sqrt{2\kappa}a^\dagger)(\mathcal{E}_{\rm lo} - \sqrt{2\kappa}a)\right\rangle_{REC}\Delta t + \frac{1}{\sqrt{2}}|\mathcal{E}_{\rm lo}|\Delta W_M, \tag{3.85b}$$

where $\frac{1}{\sqrt{2}}|\mathcal{E}_{\rm lo}|\Delta W_P$ and $\frac{1}{\sqrt{2}}|\mathcal{E}_{\rm lo}|\Delta W_M$ are the Poisson fluctuations, the shot noise, from the local oscillator field. Since for large mean number the Poisson distribution approaches the Gaussian distribution, we can take ΔW_P and ΔW_M to be Gaussian random numbers with zero mean and variance Δt.

From Eqs. (3.85) we have

$$q_P - q_M = |\mathcal{E}_{\rm lo}| \left(\sqrt{2\kappa} \langle e^{i\theta} a^\dagger + e^{-i\theta} a \rangle_{REC} \Delta t + \Delta W \right), \tag{3.86}$$

where

$$\Delta W = \frac{1}{\sqrt{2}} (\Delta W_P - \Delta W_M), \tag{3.87}$$

which is, again, a Gaussian random number with variance Δt and zero mean. In the limit $\Delta t \to 0$, the ΔW term becomes a Wiener increment.[9] So using the Ito rule, $(\Delta W)^2 = \Delta t$, we get

$$(q_P - q_M)^2 = |\mathcal{E}_{\rm lo}|^2 \Delta t. \tag{3.88}$$

Finally, we have

$$q_P + q_M = |\mathcal{E}_{\rm lo}|^2 \Delta t, \tag{3.89}$$

keeping the dominant terms only. Putting Eq. (3.83), Eq. (3.84), Eq. (3.86), Eq. (3.88) and Eq. (3.89) together, we obtain

$$\begin{aligned} \tilde{K}_{\rm REC}(\Delta t) = e^{-\frac{1}{2}|\mathcal{E}_{\rm lo}|^2 \Delta t} \left(\frac{\mathcal{E}_{\rm lo}}{\sqrt{2}} \right)^{q_P + q_M} \Big[1 - \kappa a^\dagger a \Delta t \\ + \sqrt{2\kappa} \left(\sqrt{2\kappa} \langle e^{i\theta} a^\dagger + e^{-i\theta} a \rangle_{REC} \Delta t + \Delta W \right) e^{-i\theta} a \Big]. \end{aligned} \tag{3.90}$$

Redefining the conditional state as

$$|\tilde{\tilde{\psi}}_{REC}(t)\rangle = \mathcal{E}_{\rm lo}^{-(q_P + q_M)} e^{\frac{1}{2}|\mathcal{E}_{\rm lo}|^2 t} |\tilde{\tilde{\psi}}_{REC}(t)\rangle, \tag{3.91}$$

removes the factor outside the square bracket in Eq. (3.90), allowing us to write a stochastic differential equation

$$d|\tilde{\tilde{\psi}}_{REC}(t)\rangle = \left[-\kappa a^\dagger a \Delta t + (Ge|\mathcal{E}_{\rm lo}|)^{-1}) \sqrt{2\kappa} e^{-i\theta} a dq \right] |\tilde{\tilde{\psi}}_{REC}(t)\rangle, \tag{3.92}$$

where

$$dq = Ge|\mathcal{E}_{\rm lo}| \left(\sqrt{2\kappa} \langle e^{i\theta} a^\dagger + e^{-i\theta} a \rangle_{REC} \Delta t + \Delta W \right), \tag{3.93}$$

[9] See Gardiner [35] about Wiener increment and Ito calculus.

is the infinitesimal charge deposited in the output of the balanced homodyne detector (cf. Figure 3.2). G is the gain and e is the electronic charge.

Eq. (3.92) with Eq. (3.93) is our final result. It is the *stochastic Schrödinger equation for balanced homodyne detection in quantum trajectory theory*. Figure 3.3 shows the conditioned photon numbers calculated from this stochastic Schrödinger equation; the result agrees perfectly with Figure 3.1(b) showing the equivalence between the two different methods. The difference between the two methods was our different choice of $\mathcal{S}$, hence different unravelling of the master equation. As we would expect, all the different unravellings – corresponding to different choices of $\mathcal{S}$ – yield the same answer. Note, however, that the physical interpretation of a trajectory can be given, for a given experiment setup, only if the choice of $\mathcal{S}$ is such that the jump operators (comprising $\mathcal{S}$) correspond to the field operators impinging on the detectors.

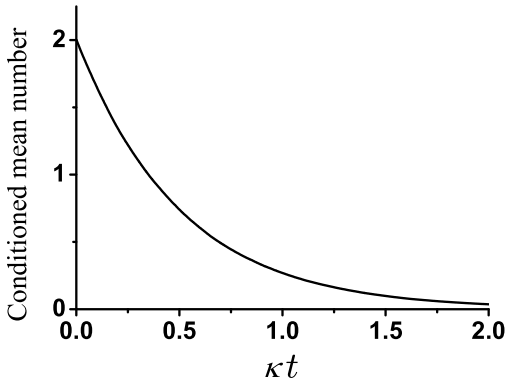

Figure 3.3: Conditioned photon numbers calculated by the stochastic Schrödinger equation [Eq. (3.92)], for an initial two-photon Fock state. 10,000 trajectories were averaged.

Chapter 4

Quantum teleportation

Before we talk about quantum teleportation, it will be helpful if we ask ourselves a question first: can we clone a quantum state? In other words, can we create a copy of a quantum state without destroying the original state? Classically this is easy. All we have to do is measure all the properties of the system, hence finding out the state, and make a copy. In quantum mechanics, however, it is generally impossible to measure all the properties of a system due to the Heisenberg Uncertainty Principle (HUP). If the system is in an eigenstate of an observable, there exists a measurement to discover its state (e.g. a photon counting experiment for a number state), but generally the system is in a superposition of non-orthogonal states, for which no set of measurements that can obtain all the information exists. Quantum states are usually destroyed by the very process of measurement, making subsequent measurement of the same state impossible.

So we cannot measure all the properties to make a copy, but is there a way to create a clone without actually measuring the state, i.e., without obtaining information about the state? The answer is no; it has been proved that cloning a quantum state is an impossibility [36]. But the question leads us to a new interesting hypothesis: we cannot clone a quantum state, but maybe we can create a copy if the original state is destroyed in the process, and no information about the original state is obtained. This is exactly what Bennett *et al.* [4] found. They found that by obtaining minimal information about the original system and using quantum entanglement they can *move* the quantum state from one system to another. If the two systems are far apart, the state is *teleported*.

This chapter first introduces quantum entanglement, the essential ingredient in quantum teleportation, and then explains the spin-state teleportation of Bennett *et*

al.. Finally, the teleportation will be extended to continuous variable systems.

4.1 Entanglement

An entangled state was first introduced in a classic paper by Einstein, Podolsky and Rosen (called the EPR paper in most literature) [1]. Their main interest, however, was not on the entangled state itself; they merely used it to prove the incompleteness of quantum mechanics.[1] The importance of entanglement was immediately recognized by the Austrian physicist Erwin Schrödinger, who hailed entanglement as [38]

> ...*the* characteristic trait of quantum mechanics, the one that enforces its entire departure from classical lines of thought.

In fact, it was Schrödinger who introduced the term 'quantum entanglement'.

In this section, we use David Bohm's version of the EPR state, rather than the original EPR state. This will make the analysis easier, because Bohm's version has correlations in spin, whereas the original version has correlations in the continuous variables position and momentum; the Hilbert space of the state decreases enormously by using Bohm's version. The EPR-Bohm state (for simplicity we will call it the EPR state from now on) can be created by a source emitting two electrons (see Figure 4.1).

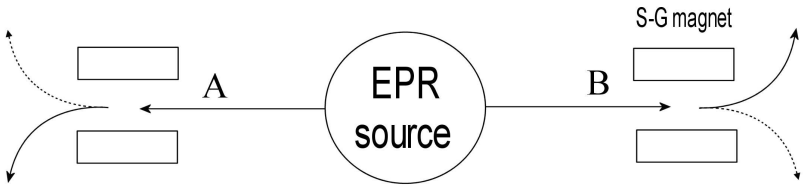

Figure 4.1: EPR source creates two electrons, traveling in opposite directions and having opposite spins. The electrons go to Alice (A) and Bob (B), who then pass them through Stern-Gerlach magnets. The electrons move up or down depending on their spin.

Angular momentum conservation forces the two electrons to have opposite spins; when one electron has spin up the other must have spin down and vice versa. So

[1] They used the idea of 'local realism' in proving the incompleteness, but thanks to Bell we now know that it is rather the concept of local realism which we must abandon. EPR were wrong in concluding that quantum mechanics is incomplete. A readable introduction on this subject is given in Sakurai [37].

the EPR state can be written as

$$|\mathrm{EPR}\rangle = \frac{1}{\sqrt{2}}\big(|\uparrow_1\rangle|\downarrow_2\rangle - |\downarrow_1\rangle|\uparrow_2\rangle \big), \tag{4.1}$$

where the arrows represent spin up or spin down in the z direction, and 1 and 2 denote electron 1 and 2 respectively.

Now let us analyze the measurement results obtained by Alice and Bob: if Alice gets spin up Bob gets spin down, if Alice gets spin down Bob gets spin up. So far there is nothing peculiar; this is just a classical correlation: to see what the classical correlation is, consider the following situation. There are two marbles of different color, say red and blue. They are in a black box so when Alice and Bob come and take one marble each they do not know which marble they have. When Alice and Bob go back to their rooms and look at their marbles, they must have different colored marbles: if Alice gets red Bob has blue and vice versa. This is a classical correlation between the colors of the marbles. The EPR state works exactly the same, so long as measurements of the spin are made in the z-direction only; the colors red and blue correspond to spin up and spin down.

To see the difference between the quantum entanglement and classical correlation, let us note that we can also measure the x component of spin by rotating the magnet.[2] Now there are four different measurement schemes, because each S-G magnet can detect the x or z component of spin. The results are summarized in Table 4.1.

Alice	Bob	Alice	Bob
$x:\uparrow$	$x:\downarrow$	$z:\uparrow$	$x:\uparrow$ or $\downarrow$
$x:\downarrow$	$x:\uparrow$	$z:\downarrow$	$x:\uparrow$ or $\downarrow$
$x:\uparrow$	$z:\uparrow$ or $\downarrow$	$z:\uparrow$	$z:\downarrow$
$x:\downarrow$	$z:\uparrow$ or $\downarrow$	$z:\downarrow$	$z:\uparrow$

Table 4.1: Measurement results for Alice and Bob.

The table tells us all possible measurement results; for example, if Alice measured the x component of spin and obtained 'up', there are two possible cases: Bob measures the x component and invariably gets 'down', or Bob measures the z component and gets 'up' or 'down' randomly. Now suppose that the EPR source emits the en-

[2]The EPR state looks the same when spin components are taken in the x direction, i.e., Eq. (4.1) works for both x and z component of spin.

tangled pairs regularly, allowing Alice and Bob to perform a series of measurements; they write down the directions and measurement results. After a while they will have a string of directions and arrows; suppose that Alice and Bob meet, later on, with their results to compare them. They will notice a very peculiar fact: whenever they happened to have measured the same component, they invariably obtained the opposite spins. However, when they have measured different components, there exists no correlation. This observation seems to suggest that, somehow, Bob's measurement result depends on what component Alice decided to measure. Electrons have communicated to tell each other which kind of S-G magnet they went through, even if the electrons are separated by a space-like distance. This communication between electrons is what Einstein called 'spooky action at a distance'.

So, we ask, is this really true? Is 'action at a distance' the only possible explanation? Can we not extend the marble analogy to explain this? For this case, we can. Let us see how. Suppose that marbles are more sophisticated; their two hemispheres have different colors. Northern hemispheres have blue or red, southern hemispheres have green or yellow. Now, suppose when the marbles are created in the factory it was made so that for a given pair of marbles, the colors in the same hemispheres are perfectly correlated (different color), while the colors between the different hemispheres have no correlation. This situation is represented in Table 4.2. From the similarity of this table and Table 4.1, we can see that this ensemble of mar-

Alice	Bob	Alice	Bob
S : Y	S : G	N : R	S : Y/G
S : G	S : Y	N : B	S : Y/G
S : Y	N : R/B	N : R	N : B
S : G	N : R/B	N : B	N : R

Table 4.2: The marble analogy of entangled states. N (northern hemisphere) can have one of the two colors R (red) and B (blue), S (southern hemisphere) can have one of the two colors Y (yellow) and G (green).

bles behaves in the same way as an ensemble of EPR pairs if we say that measuring the z component corresponds to looking at the northern hemisphere and measuring the x component corresponds to looking at the southern hemisphere. Everything is predetermined (at the factory), but we still get the same behaviour as for the EPR pair.

So, for this case, there is no 'spooky action at a distance' *required*. This does not rule out quantum mechanics, however, since both theories give the same prediction, either is as right as the other. After the EPR paper, this was recognized by most physicists and caused trouble. They knew the concept of probability (amplitude) in quantum mechanics is fundamentally different to those of classical mechanics, but they could not find any evidence that ruled out 'hidden-variable' theories. The situation continued until John S. Bell entered the scene in 1964. He recognized that there is a statistical difference between the 'local hidden-variable theory' and quantum mechanics, one that can be *observed*. Bell found an inequality that probabilities obey, which can be used to settle the score once and for all. This is the celebrated Bell inequality [39]. The Bell inequality has been tested experimentally in many ingenious ways [40, 41, 42], declaring quantum mechanics triumphant.[3] Local hidden-variable theories are not reconcilable with experiments.

4.2 Quantum teleportation

In this section we study the proposal of Bennett *et al.*, which opened up the field of quantum teleportation. As we have seen in the previous section, an entangled pair of particles show non-local correlations; that is, a certain property of one particle depends, *instantaneously*, on both the outcome and choice of measurement on the other particle at a distant location.

At first sight, there seems to be a problem; we know that information cannot travel faster than light,[4] and certainly, electrons 'communicating' instantaneously sounds like a contradiction. Of course, there is no contradiction; although there is a non-local correlation between the pairs, it cannot be used to transmit any useful information.

To see that there is no contradiction, consider the following example. Suppose Alice and Bob share a collection of EPR pairs, Alice is trying to send to Bob some information, using the collection of entangled pairs. Furthermore, Alice and Bob can only align their S-G magnets in two directions x and z. To make communication possible, Bob has to have a promised sequence of measurements (say x,z,x,z), otherwise his data is a completely random sequence. Also, Alice can only control her measurement sequence – the results are uncontrollable. Their hope is that when

[3] Actually, in the experiments, a generalized type of Bell inequality called the CHSH inequality [43] is used. However, the principles are the same.

[4] By special relativity, the speed of any signal is bounded by the speed of light, since the signal must be a physical object.

Alice uses a different measurement sequence, Bob would get different measurement results. As an example, suppose that Alice measures x, x, x, x and gets 'up', 'up', 'down', 'up', then Bob will get 'down', 'up or down', 'up', 'up or down' (see Table 4.3). Contrary to their hope, there are already four possible sequences (Table 4.4)

Alice	Bob
$x : \uparrow$	$x : \downarrow$
$x : \uparrow$	$z : \uparrow$ or $\downarrow$
$x : \downarrow$	$x : \uparrow$
$x : \uparrow$	$z : \uparrow$ or $\downarrow$

Table 4.3: Possible pair of measurement results. x and z denote the x and z direction, respectively, and $\uparrow$ and $\downarrow$ denote the spin measurement results 'up' and 'down', respectively.

for Bob, for Alice's particular sequence of measurements. Furthermore, the same sequence of Bob's results could come from a number of different measurement sequences of Alice. For example, look at the fourth column of Table 4.4: Bob measures 'down', 'up', 'up', 'down'. This particular sequence can arise from Alice measuring either x, x, x, x or z, z, z, z.

direction	1	2	3	4
x	$\downarrow$	$\downarrow$	$\downarrow$	$\downarrow$
z	$\uparrow$	$\downarrow$	$\downarrow$	$\uparrow$
x	$\uparrow$	$\uparrow$	$\uparrow$	$\uparrow$
z	$\uparrow$	$\uparrow$	$\downarrow$	$\downarrow$

Table 4.4: All the possible results of Bob.

This particular example shows there is no contradiction, that superluminal communication, using quantum entanglement, is impossible. We can also see that any other scheme will fail as well, because, in the end, no matter what Alice does, Bob can only get a random sequence of data not allowing him to infer the direction of Alice's measurement sequence.

Although we cannot communicate instantaneously using the EPR pair, it can assist in teleportation of a quantum state. The proposal of Bennett *et al.* [4] is summarized here, showing how quantum entanglement can be used to assist teleportation. First, let us specify the situation. Initially Alice and Bob share the EPR

pair with the state given by

$$|\text{EPR}\rangle = \frac{1}{\sqrt{2}}\big(|\uparrow_1\rangle|\downarrow_2\rangle - |\downarrow_1\rangle|\uparrow_2\rangle \big), \tag{4.2}$$

where the subscripts 1 and 2 refer to Alice and Bob, respectively. Alice is given a particle, which has a property that can be represented by a dichotomic variable (e.g. the polarization state of a photon or spin of any spin 1/2 particle), with state $|\phi\rangle$. Neither Alice nor Bob know the quantum state of the particle, but Alice has to teleport this state to Bob, without sending the particle itself.

As we have seen at the start of this chapter, this cannot be done in a straightforward way, namely, with Alice finding out what the state is, then passing this information to Bob. This would violate the no-cloning theorem. The proposal of Bennett *et al.* was, instead of obtaining information about the state $|\phi\rangle$, to use entanglement to pass what they called the 'quantum information': the information which cannot be written down or replicated at will. In their own words, Alice could

> ... divide the full information encoded in $|\phi\rangle$ into two parts, one purely classical and the other purely non-classical...

where the 'non-classical information' would be transmitted through quantum entanglement. The situation is depicted in Figure 4.2. The question mark represents the unknown state $|\phi\rangle$.

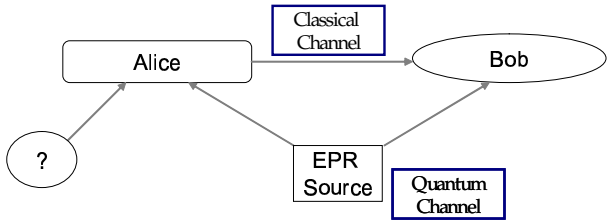

Figure 4.2: Schematic representation of teleportation.

Initially, the state that describes the total system is given by

$$|\text{total}\rangle = |\phi\rangle|\text{EPR}\rangle, \tag{4.3}$$

which is a pure product between the unknown state and the EPR state. Because they are in a pure product state, nothing interesting can happen. No measurement

can transfer information about the unknown state to Bob's share of the EPR pair. So our next step is to create a correlation between the states. This is done by performing what is called the Bell-operator measurement: Alice performs a joint measurement such that she measures one of the four states given by

$$|\Psi_{12}^{(\pm)}\rangle = \frac{1}{\sqrt{2}}\big(\,|\uparrow_1\rangle|\downarrow_2\rangle \pm |\downarrow_1\rangle|\uparrow_2\rangle\,\big), \tag{4.4a}$$

$$|\Phi_{12}^{(\pm)}\rangle = \frac{1}{\sqrt{2}}\big(\,|\uparrow_1\rangle|\uparrow_2\rangle \pm |\downarrow_1\rangle|\downarrow_2\rangle\,\big). \tag{4.4b}$$

Note that these four states form a complete orthogonal basis for particles 1 and 2, i.e., any (spin) state for the particles 1 and 2 can be written as a superposition of these four states. Let us write the unknown state as

$$|\phi\rangle = \alpha|\uparrow_0\rangle + \beta|\downarrow_0\rangle, \tag{4.5}$$

then Eq. (4.3) becomes

$$\begin{aligned}|\text{total}\rangle = {} & \frac{\alpha}{\sqrt{2}}\big(\,|\uparrow_0\rangle|\uparrow_1\rangle|\downarrow_2\rangle - |\uparrow_0\rangle|\downarrow_1\rangle|\uparrow_2\rangle\,\big) \\ & + \frac{\beta}{\sqrt{2}}\big(\,|\downarrow_0\rangle|\uparrow_1\rangle|\downarrow_2\rangle - |\downarrow_0\rangle|\downarrow_1\rangle|\uparrow_2\rangle\,\big).\end{aligned} \tag{4.6}$$

Now we change the basis to the Bell states given in Eq. (4.4). Upon this change the total state becomes

$$\begin{aligned}|\text{total}\rangle = \frac{1}{2}\Big[& |\Psi_{01}^{(-)}\rangle(-\alpha|\uparrow_3\rangle - \beta|\downarrow_3\rangle) + |\Psi_{01}^{(+)}\rangle(-\alpha|\uparrow_3\rangle + \beta|\downarrow_3\rangle) \\ & + |\Phi_{01}^{(-)}\rangle(\alpha|\downarrow_3\rangle + \beta|\uparrow_3\rangle) + |\Phi_{01}^{(+)}\rangle(\alpha|\downarrow_3\rangle - \beta|\uparrow_3\rangle)\Big].\end{aligned} \tag{4.7}$$

If Alice measures one of the four Bell states given in Eq. (4.4), Bob obtains one of the four states given by

$$-\alpha|\uparrow_3\rangle - \beta|\downarrow_3\rangle, \qquad -\alpha|\uparrow_3\rangle + \beta|\downarrow_3\rangle,$$

$$\alpha|\downarrow_3\rangle + \beta|\uparrow_3\rangle, \qquad \alpha|\downarrow_3\rangle - \beta|\uparrow_3\rangle.$$

By performing a joint measurement (Bell-state measurement), Alice has sent the quantum information to Bob.

Alice now has to send her measurement result to Bob, namely which of the

four Bell states she has obtained. Note that this measurement result does not reveal information about the input state (it does not depend on α or β at all); nevertheless, this information is vital to complete the teleportation. Once Bob gets the classical information he can perform a unitary operation to get the original state back. For example, suppose that Alice detected $|\Psi_{01}^{(-)}\rangle$, then Bob has the original state except for the overall minus sign, which is irrelevant (an overall phase factor does not change the state). If Alice detected $|\Phi_{01}^{(-)}\rangle$, Bob will get $\alpha|\downarrow_3\rangle+\beta|\uparrow_3\rangle$ in his hand, then he has to apply a spin flipping operation to get the original state back.[5] Other results of Bell-state measurements for Alice mean other unitary transformations for Bob. Because of this need of classical information, the whole teleportation process cannot happen instantaneously.[6]

In this section we have seen how we could teleport an arbitrary spin-state of a spin-1/2 particle. The whole process can be summarized as five steps:

1. Alice and Bob initially share an EPR pair.

2. Alice gets an unknown state that she has to teleport.

3. Alice performs a joint measurement on the unknown state and the EPR state.

4. Alice sends the measurement result to Bob.

5. Bob performs a unitary operation, on his share of the EPR pair, and gets the unknown state in his hand.

Experiments have been done on teleporting the polarization state of a photon [44, 45], and were successful in showing the validity of quantum teleportation.

So far, we have restricted ourselves to teleportation of spin-1/2 variables. We have no way of teleporting any states that live in a bigger Hilbert space. In quantum optical language, we can teleport the polarization state of photons, but we cannot teleport other interesting features: whether the state is in a coherent state, a squeezed state or a thermal state. To do this, we have to extend our analysis to continuous variables. This is the topic of the next section.

[5] How we can do this operation depends on what kind of particles we are using. For example, if we use photons, we can use a half-wave plate for this particular operation.

[6] More correctly, it cannot happen at speeds faster than light.

4.3 Continuous variable quantum teleportation

In this section, we will deal with continuous variable quantum teleportation (CVQT). CVQT allows us to teleport a much broader range of states, since any quantum optical state can be represented by continuous variables.

CVQT was first proposed in 1994 by Vaidman [8]. Essentially, he used the original EPR state (which has perfect correlations in position and momentum) to show that one can teleport quantum states that can be represented by position and momentum variables. After four years, in 1998, Braunstein and Kimble [9] came up with a quantum optical protocol for CVQT. Their entangled source was the two-mode squeezed state, which, in the limit of infinite squeezing, becomes the EPR state. Their protocol forms the basis of the teleportation protocol in this thesis, so we shall study it in detail.

Basically, the procedures are the same as in teleportation of dichotomic variables. Alice and Bob share an EPR pair; Alice also gets the state to be teleported; she performs a joint measurement and sends the information to Bob; Bob then performs a unitary operation (Figure 4.2). The difference is in the EPR pair, the detail of Alice's measurements (because we are dealing with continuous variables we have infinitely many entangled states, rather than four Bell states) and hence Bob's operation. We should now look at the detailed analysis, done in the Wigner representation.

The Wigner representation of the two-mode squeezed state (the quantum optical analogue of the EPR state) is given by [9]

$$W_{\mathrm{EPR}}(x_a,p_a,x_b,p_b) = \frac{4}{\pi^2}\exp\left\{-e^{-2r}[(x_a-x_b)^2+(p_a+p_b)^2] \right. \\ \left. -e^{+2r}[(x_a+x_b)^2+(p_a-p_b)^2]\right\}, \qquad (4.8)$$

where x_a and p_a refer to the x and p quadratures of the mode that goes to Alice, and similarly x_b and p_b are the quadratures for Bob. In the limit of infinite r, the above equation becomes

$$W_{\mathrm{EPR}}(x_a,p_a,x_b,p_b) = C\delta(x_a+x_b)\delta(p_a-p_b), \qquad (4.9)$$

where C is just a normalization constant. This Wigner distribution has exactly the same form as the Wigner distribution of the original EPR state. This limit, however, is not realizable even in the ideal situation (it requires infinite energy), so

instead of this Wigner distribution, we will use Eq. (4.8). Using Eq. (4.8) for finite r corresponds to using entangled states which are not maximally entangled.

Having the pulses of light described by Eq. (4.8), initially shared between Alice and Bob, Alice now obtains another light pulse, which is to be teleported. The quantum state of the light pulse is represented by the Wigner function $W_{\text{in}}(x_c, p_c)$. At this moment the total state is represented by

$$W_{\text{total}}(x_c, p_c, x_a, p_a, x_b, p_b) = W_{\text{in}}(x_c, p_c) W_{\text{EPR}}(x_a, p_a, x_b, p_b). \tag{4.10}$$

Because the total state is a direct product between the input and EPR states, the Wigner functions are merely multiplied.

Carrying on with teleportation, Alice performs a joint measurement: she first entangles the two modes of light x_c, p_c and x_a, p_a, by passing them through a 50/50 beam splitter. The resulting output mode quadrature operators, x_d, p_d and x_e, p_e, can be written as[7]

$$x_d = \frac{1}{\sqrt{2}}(x_c + x_a), \tag{4.11a}$$

$$p_d = \frac{1}{\sqrt{2}}(p_c + p_a), \tag{4.11b}$$

$$x_e = \frac{1}{\sqrt{2}}(x_c - x_a), \tag{4.11c}$$

$$p_e = \frac{1}{\sqrt{2}}(p_c - p_a), \tag{4.11d}$$

which, combined with Eq. (4.10) gives

$$\begin{aligned} &W_{\text{total}}(x_d, p_d, x_e, p_e, x_b, p_b) = \\ &W_{\text{in}}\left(\frac{1}{\sqrt{2}}(x_d + x_e), \frac{1}{\sqrt{2}}(p_d + p_e)\right) W_{\text{EPR}}\left(\frac{1}{\sqrt{2}}(x_d - x_e), \frac{1}{\sqrt{2}}(p_d - p_e), x_b, p_b\right). \end{aligned} \tag{4.12}$$

After entangling the two modes of light, Alice measures x_d and p_e. Calling the measured values q_x and q_y, this step corresponds to making the substitutions $x_d \to q_x, p_e \to q_y$ and integrating over the variables p_d, x_e in the Wigner function. Defining

[7] In real life, it is difficult to control the phase factor to get exactly this transformation. If we get a different transformation Bob's operation must change.

the complex Gaussian as

$$G_\sigma(\alpha) = \frac{1}{\pi\sigma} \exp\left(\frac{-|\alpha|^2}{\sigma}\right), \tag{4.13}$$

the state after the measurement can be written as

$$W'_{\text{total}}(\alpha_b) = 4NG_\nu(\alpha_b) \int d^2\alpha_c W_{\text{in}}(\alpha_c) G_\tau(\sqrt{2}(q_x + iq_y) + \tanh(2r)\alpha_b - \alpha_c), \tag{4.14}$$

where $\nu = \cosh(2r)/2$ and $\tau = 1/2\cosh(2r)$. N is a normalization constant, which is required because the conditional output state is not necessarily normalized (after the substitutions $x_d \to q_x, p_e \to q_y$). We have also introduced a shorthand notation $\alpha = x + ip$.

From this we can see that as $r \to \infty$, $\tanh(2r) \to 1$ and $\tau \to 0$, meaning that the complex Gaussian G_τ becomes a delta function. Then, all Bob has to do is displace the output Wigner distribution by $\sqrt{2}(q_x + iq_y)$. We will call this final state the output state. It is given by

$$W_{\text{out}}(\alpha_b) = W'_{\text{total}}(\alpha_b - \sqrt{2}(q_x + iq_y)). \tag{4.15}$$

This ends the teleportation procedure proposed by Braunstein and Kimble. A summary of the procedure will be useful:

1. Alice and Bob share a two-mode squeezed state.
2. When Alice gets the input state (an unknown optical state), she mixes the input light pulse and squeezed light pulse by passing them through a 50/50 beam splitter. Then she measures the x and y quadratures of each output light pulse. (Balanced homodyne detection is used to measure the quadratures.)
3. Alice passes the information (q_x, q_y), obtained in Step 2, to Bob.
4. Bob displaces his share of the two-mode squeezed state by $\sqrt{2}(q_x + iq_y)$.

In this chapter, we started from quantum entanglement, explained dichotomic variable teleportation, then finished with continuous variable teleportation. It should be mentioned, however, that the version introduced in this section is not a complete version.

The version in this section is single-mode teleportation; the two modes of the two-mode squeezed state have the same spatio-temporal structure, the input mode

is mode-matched (spatio-temporal mode matching[8]), and frequency-matched to the two-mode squeezed state.

The more complete version is broadband teleportation, taking into account the finite bandwidth of the squeezing and the input light, making it easier to compare theory with experiments. The extension of the Braunstein and Kimble scheme to the broadband case was given by Loock, Braunstein and Kimble [6].

The broadband nature does not pose too great a restriction, however; if the bandwidth of the input state is narrow (called quasi single-mode) compared with the bandwidth of the squeezed state, then we could treat the teleportation as single-mode teleportation around the frequency of the input light pulse.[9] The difficulty in an experiment is with Bob holding on to his EPR share; since the squeezed light pulses are traveling at the speed of light it is a very difficult job.

[8]See Section 5.1, and for a more concrete discussion, Raymer *et al.* [46], about mode matching.
[9]This requires the central squeezed frequency to be the same as the central input mode.

Chapter 5

Fock state teleportation: methods of analysis

We now have all the theoretical machinery we need to investigate quantum teleportation in detail. In this chapter, a teleportation protocol implementing the scheme of Braunstein and Kimble will be introduced and explained in detail. Then numerical and analytical methods are used to investigate the protocol. The stochastic Schrödinger equation of the protocol will be developed, and then solved numerically. We will confine ourselves to Fock state inputs; we choose Fock states for two reasons: (1) it is one of the simplest states, if not the simplest, one might think of in numerical simulations; (2) it is a non-classical state, unlike coherent states. More will be said about non-classicality later. The analytical expressions are obtained from the Wigner function analysis, as in Braunstein and Kimble [9], as well as from solving the SSE directly.

Our focus is on a *theoretical* study of teleportation, especially the teleportation of a Fock state. Experimental realization of our protocol suffers some problems, one being that the generation of a Fock state of the electromagnetic field is very difficult, and we do not have a readily available method yet. There is also the problem of keeping Bob's share of the entangled state at his location while waiting for Alice's results. This is quite a formidable challenge, mainly because light travels at tremendous speed. All the experimental teleportations up to now employ the continuous feed-forward mechanism where everything runs continuously in time, including Alice's feed-forward of her results to Bob. Coherent state teleportation was done in this way by Furusawa *et al.* [5] and Bowen *et al.* [10].

The above problems, however, are only experimental; in principle the problems

can be, and probably will be, solved. Thus studying the single-mode (or quasi single-mode) teleportation protocol described in this chapter is not entirely without merit. Our focus is on the single-shot results, rather than on the ensemble averages, as it has been so far; the single-shot results can also tell us, when taken along with the probabilities of obtaining the measurement record, what the average is going to be, as well as whether the teleportation works shot by shot, and if they do, how well it works.

5.1 Teleportation protocol

This section introduces the teleportation protocol, and explains a few detailed topics with regard to it. The topics discussed are mode matching, the EPR state, displacement, and non-classicality of the Fock states.

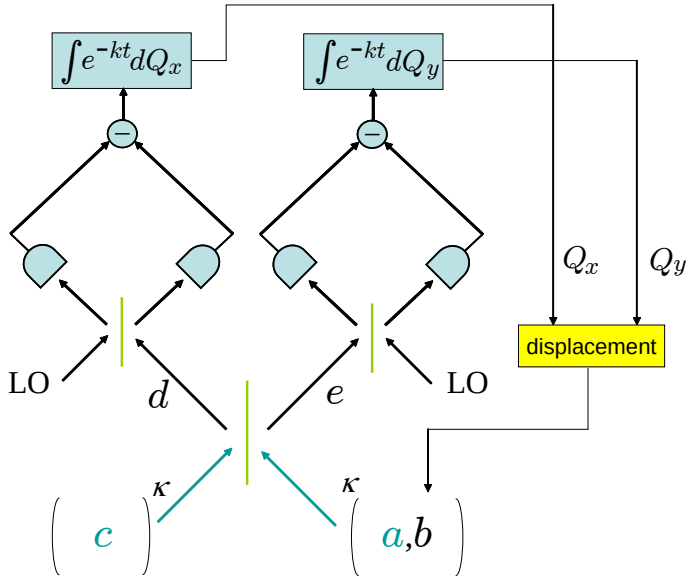

Figure 5.1: Teleportation scheme.

Figure 5.1 is a schematic representation of the protocol we investigate. Initially, a Fock state is prepared in a cavity with damping rate κ, κ tells us how fast light leaks out of the cavity – the higher the damping rate the faster the leak. The EPR state is imagined to be prepared in another cavity with the same damping rate.[1]

[1]More realistically we can include a model, such as the optical parametric oscillator, which generates the entangled light pulses.

a, b, and c are the annihilation operators for the two modes of the EPR state and the input Fock state, respectively. All three modes have the same frequency. At time $t = 0$, the input field and one of the entangled fields, the fields described by the mode annihilation operators c and a respectively,[2] start to leak through the cavities – as represented by the arrows at the bottom of the diagram. The field in mode b, Bob's mode, stays in the cavity. Following the arrows in the diagram, fields in modes a and c pass through a 50/50 beam splitter, producing the two output fields in modes d and e. Subsequently, the x and y quadratures of the output fields are measured – the results are called Q_x and Q_y in the diagram. The measurement results are then passed to Bob, who displaces the field in mode b by $Q_x + iQ_y$. The quadratures are measured with two balanced homodyne detectors; the results Q_x and Q_y correspond to the integrated photocurrents coming out of each detectors. Note that there is an integrating factor $e^{-\kappa t}$ involved; the inclusion of this factor is required by the mode matching.

Mode matching

The concept of mode matching was introduced earlier in Chapter 2 when we introduced the balanced homodyne detection scheme. It simply states that the mode of the local oscillator field has to be matched to that of the input field, both spatially and temporally, meaning they must overlap in space and time completely for perfect detection. This is because we want exactly the same contributions from the local oscillator field and the input field; a wider and/or longer local oscillator field compared with the input field would certainly be undesirable.

Now, let us go back to our protocol and assume the spatial modes are matched. How do we match the temporal modes? If the local oscillator field is fed continuously in time, it is certainly not mode matched to the input field, which is a pulse. One way to mode match the two fields is to simply put the local oscillator field in a cavity with damping rate κ. For the local oscillator field, which is essentially a classical field, this corresponds to a decaying amplitude. That is, $\mathcal{E}_{\rm lo} \to e^{-\kappa t}\mathcal{E}_{\rm lo}$. If we put this into Eq. (3.93), the infinitesimal charge acquires the integrating factor.

There is also another probability. Actually, it is unnecessary to put the local

[2]Here, a little warning should be given about the notation. a, b, c, d, e are the annihilation operators, and a,b,c,d,e denote the respective modes. Thus, a is the annihilation operator for the mode a. The difference is that the mode names are in the normal font, whereas the annihilation operators are written in the math font. At any rate, it should be clear from the context which one is being used.

oscillator in a cavity but we can run the local oscillator without the decaying amplitude and introduce the integrating factor later when we integrate the photocurrents – both ways are equivalent. In practice the latter method is adopted because it is easier to use.

Two-mode squeezed state

Before we develop quantum trajectory theory of the protocol, we need to know what the EPR state is. It was already mentioned that the quantum optical analogue of the EPR state is the two-mode squeezed state – specifically, it is the two-mode squeezed vacuum state. The two-mode squeezed state can be made from two separate squeezed states, by mixing them using a 50/50 beam splitter. To create a two-mode squeezed vacuum state, we prepare two squeezed vacuum states, one squeezed in the x quadrature, and the other in the p quadrature, each squeezed by the same amount. From the definition of the squeezing operator given in Chapter 2, we can work out the squeezed vacuum states:

$$|S_x\rangle = S(r)|0\rangle = \exp\left[\frac{r}{2}(a_1^2 - a_1^{\dagger 2})\right]|0\rangle, \tag{5.1a}$$

$$|S_p\rangle = S(-r)|0\rangle = \exp\left[-\frac{r}{2}(a_2^2 - a_2^{\dagger 2})\right]|0\rangle. \tag{5.1b}$$

The total state before the mixing is given by

$$|S_x\rangle \otimes |S_p\rangle = \exp\left\{\frac{r}{2}[(a_1^2 - a_1^{\dagger 2}) - (a_2^2 - a_2^{\dagger 2})]\right\}|0,0\rangle. \tag{5.2}$$

After passing them through a beam splitter the annihilation operators transform according to

$$a_1 = \frac{1}{\sqrt{2}}(a+b), \tag{5.3a}$$

$$a_2 = \frac{1}{\sqrt{2}}(a-b), \tag{5.3b}$$

where a and b are the annihilation operators of the beamsplitter output modes. Substituting these into Eq. (5.2), we obtain the two-mode squeezed vacuum state, given by

$$\begin{aligned} |\text{TMSV}\rangle &= \exp\left[r(ab - a^\dagger b^\dagger)\right]|0,0\rangle, \\ &\equiv S_{TM}(r)|0,0\rangle, \end{aligned} \tag{5.4}$$

where

$$S_{TM}(r) = \exp\left[r(ab - a^\dagger b^\dagger)\right] \tag{5.5}$$

is the two-mode squeezing operator. Note that the vacuum state of modes a_1 and a_2 transforms to the vacuum state of modes a and b; it is obvious from the physics that the vacuum state is invariant under this transformation. That this state is equivalent to the EPR state introduced earlier is proved, in the Wigner representation, in Appendix C.

The displacement

If we look at the end of Chapter 4, the Wigner function analysis of Braunstein and Kimble showed that the displacement should be $\sqrt{2}(q_x + iq_y)$, assuming q_x and q_y corresponds to x_d and p_e. Yet we claimed earlier in this section that the displacement has to be $Q_x + iQ_y$. This discrepancy arises from the fact that the measured values Q_x and Q_y are not exactly the same as the x and p quadrature amplitudes as usually defined. We can see the exact displacement required by considering a special case: teleportation of a classical field with an unentangled EPR source ($r = 0$). In this case, each of the two modes are in the vacuum state, completely uncorrelated. The teleportation procedure now amounts to measuring the amplitude of the input field and displacing the vacuum field by the measured amplitude.

From Section 5.2.1, we can see that the infinitesimal charge is given by [cf. Eq. (5.11b)]

$$\begin{aligned} dq_x &= \sqrt{\kappa}\langle c + c^\dagger\rangle_{REC} dt + dW, \\ &= 2\sqrt{\kappa} x_c(t) dt + dW \end{aligned}$$

if the EPR state is unentangled so that the mode a is in the vacuum; $x_c(t)$ stands for the expectation value of the quadrature operator. Now suppose that the input field is in a classical state (coherent state). Then $x_c(t)$ becomes a classical amplitude, decaying exponentially at rate κ, i.e., we can write

$$\begin{aligned} Q_x &= \int_0^\infty dt 2\sqrt{\kappa} x_c(0) e^{-\kappa t} e^{-\kappa t}, \\ &= \frac{1}{\sqrt{\kappa}} x_c(0). \end{aligned}$$

and

$$Q_y = \frac{1}{\sqrt{\kappa}} p_c(0).$$

For $\kappa = 1$ our displacement should be $Q_x + iQ_y$. From now on we will assume that $\kappa = 1$, without loss of generality; it just changes the unit of time.

The result is that between the simulation and the Wigner function analysis there exists a relation

$$\sqrt{2} q_x = Q_x. \tag{5.6}$$

Non-classicality of Fock states

It was claimed that the Fock states are non-classical, but in what sense is it non-classical? What is a classical state? In the literature, non-classicality usually refers to the non-existence of a positive-definite P distribution.[3] The P representation is similar to the Wigner representation, in that the P function acts like a probability distribution. The difference is that the P distribution gives us normal-ordered operator averages rather than symmetric-ordered ones. Since photoelectric detection is intimately related to normal ordering – because the main process is the absorption of photons – it is in turn related to the P distribution. If the P distribution of a state is a positive-definite function, as it is for all mixture of coherent states, the state can be considered classical[4] in the sense that the sub-Poissonian statistics or anti-bunching are impossible. To put it another way, those states that have positive-definite P representations can be described by the semiclassical theory of photoelectric detection, hence they are called classical states; states that cannot be described by a positive-definite P distribution cannot be described by the semiclassical theory, hence they are called non-classical states.

In our case, however, the non-classicality of a Fock state refers to the existence of a negative region in the Wigner distribution (shown in Figure 5.2 for a one-photon Fock state). If we are worried about the details of the detection process, this definition of classicality does not suffice; we have to resort to the P distribution. However, if we take the detection as granted, and just say that the balanced ho-

[3] The P representation or Glauber-Sudarshan P representation was introduced independently by Glauber [47], and Sudarshan [48], concerned with the representation of mixed coherent states describing a general laser output.

[4] In addition, the P distribution cannot be more singular than a δ-function if it represents a classical state.

modyne detectors measure the quadratures, then, because the quadrature operators are symmetrically ordered, we can think of the Wigner distribution as a probability distribution of the x and p quadratures. This means we could think of the quadratures as pre-existing statistical quantities, unlike observables in quantum mechanics. This is what stochastic electrodynamics (SED) [49] does; it treats the quadratures as real predetermined quantities and adds the vacuum fluctuations by hand, treating them as real fluctuations. This certainly fails when we think about the photoelectric detection process, since the vacuum never makes a detector click. However, the expectation values of any function of x and p can be calculated this way, yielding the right answer. So, in our protocol, where two balanced homodyne detectors are used, the negativity of Wigner distribution provides a good definition of non-classicality.

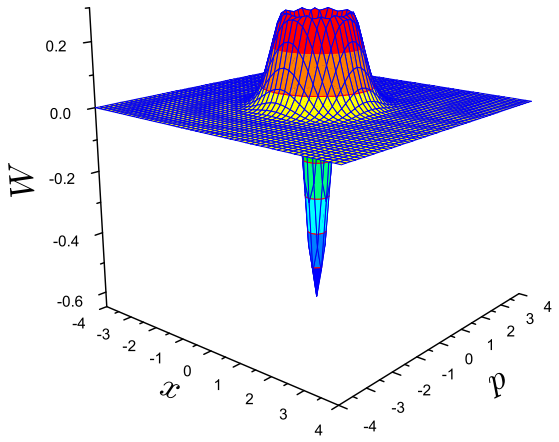

Figure 5.2: Wigner representation of a one-photon Fock state.

Continuous variable teleportation has been studied within SED for classical input states – classical in the Wigner sense – by Carmichael and Nha [50]. This could be done because the two-mode squeezed state is classical in the Wigner sense, although it is not classical in the P distribution sense. This cannot be done, however, for a Fock state input because the Wigner distribution of a Fock state can take negative values. Thus we can expect features that cannot be described by a *real* fluctuating field to happen in the teleportation of Fock states.

5.2 Simulation

In this section we first develop the quantum trajectory theory of the teleportation protocol which results in a stochastic Schrödinger equation. We then talk about how it can be solved numerically.

5.2.1 Stochastic Schrödinger equation for the protocol

We are now left with the task of deriving the stochastic Schrödinger equation as promised at the start of this chapter. Having seen the derivation of the stochastic Schrödinger equation for balanced homodyne detection, our derivation will not be too difficult; the only complication is that we now have two balanced homodyne detectors rather than one. We will assume that the two local oscillators have the same strength, although they have to have different phases. When we write the propagator as in Eq. (3.80), instead of two kinds of jumps, J_P and J_M, we have now four kinds of jumps, J_{P1}, J_{M1}, J_{P2}, and J_{M2}, 1 and 2 referring to different detectors. Consequently, instead of J defined below Eq. (3.82), we will have

$$J_1 = \frac{1}{\mathcal{E}_{\rm lo}}(c + a), \tag{5.7a}$$

$$J_2 = \frac{1}{\mathcal{E}_{\rm lo}}(c - a), \tag{5.7b}$$

where we have used $\kappa = 1$. With these changes Eq. (3.83) becomes

$$\begin{aligned}\tilde{K}_{\rm REC}(\Delta t) = e^{-\frac{1}{2}|\mathcal{E}_{\rm lo}|^2\Delta t}\left(\frac{\mathcal{E}_{\rm lo}}{\sqrt{2}}\right)^{q_{tot}}\Big[e^{-(c^\dagger c + a^\dagger a)(\Delta t - t_{q_{tot}})}(1 \pm J_{\mu_{q_{tot}}})\cdots \\ \cdots(1 \pm J_{\mu_2})e^{-(c^\dagger c + a^\dagger a)(t_2 - t_1)}(1 \pm J_{\mu_1})e^{-(c^\dagger c + a^\dagger a)t_1}\Big],\end{aligned} \tag{5.8}$$

where $q_{tot} = q_{P1} + q_{M1} + q_{P2} + q_{M2}$ and $J_{\mu_i} \in \{J_1, J_2\}$. After expanding this term in a similar way to what we did below Eq. (3.83), and then applying the same limits regarding the local oscillator strength and coarse graining of time, we obtain

$$\begin{aligned}&1 - (c^\dagger c + a^\dagger a)\Delta t + (q_{P1} - q_{M1})J_1 + (q_{P2} - q_{M2})J_2 \\ &\quad = 1 - (c^\dagger c + a^\dagger a)\Delta t + \frac{(q_{P1} - q_{M1})}{\mathcal{E}_{\rm lo}}(c + a) + \frac{(q_{P2} - q_{M2})}{\mathcal{E}_{\rm lo}}(c - a),\end{aligned} \tag{5.9}$$

for the terms inside the square brackets of Eq. (5.8). Again, the terms of higher order in the jump operators disappear; one way to think of this is that the coarse

graining was taken such that only one jump of the source (not the local oscillator) occurs within Δt, and such that two jumps, J_1 and J_2, do not occur within the same time interval. We now follow exactly the same steps as we did towards the end of Chapter 3: write the q's as a mean plus fluctuations, put them into Eq. (5.9) and put the corresponding result into Eq. (5.8). Doing that gives us the *stochastic Schrödinger equation for the teleportation protocol*:

$$d|\tilde{\tilde{\psi}}_{REC}\rangle = \left\{-(c^\dagger c + a^\dagger a)dt + (dq_x - i dq_y)c + (dq_x + i dq_y)a\right\}|\tilde{\tilde{\psi}}_{REC}\rangle, \quad (5.10)$$

with

$$dq_x = \left(\langle c^\dagger + c\rangle_{REC} + \langle a^\dagger + a\rangle_{REC}\right)dt + dW_x, \quad (5.11a)$$

$$dq_y = i\left(\langle c^\dagger - c\rangle_{REC} - \langle a^\dagger - a\rangle_{REC}\right)dt + dW_y. \quad (5.11b)$$

$\theta = 0$ and $\theta = \pi/2$ has been put in for dq_x and dq_y, respectively – cf. Eq. (3.93). The expectation values denoted $\langle\ \rangle_{REC}$ are to be taken with the normalized conditional state; the i in Eq. (5.11b) comes from $\exp(i\pi/2) = i$, and dW_x and dW_y are two independent Gaussian random numbers. $|\tilde{\tilde{\psi}}_{REC}\rangle$ is an unnormalized conditional state similar to the one given in Eq. (3.91), but the detail is not important; we will evolve the unnormalized state, normalizing only to find the expectation values. The only change the different normalization makes is that we cannot write

$$P_{(REC)} = \langle\tilde{\tilde{\psi}}_{REC}|\tilde{\tilde{\psi}}_{REC}\rangle, \quad (5.12)$$

which has no direct consequence for us, since we are not directly interested in this quantity. Later on, we will be interested in finding the probability distribution of Alice's measurement records Q_x and Q_y, but there again, it is not this quantity we are interested in. The probability given above does not give the probability distribution of Alice's measurement results, since there is likely to be more than one trajectory that leads to the same values of Q_x and Q_y; we will find the probability by going over many trajectories.

5.2.2 Numerical simulation

The simplest way to solve Eq. (5.10) is to use numerical simulation, implementing the Monte-Carlo technique. First, we choose a small time step dt, and then evolve the conditional state through a series of discrete time steps using Eq. (5.10). At each

step we have to generate two Gaussian random numbers, dW_x and dW_y, with mean zero and variance dt. To generate the random numbers, an algorithm from Ref. [51] was used, which generates pseudo-random (rather than truly random) numbers. It is believed that this pseudo-randomness does not change our results; the belief is supported by the fact that the probability distributions from the simulations match those from the analytically calculated distributions. See Section 6.3.

Quantum states are represented in the Fock state basis, an obvious choice given that our input state is a Fock state. The initial states consist of the input Fock state and the two-mode squeezed state. The Fock state representation of the two-mode squeezed state is given by

$$|\psi_{\rm EPR}\rangle = \frac{1}{\cosh(r)} \sum_{n=0}^{\infty} (-1)^n \tanh^n(r) |n,n\rangle, \tag{5.13}$$

where, as mentioned earlier, r is the squeezing parameter of the squeezed beams that constitute the EPR state. A higher squeezing value means better correlation, or entanglement, as can be seen from Eq. (4.8).

Since Eq. (5.13) specifies an infinite series, we need to truncate the series at some point. The truncation was made such that the last term of the series is less than one thousandth of the first term for any given value of r. For a good squeezing value, say $r \approx 2$,[5] about 200 terms are needed in the series, and since there are two modes we will need 200×200 matrix for keeping the coefficients, which, to give the total number of storage spaces we need, has to be further multiplied by the number of photons in the input Fock state. However, for a small value of squeezing, e.g. $r = 0.7$ (about 50% noise reduction), only 15 terms are needed, making the simulation quite efficient. A time step $dt = 0.001$ was chosen going through $10,000$ steps, which means the total time of evolution is ten, providing ten cavity lifetimes for each trajectory – remember, $\kappa = 1$. All the simulations are done with Visual Fortran. The code is provided in Appendix F.1.

Displacement in simulation

In the simulations, the displacement was made by calculating the matrix elements of the displacement operator, and then doing the matrix multiplication with the output state before displacement. An iterative method, which is suitable for computers, was used to calculate the matrix element. The method is described here.

[5] For this value $\exp(-r) \approx 0.13$, meaning about 90% noise reduction in a selected quadrature.

First, note that

$$\langle m|D(\alpha)|0\rangle = \langle m|\alpha\rangle = \exp\left(-\frac{|\alpha|^2}{2}\right)\frac{\alpha^m}{\sqrt{m!}}, \tag{5.14a}$$

and consequently,

$$\langle 0|D(\alpha)|n\rangle = \langle n|D^\dagger(\alpha)|0\rangle^* = \exp\left(-\frac{|\alpha|^2}{2}\right)\frac{(-\alpha^*)^n}{\sqrt{n!}}, \tag{5.14b}$$

where we have used $D^\dagger(\alpha) = D(-\alpha)$. We will now derive relationships that will allow us to calculate $\langle m|D(\alpha)|n\rangle$ given $\langle m-1|D(\alpha)|n-1\rangle$ and $\langle m|D(\alpha)|n-1\rangle$ or $\langle m-1|D(\alpha)|n\rangle$. The first one is

$$\begin{aligned}\langle m|D(\alpha)|n\rangle &= \langle m|D(\alpha)\frac{a^\dagger}{\sqrt{n}}|n-1\rangle,\\ &= \frac{1}{\sqrt{n}}\langle m|(a^\dagger-\alpha^*)D(\alpha)|n-1\rangle,\\ &= \frac{1}{\sqrt{n}}(\sqrt{m}\langle m-1|D(\alpha)|n-1\rangle - \alpha^*\langle m|D(\alpha)|n-1\rangle),\end{aligned} \tag{5.15a}$$

and the second one is, similarly,

$$\begin{aligned}\langle m|D(\alpha)|n\rangle &= \langle m-1|\frac{a}{\sqrt{m}}D(\alpha)|n\rangle,\\ &= \frac{1}{\sqrt{m}}(\sqrt{n}\langle m-1|D(\alpha)|n-1\rangle + \alpha\langle m-1|D(\alpha)|n\rangle).\end{aligned} \tag{5.15b}$$

Combining Eqs. (5.14) and Eqs. (5.15), we can iteratively build up the matrix representation of the displacement operator. For example, we can calculate $\langle m|D(\alpha)|1\rangle$ and $\langle 1|D(\alpha)|n\rangle$ by first using Eqs. (5.15) to obtain

$$\begin{aligned}\langle m|D(\alpha)|1\rangle &= \sqrt{m}\langle m-1|D(\alpha)|0\rangle - \alpha^*\langle m|D(\alpha)|0\rangle,\\ \langle 1|D(\alpha)|n\rangle &= \sqrt{n}\langle 0|D(\alpha)|n-1\rangle + \alpha\langle 0|D(\alpha)|n\rangle,\end{aligned}$$

then substitute Eqs. (5.14) into the above equation to calculate the matrix elements. Once we finish this, we can repeat the procedure to find the matrix elements $\langle m|D(\alpha)|2\rangle$ and $\langle 2|D(\alpha)|n\rangle$, which can in turn be used to calculate the next matrix elements. This process is continued until we obtain all the matrix elements we require. The code was checked by looking at the Wigner distribution of a given state before and after the displacement, using the fact that the Wigner function of

a displaced state (displaced by α) is the same as the Wigner function of the state without displacement shifted by $\alpha = x + ip$.

Wigner function plots

Once a displaced output state is calculated, the state is written out in the form of a density operator, and then passed out in an ASCII text format. This density operator (or the matrix elements of it) is then read by another program written in Fortran, which produces the Wigner functions that can be plotted by a plotting program such as ORIGIN. The original Wigner-plotting code was provided by Howard Carmichael, which only needed a minor touch. The full working to get the expression for the Wigner function in terms of ρ_{nm}, the matrix representation of the density operator ρ, is quite cumbersome, forcing us to give only a brief sketch.

The characteristic function can be written as

$$\begin{aligned}\chi_s &= \mathrm{tr}\left[\rho \exp\left(iz^* a^\dagger + iza\right)\right], \\ &= \exp\left(-\frac{1}{2}|z|^2\right) \sum_{k=0}^{N} \sum_{n,m=0}^{N} \rho_{nm} c_{kn}(z) c^*_{km}(-z), \end{aligned} \tag{5.16}$$

where

$$\begin{aligned} c_{kn}(z) &\equiv \langle k| \exp\left(iza\right) |n\rangle, \\ &= (iz)^{n-k} \sqrt{\frac{n!}{k!}} \frac{1}{(n-k)!}, \qquad\qquad n \geq k. \end{aligned}$$

Here, N is the upper limit of the Fock state basis. When the above equation is put into the definition of the Wigner distribution [Eq. (2.42)], we find that we have to solve integrals of the type

$$I_{pq} = \int d^2 z \exp\left(-\frac{1}{2}|z|^2\right) (iz)^p (iz^*)^q e^{-iz^*\alpha^* - iz\alpha}. \tag{5.17}$$

The solution of this integral plus Eq. (5.16) and Eq. (2.42) gives, after a lot of

rearranging,

$$W(\alpha,\alpha^*) = \frac{2}{\pi}e^{-2|\alpha|^2}\left[\sum_{n=0}^{N}\rho_{nn}\sum_{l=0}^{n}(-1)^{n-l}\frac{n!|2\alpha|^{2l}}{(n-l)!(l!)^2} + \sum_{n=0}^{N}\sum_{m=0}^{n-1}\rho_{nm}\sum_{l=0}^{m}(-1)^{m-l}\frac{n!m!}{(n-m+l)!l!(m-l)!}2Re\left((2\alpha^*)^{n-m+l}(2\alpha)^l\right)\right]. \tag{5.18}$$

The fact that the density operators are Hermitian, i.e., $\rho_{nm} = \rho^*_{mn}$, was used to derive this result. The computer program `wigplot` which calculates this function numerically, is given in Appendix F.2.

5.3 Analytical methods

5.3.1 Wigner function analysis

In Section 4.3 we have seen that the output Wigner distribution is given by

$$W_{\rm out}(\alpha_b) = 4NG_\nu(\alpha_b)\int d^2\alpha_c W_{\rm in}(\alpha_c)G_\tau\left(Q_x + iQ_y + \tanh(2r)\alpha_b - \alpha_c\right), \tag{5.19}$$

where $\nu = \cosh(2r)/2$, $\tau = 1/2\cosh(2r)$, and

$$G_\sigma(\alpha) = \frac{1}{\pi\sigma}\exp\left(\frac{-|\alpha|^2}{\sigma}\right). \tag{5.20}$$

This can be expanded to give

$$W_{\rm out}(x_b,p_b) = N\frac{8}{\pi^2}\int dx_c dp_c W_{\rm in}(x_c,p_c)\exp\left[-\frac{2(x_b^2+p_b^2)}{\cosh(2r)}\right] \times\exp\left[-2\cosh(2r)(Q_x + x_b\tanh(2r) - x_c)^2\right] \times\exp\left[-2\cosh(2r)(Q_y + p_b\tanh(2r) - p_c)^2\right]. \tag{5.21}$$

Our objective is to solve the integrals in Eq. (5.21) for a Fock state input, which has the Wigner function (see, for example Barnett [52], p. 120.)

$$W_{\rm in}(x_c,p_c) = \frac{2}{\pi}\frac{1}{l!}\exp\left[-2(x_c^2+p_c^2)\right]\sum_{k=0}^{l}(-1)^{l-k}\frac{l!}{k!(l-k)!}\frac{l!}{k!}4^k(x_c^2+p_c^2)^k, \tag{5.22}$$

where l is the number of photons in the Fock state. Thus, we are required to solve an integral of the type

$$\begin{aligned} K(n) = \int dx_c dp_c (x_c^2 + p_c^2)^n \exp\left[-2(x_c^2 + p_c^2)\right] \\ \times \exp\left[-2\cosh(2r)(Q_x + x_b \tanh(2r) - x_c)^2\right] \\ \times \exp\left[-2\cosh(2r)(Q_y + p_b \tanh(2r) - p_c)^2\right]. \end{aligned} \tag{5.23}$$

$K(n)$ is worked out in Appendix B, and shown to be equal to

$$K(n) = \left(\frac{-1}{2}\right)^n \frac{\pi}{2} \frac{(-1)^n n!}{(1+A)^{n+1}} \exp\left(-\frac{2AB^2}{1+A}\right) L_n\left(-\frac{2A^2B^2}{1+A}\right), \tag{5.24}$$

where $A = \cosh(2r)$, $B^2 = (Q_x + x_b \tanh(2r))^2 + (Q_y + p_b \tanh(2r))^2$, and L_n is the Laguerre polynomial [53]. Combining Eq. (5.21) – Eq. (5.24), we obtain

$$\begin{aligned} W_{\text{out}}(x_b, p_b) = N \exp\left[-\frac{2(x_b^2 + p_b^2)}{A}\right] \exp\left[-\frac{2AB^2}{A+1}\right] \\ \times \sum_{k=0}^{l} (-1)^{l-k} \frac{l!}{k!(l-k)!} \frac{2^k}{(1+A)^{k+1}} L_k\left(-\frac{2A^2B^2}{1+A}\right) \end{aligned} \tag{5.25}$$

This is our final result, the output Wigner function for an l-photon Fock state input. From this equation we can work out the single-shot output results, which will be compared with the results from the simulations in the next chapter.

5.3.2 Solving the stochastic Schrödinger equation

In this subsection we solve the stochastic Schrödinger equation [Eq. (5.10)]

$$d|\tilde{\tilde{\psi}}_{REC}(t)\rangle = \left\{-(c^\dagger c + a^\dagger a)dt + (dq_x - i dq_y)c + (dq_x + i dq_y)a\right\} |\tilde{\tilde{\psi}}_{REC}(t)\rangle, \tag{5.26}$$

with

$$Q_x(t) = \int_0^t e^{-t'} dq'_x, \tag{5.27a}$$

$$Q_y(t) = \int_0^t e^{-t'} dq'_y. \tag{5.27b}$$

The primes in dq_x' and dq_y' is to remind us that dq_x and dq_y depends on t and the t must be primed for the integration. To solve the SSE we first define a new ket $|\chi\rangle$ such that

$$|\tilde{\tilde{\psi}}_{REC}(t)\rangle = \exp\left[-(c^\dagger c + a^\dagger a)t\right]|\chi(t)\rangle, \tag{5.28}$$

with which we can rewrite Eq. (5.26) as

$$\begin{aligned} &d|\chi(t)\rangle \\ &= \exp\left[(c^\dagger c + a^\dagger a)t\right]\left[(dq_x - idq_y)c + (dq_x + idq_y)a\right]\exp\left[-(c^\dagger c + a^\dagger a)t\right]|\chi(t)\rangle, \\ &= \left[(dq_x - idq_y)ce^{-t} + (dq_x + idq_y)ae^{-t}\right]|\chi(t)\rangle, \\ &= \left[d\tilde{Q}^* c + d\tilde{Q}a\right]|\chi(t)\rangle, \end{aligned} \tag{5.29}$$

where $d\tilde{Q} = \exp(-t)(dq_x + idq_y)$. Caution is required in solving this equation; since $d\tilde{Q}$ is a stochastic quantity, Eq. (5.29) does not obey the rules of ordinary calculus. Specifically, $d\tilde{Q}$ contains a Wiener increment dW [Eqs. (5.11)], so we cannot ignore $(d\tilde{Q})^2$ as we would do normally. Keeping this in mind, it is not too difficult to see that Eq. (5.29) has the solution (Appendix E)

$$\begin{aligned} |\chi(t)\rangle &= \exp\left(-2ac\int_0^t dt' e^{-2t'} + \tilde{Q}a + \tilde{Q}^* c\right)|\chi(0)\rangle, \\ &= \exp\left[ac(e^{-2t} - 1) + \tilde{Q}a + \tilde{Q}^* c\right]|\chi(0)\rangle. \end{aligned} \tag{5.30}$$

A quick way to see this is by taking the differential of $|\chi(t)\rangle$ and noting that, following the Ito rule, $d\tilde{Q}d\tilde{Q}^* = 2\exp(-2t)dt$ and $d\tilde{Q}d\tilde{Q} = d\tilde{Q}^* d\tilde{Q}^* = 0$. The final solution to Eq. (5.26) is then given by

$$|\tilde{\tilde{\psi}}_{REC}(t)\rangle = \exp\left[-(c^\dagger c + a^\dagger a)t\right]\exp\left[ac(e^{-2t} - 1) + \tilde{Q}a + \tilde{Q}^* c\right]|\tilde{\tilde{\psi}}_{REC}(0)\rangle. \tag{5.31}$$

The output state before displacement is given by the state described in the above equation in the limit of a long time, i.e.,

$$\begin{aligned} |\text{out}\rangle &= N|0_a, 0_c\rangle\langle 0_a, 0_c|\exp(-ac + \tilde{Q}a + \tilde{Q}^* c)|\tilde{\tilde{\psi}}_{REC}(0)\rangle, \\ &= N|0_a, 0_c\rangle\langle 0_a, 0_c|\exp(-ac + \tilde{Q}a + \tilde{Q}^* c)|\psi(0)\rangle, \end{aligned} \tag{5.32}$$

where we have used the fact that[6]

$$\lim_{t\to\infty} \exp\left[-(c^\dagger c + a^\dagger a)t\right] = |0_a, 0_c\rangle\langle 0_a, 0_c|, \tag{5.33}$$

where $|0_a, 0_c\rangle$ is the vacuum state of the modes a and c. N in Eq. (5.32) is a normalization factor, such that $\langle \text{out}|\text{out}\rangle = 1$.

For a general input state

$$|\text{in}\rangle = \sum_{n=0}^{\infty} c_n |n\rangle, \tag{5.34}$$

we have

$$\begin{aligned} |\psi(0)\rangle &= |\text{in}\rangle \otimes |\text{TMSS}\rangle \\ &= \frac{1}{\cosh(r)} \sum_{m,n=0}^{\infty} c_m (-1)^n \tanh^n(r) |m\rangle \otimes |n, n\rangle. \end{aligned} \tag{5.35}$$

Then Eq. (5.32) becomes

$$|\text{out}\rangle = \frac{N}{\cosh(r)} \sum_{m,n=0}^{\infty} c_m (-1)^n \tanh^n(r) \langle 0_a, 0_c| \exp(-ac + \tilde{Q}a + \tilde{Q}^* c)|m, n, n\rangle, \tag{5.36}$$

where we have not written down the vacuum states for modes a and c. From now on the output state refers to the state of mode b only. The above equation is our final solution of Eq. (5.26), the state at Bob's location before he makes the displacement.

Special case, $Q_x = Q_y = 0$

Our next aim is to show the connection between Eq. (5.36) and the Wigner representation of the output state (before displacement). However, before we move on, there is one interesting result we can easily see: if the input state is a number state, $|m\rangle$, and $Q_x = Q_y = 0$, the teleportation is perfect. We will prove this now.

[6]This result can be shown easily by thinking about the operator acting on an arbitrary state expanded in number states.

In this special case, Eq. (5.36) becomes

$$|\text{out}\rangle = \frac{N}{\cosh(r)} \sum_{n=0}^{\infty} (-1)^n \tanh^n(r) \langle 0_a, 0_c| \exp(-ac) |m, n, n\rangle, \tag{5.37}$$

from which (noting that $\langle 0_a, 0_c| \exp(-ac)|m, n\rangle = (-1)^m \delta_{mn}$) we get

$$|\text{out}\rangle = \frac{N}{\cosh(r)} \tanh^m(r)|m\rangle = N'|m\rangle, \tag{5.38}$$

where N' is a new normalization constant. Equation (5.38) is saying that, for Fock state teleportation, whenever Alice obtains $Q_x = Q_y = 0$, Bob gets the input Fock state.[7] Note that this result only holds true for Fock state teleportation (it works for a Fock state input, since the EPR state has a perfect correlation in photon numbers). Similar results do not hold true for other input states, as can easily be seen from the working.

5.3.3 Equivalence between the simulation and the Wigner analysis

Now we show the equivalence between the stochastic Schrödinger equation (simulation), and the Wigner function analysis. This will be done by comparing the characteristic functions from Eq. (5.36) and Eq. (5.19).

Characteristic function from the solution of the stochastic Schrödinger equation

We first recast Eq. (5.36) into a form that is easier to compare with the Wigner method. Noting that

$$\langle 0| = \langle 0| e^{-\tilde{Q}c^\dagger}, \tag{5.39}$$

we can rewrite Eq. (5.36) as

$$|\text{out}\rangle = N \sum_{m,n=0}^{\infty} c_m s_n(r) \langle 0_a, 0_c| \exp(-\tilde{Q}c^\dagger) \exp(-ac + \tilde{Q}a + \tilde{Q}^* c)|m, n, n\rangle, \tag{5.40}$$

[7] Note that in this case, Bob's displacement is exactly zero.

where

$$s_n(r) = \frac{(-1)^n \tanh^n(r)}{\cosh(r)}. \tag{5.41}$$

Now, using the Baker-Hausdorff theorem [31], we can see that

$$\exp(-\tilde{Q}c^\dagger)\exp(-ac) = \exp(-ac)\exp(-\tilde{Q}c^\dagger)\exp(-\tilde{Q}a). \tag{5.42}$$

Putting this into Eq. (5.40) we obtain

$$\begin{aligned} |\text{out}\rangle &= N\sum_{m,n=0}^{\infty} c_m s_n(r)\langle 0_a, 0_c|\exp(-ac)\exp(-\tilde{Q}c^\dagger)\exp(\tilde{Q}^* c)|m,n,n\rangle, \\ &= N'\sum_{m,n=0}^{\infty} c_m s_n(r)\langle 0_a, 0_c|\exp(-ac)D_c(-\tilde{Q})|m,n,n\rangle, \end{aligned} \tag{5.43}$$

where $N' = N\exp(|\tilde{Q}|^2/2)$, and $D_c(-\tilde{Q})$ is the displacement operator for the mode c. Defining $|\text{in} - \tilde{Q}\rangle \equiv D_c(-\tilde{Q})|\text{in}\rangle = D_c(-\tilde{Q})\sum_{m=0}^{\infty} c_m|m\rangle$, we can rewrite the above equation as

$$|\text{out}\rangle = N'\sum_{n=0}^{\infty} s_n(r)\langle 0_a, 0_c|\exp(-ac)|\text{in} - \tilde{Q}, n, n\rangle. \tag{5.44}$$

We can expand $|\text{in} - \tilde{Q}\rangle$ in terms of number states, $|\text{in} - \tilde{Q}\rangle = \sum_{m=0}^{\infty} d_m|m\rangle$, giving

$$\begin{aligned} |\text{out}\rangle &= N'\sum_{m,n=0}^{\infty} s_n(r)d_m\langle 0_a, 0_c|\exp(-ac)|m,n,n\rangle, \\ &= N'\sum_{m=0}^{\infty}(-1)^m s_m(r)d_m|m\rangle. \end{aligned} \tag{5.45}$$

Note that as $r \to \infty$, $(-1)^m s_m(r)$ becomes constant, i.e., it does not depend on m,[8] which means that $|\text{out}\rangle = \sum_{m=0}^{\infty} d_m|m\rangle$, i.e., it becomes the displaced input state. Thus, in the limit of infinite squeezing, which means maximum degree of entanglement, teleportation is perfect as we expect.

We now find an expression for the characteristic function of the output state described in Eq. (5.45), so we can compare it to the characteristic function of the output state obtained from the Wigner function analysis. The characteristic function

[8] $\tanh(r) \to 1$, so $(-1)^m s_m(r) \to 1/\cosh(r)$.

of this state is[9]

$$\chi_{\rm out}(z,z^*) = \langle {\rm out}|e^{ibz+ib^\dagger z^*}|{\rm out}\rangle, \\ = \sum_{m,n=0}^{\infty}(-1)^{m+n}[s_n(r)c_n]^*[s_m(r)c_m]\langle n|e^{ibz+ib^\dagger z^*}|m\rangle. \tag{5.46}$$

Using real variables rather than complex variables, it can be written as

$$\chi_{\rm out}(u,v) = \sum_{m,n=0}^{\infty}(-1)^{m+n}[s_n(r)c_n]^*[s_m(r)c_m]\langle n|e^{iu(b+b^\dagger)-v(b-b^\dagger)}|m\rangle, \tag{5.47}$$

where we have used $z = u + iv$.

5.3.4 Characteristic function from the output Wigner distribution

Our objective now is to manipulate

$$W_{\rm out}(x_2,p_2) = N\int dx_e dp_d W_{\rm in}\left(\frac{1}{\sqrt{2}}(q_x+x_e),\frac{1}{\sqrt{2}}(p_d+q_y)\right) \\ \times W_{\rm EPR}\left(\frac{1}{\sqrt{2}}(q_x-x_e),\frac{1}{\sqrt{2}}(p_d-q_y)\right) \tag{5.48}$$

into the form that has the same characteristic function as the one in Eq. (5.47). To this end, we first rewrite Eq. (5.48) so that it shows the characteristic function explicitly. Using the definitions of the Wigner distribution [Eq. (2.42)] and the characteristic function [Eq. (2.43)], we have

$$W_{\rm out}(x_2,p_2) = \frac{N}{\pi^4}\int dx_e dp_d du dv\ \chi_{\rm in}(u_c,v_c)\chi_{\rm EPR}(u_a,v_a,u_b,v_b) \\ \times \exp\left\{-\sqrt{2}i\left[u_c\left(q_x+x_e\right)-v_c\left(p_d+q_y\right)\right]\right\} \\ \times \exp\left\{-\sqrt{2}i\left[u_a\left(q_x-x_e\right)-v_a\left(p_d-q_y\right)\right]-2i(u_b x_b - v_b p_b)\right\}, \tag{5.49}$$

where $\int dudv$ refers to the integration over all three modes (a,b, and c) of u and v. Integrating over the variables x_e and p_d, we obtain delta functions $\delta(u_c - u_a)$ and

[9] Note that we have the subscript 'out', instead of s [Eq. (2.43)], where s refers to symmetric ordering. There are other characteristic functions for normal and anti-normal ordering – see, for example, Walls [13] p. 62. The subscript out refers to the (output) state.

$\delta(v_c + v_a)$. Further integration over the variables u_c and v_c leaves us with

$$W_{\text{out}}(x_2, p_2) = \frac{2N}{\pi^2} \int du_a du_b dv_a dv_b \chi_{\text{in}}(u_a, -v_a) \chi_{\text{EPR}}(u_a, v_a, u_b, v_b) \times \exp\left[-2\sqrt{2}i\left(q_x u_a + q_y v_a\right)\right] \exp\left[-2i(u_b x_b - v_b p_b)\right]. \quad (5.50)$$

Now all we have to do is prove that

$$\chi_{\text{out}}(u_b, v_b) \propto \int du_a dv_a \chi_{\text{in}}(u_a, -v_a) \chi_{\text{EPR}}(u_a, v_a, u_b, v_b) \exp\left[-2\sqrt{2}i\left(q_x u_a + q_y v_a\right)\right]. \quad (5.51)$$

First, note that (see Appendix D.4),

$$\chi_{\text{in}}(u_a, -v_a) \exp\left[-2\sqrt{2}i\left(q_x u_a + q_y v_a\right)\right] = \chi_{\text{in}-\sqrt{2}\tilde{q}}(u_a, -v_a), \quad (5.52)$$

where

$$\chi_{\text{in}-\sqrt{2}\tilde{q}}(u_a, -v_a) = \langle \text{in} - \sqrt{2}\tilde{q} | e^{iu_a(a+a^\dagger) + v_a(a-a^\dagger)} | \text{in} - \sqrt{2}\tilde{q} \rangle. \quad (5.53)$$

Rewriting Eq. (5.53) using Eq. (5.6) gives

$$\chi_{\text{in}-\tilde{Q}}(u_a, -v_a) = \langle \text{in} - \tilde{Q} | e^{iu(a+a^\dagger) + v(a-a^\dagger)} | \text{in} - \tilde{Q} \rangle. \quad (5.54)$$

Then, Eq. (5.51) becomes

$$\chi_{\text{out}}(u, v) \propto \int du_a dv_a \chi_{\text{in}-\tilde{Q}}(u_a, -v_a) \chi_{\text{EPR}}(u_a, v_a, u_b, v_b). \quad (5.55)$$

We now expand $\chi_{\text{EPR}}(u_a, v_a, u_b, v_b)$ and rewrite it in a different form:

$$\begin{aligned}
&\chi_{\text{EPR}}(u_a, v_a, u_b, v_b) \\
&\quad = \sum_{m,n=0}^{\infty} s_n(r)^* s_m(r) \langle n, n | e^{iu_a(a+a^\dagger) + iu_b(b+b^\dagger) - v_a(a-a^\dagger) - v_b(b-b^\dagger)} | m, m \rangle, \\
&\quad = \sum_{k,l,m,n=0}^{\infty} s_n(r)^* s_m(r) \delta_{n,k} \delta_{m,l} \langle n_a | e^{iu_a(a+a^\dagger) - v_a(a-a^\dagger)} | m_a \rangle \\
&\qquad\qquad \times \langle k_b | e^{iu_b(b+b^\dagger) - v_b(b-b^\dagger)} | l_b \rangle, \\
&\quad = \sum_{k,l=0}^{\infty} \chi_{\text{EPRa}}(u_a, v_a) \chi_{\text{EPRb}}(u_b, v_b), \quad (5.56)
\end{aligned}$$

where

$$\chi_{\mathrm{EPRa}}(u_a, v_a) = \sum_{m,n=0}^{\infty} s_n(r)^* \delta_{n,k} s_m(r) \delta_{m,l} \langle n_a | e^{iu_a(a+a^\dagger) - v_a(a-a^\dagger)} | m_a \rangle, \tag{5.57a}$$

and

$$\chi_{\mathrm{EPRb}}(u_b, v_b) = \langle k_b | e^{iu_b(b+b^\dagger) - v_b(b-b^\dagger)} | l_b \rangle. \tag{5.57b}$$

We also need to use a relation (see Appendix D.2)

$$\chi_\psi(u, -v) = \chi_{\psi'}(u, v), \tag{5.58}$$

where if $|\psi\rangle = \sum_{m=0}^{\infty} c_m |m\rangle$, $|\psi'\rangle = \sum_{m=0}^{\infty} c_m^* |m\rangle$. And another relation (see Appendix D.3)

$$\chi_\psi(u, v) = \chi_{\psi_*}(-u, -v), \tag{5.59}$$

where $|\psi_*\rangle = \sum_{m=0}^{\infty} (-1)^m c_m |m\rangle$. Combining the expansion $|\mathrm{in} - \tilde{Q}\rangle = \sum_{m=0}^{\infty} d_m |m\rangle$ and Eq. (5.55) – Eq. (5.59), we obtain

$$\chi_{\mathrm{out}}(u, v) \propto \sum_{k,l=0}^{\infty} \int du_a dv_a \chi_{\mathrm{in}-\tilde{Q}'_*}(-u_a, -v_a) \chi_{\mathrm{EPRa}}(u_a, v_a) \chi_{\mathrm{EPRb}}(u_b, v_b), \tag{5.60}$$

where $\mathrm{in} - \tilde{Q}'_*$ refers to the state

$$|\mathrm{in} - \tilde{Q}'_*\rangle = \sum_{m=0}^{\infty} (-1)^m d_m^* |m\rangle. \tag{5.61}$$

Finally, from the result (see Appendix D.1)

$$\int du dv \chi_\psi(-u, -v) \chi_\phi(u, v) = |\langle \psi | \phi \rangle|^2, \tag{5.62}$$

we see that Eq. (5.60) becomes

$$\begin{aligned}
&\chi_{\text{out}}(u,v) \\
&\quad \propto \sum_{k,l=0}^{\infty} \sum_{m,n=0}^{\infty} (-1)^{m+n} [\delta_{n,k} d_n s_n(r)]^* [\delta_{m,l} d_m s_m(r)] \langle k_b | e^{iu_b(b+b^\dagger) - v_b(b-b^\dagger)} | l_b \rangle, \\
&\quad \propto \sum_{m,n=0}^{\infty} (-1)^{m+n} [d_n s_n(r)]^* [d_m s_m(r)] \langle n_b | e^{iu_b(b+b^\dagger) - v_b(b-b^\dagger)} | m_b \rangle
\end{aligned} \tag{5.63}$$

where $s_m(r)$ is given by Eq. (5.41). Apart from normalization, which is irrelevant since the Wigner distribution has an overall normalization factor, this equation matches exactly with Eq. (5.47), thus proving that the stochastic Schrödinger equation and the Wigner function analysis are equivalent to one another.

Chapter 6

Fock state teleportation: results

Using the methods of Chapter 5, we will present various results for the teleportation of Fock states. Three qualitative features will be shown: (1) the single-shot output, (2) the fidelity, and (3) the probability distribution of Alice's measurement results. Numerical and analytical results will be shown and compared.

All the results in this chapter are in the interaction picture, since all the results from Chapter 5 are in the interaction picture. The free Hamiltonian terms are just the free evolution term, so the interaction picture is equivalent to working in a rotating frame. This has the effect of rotating the Wigner function around the W, or z, axis; thus when we look at the Wigner function of the output state in the interaction picture, we are looking at the still-shot picture of a rotating graph.

6.1 Single-shot output states

Figure 6.2 shows examples of the output Wigner distribution for a one-photon Fock state input obtained from the simulations. The output states are single-shot results, i.e., the states at Bob's location after a single run of the teleportation protocol. For comparison, the Wigner function of a one-photon Fock state input is given in Figure 6.1. The three graphs in Figure 6.2 show the Wigner functions of the output states for different squeezing parameters, for $r = 0.1$, $r = 0.7$ and $r = 2.0$. Q_x and Q_y refer to Alice's measurement results; these numbers are given because the output states depend on them. The n_{max} refers to the truncation number that was used to represent the two-mode squeezed state. It increases rapidly as the squeezing parameter increases; $r = 2$ requires $n_{max} = 190$, whereas only $n_{max} = 20$ is required for $r = 0.7$.

Figure 6.3 shows the analytical results corresponding to the simulation results shown in Figure 6.2. Comparing these results to those from the simulation shows good agreement for $r = 0.1$ and $r = 0.7$ case, whereas the $r = 2.0$ case shows discrepancy. The discrepancy is a little bit misleading because in this particular example the analytical and numerical results differ only by a rotation, which is not a general feature; by comparing other single-shot results for $r = 2.0$, it was checked that discrepancies take different forms for different runs. One possible reason for this difference could be the numerical error due to the truncation, because the truncation error is larger for a higher value of r.

The Wigner distributions clearly show that, as the squeezing parameter is increased, the quality of the teleportation also increases. This is just what we had expected, since the quality of entanglement increases as the squeezing parameter is increased. In fact, it can be shown that the von Neumann entropy [54] (the standard measure of entanglement for pure states [55]) for a two-mode squeezed state is given by [56]

$$E_{TMSS} = \cosh^2(r)\log_2[\cosh^2(r)] - \sinh^2(r)\log_2[\sinh^2(r)]. \tag{6.1}$$

E_{TMSS} is an increasing function of r since $\cosh(r)$ is always greater than $\sinh(r)$, which means that the entropy (the degree of entanglement) is an increasing function of r.

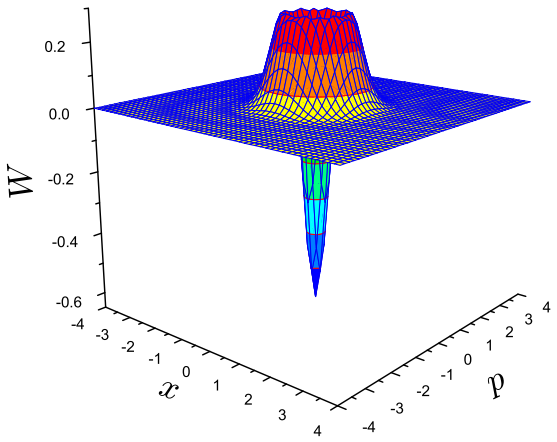

Figure 6.1: Wigner representation of a one-photon Fock state.

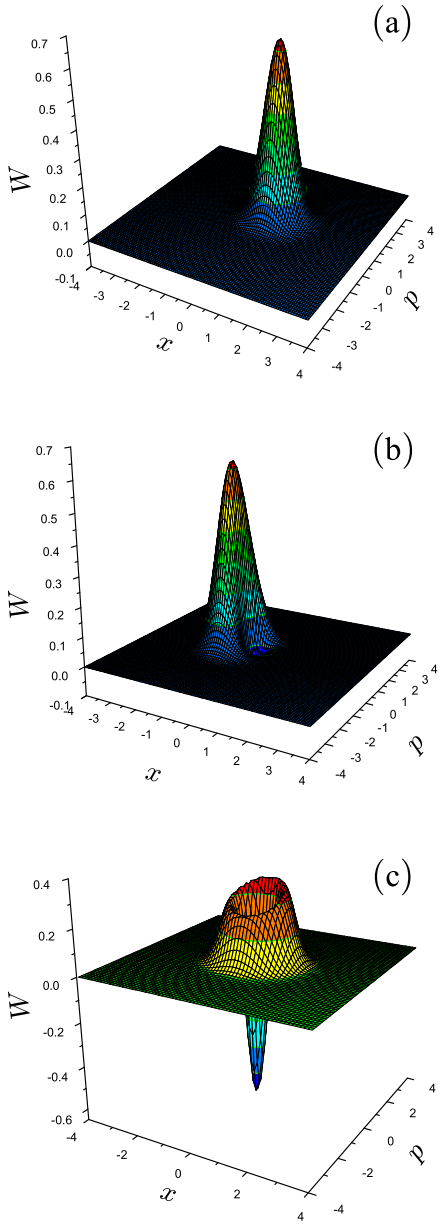

Figure 6.2: Single-shot results of a one-photon Fock state input obtained from numerical simulations, for (a) $r = 0.1$, $Q_x = 0.5$, $Q_y = 0.46$ and $n_{max} = 10$. (b) $r = 0.7$, $Q_x = -1.55$, $Q_y = 0.41$ and $n_{max} = 20$. (c) $r = 2.0$, $Q_x = 1.37$, $Q_y = 1.50$ and $n_{max} = 190$.

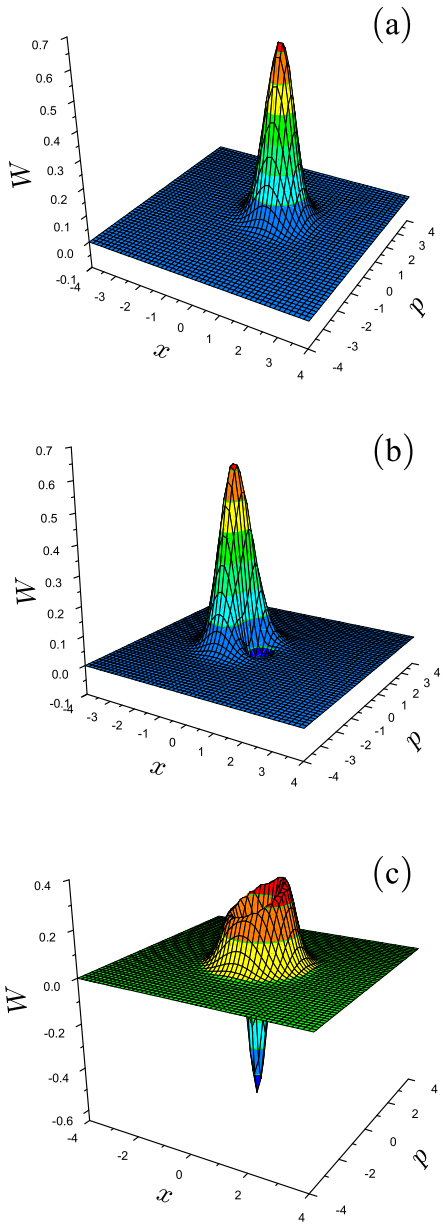

Figure 6.3: Single-shot results of a one-photon Fock state input obtained from the analytical expression, for (a) $r = 0.1$, $Q_x = 0.5$, $Q_y = 0.46$. (b) $r = 0.7$, $Q_x = -1.55$, $Q_y = 0.41$. (c) $r = 2.0$, $Q_x = 1.37$, $Q_y = 1.50$.

6.2 Fidelity

Definition and methods of calculation

Fidelity is a measure of how closely the output state mimics the input state. For pure states $F = |\langle\psi_{\rm in}|\psi_{\rm out}\rangle|^2$ is a natural candidate for fidelity. F is the probability that the output state passes an experimental test of being the same as the input state, where the test is carried out by a third party – usually called Victor for verifier – who knows the input state. The fidelity defined by F also has some intuitively satisfying properties: if the input state is the same as the output state the fidelity is 1, if they are orthogonal the fidelity is 0; the output state is completely different to the input state, in the sense that there exists a measurement that can distinguish one state from the other.

In the simulations it is very easy to calculate the fidelities for Fock state inputs, since we are in the Fock state basis. Once we obtain an output state described by $|{\rm out}\rangle = \sum c_n|n\rangle$, we simply calculate $|c_m|^2$ to get the fidelity for the input state $|m\rangle$. In the Wigner distribution analysis we use the fact that the overlap integral of Wigner distributions gives the trace of the product of the corresponding density operators [Eq. (D.4)], i.e.,

$$\mathrm{tr}\,(\hat{\rho}_{\rm in}\hat{\rho}_{\rm out}) = \frac{1}{\pi}\int d^2\alpha W_{\rm in}(\alpha,\alpha^*)W_{\rm out}(\alpha,\alpha^*). \tag{6.2}$$

From the $W_{\rm out}$ obtained in the previous chapter and Eq. (6.2) we can work out the analytical expression of a conditional fidelity distribution, $F(Q_x, Q_y)$, for a given input state. Here, by conditional fidelity we mean the fidelity for given values of Q_x and Q_y. Rather than carrying out the calculation analytically, we do a numerical integration, using Eq. (5.25) to work out $W_{\rm out}$.

In quantum teleportation the output states, and hence the fidelities, depend on Alice's results Q_x and Q_y. In fact, for a Fock state input, it turns out that the fidelity depends only on $\mathrm{q} = \sqrt{Q_x^2 + Q_y^2}$, because the phase information cannot change the result for a phase-independent input state. Figure 6.4 shows the simulated conditional fidelity distribution for a one-photon Fock state input with $r = 0.7$. The simulation result was obtained by running $200,000$ trajectories, computing the conditional fidelities at each run. To collect the data, bins are created for both Q_x and Q_y ranging from -4 to 4 with spacing $dq = 0.05$, and at the end of each run the conditional fidelity is recorded in the appropriate bin according to the values of Q_x and Q_y obtained for the run. If the value of either Q_x and/or Q_y lies outside

the range, the data is discarded.

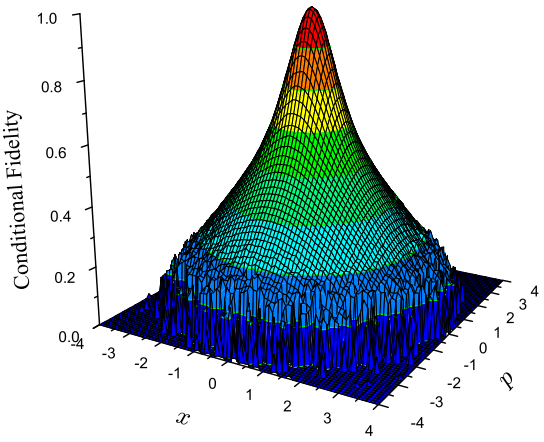

Figure 6.4: Conditional fidelity distribution for a one-photon Fock state input and $r = 0.7$. 200,000 trajectories.

Radial conditional fidelity distribution

We see that the fidelity depends only on the radial distance of Q_x and Q_y from the origin. Thus, we introduce $\mathrm{q} = \sqrt{Q_x^2 + Q_y^2}$ and compute the *radial* conditional fidelity distribution. The results are shown in Figures 6.5, 6.6, and 6.7 for various input Fock states.

The simulation data is collected in a similar manner to that described earlier, changing the bin to depend on q rather than Q_x and Q_y, with $d\mathrm{q} = 0.005$ and range 0 – 5. An analytical calculation is also carried out in the manner described above, but we change to the radial coordinate system with $dQ_x dQ_y \rightarrow 2\pi \mathrm{q} d\mathrm{q}$. This has the consequence that the radial distribution is given by $\mathrm{q}F(\mathrm{q})$, not $F(\mathrm{q})$, where $F(\mathrm{q})$ is obtained from $F(Q_x, Q_y)$ using $\mathrm{q} = \sqrt{Q_x^2 + Q_y^2}$.

Analytical and numerical results are shown on separate axes for visibility. For the vacuum and a one-photon Fock state input the two results agree very well with each other, whereas for a two-photon Fock state input there are discrepancies. Graphs showing the analytical and numerical results on the same plot are shown in Figure 6.8 and Figure 6.9. The results for the vacuum input are not given but they agree very well, as in the case of the one-photon Fock state input shown in Figure 6.8.

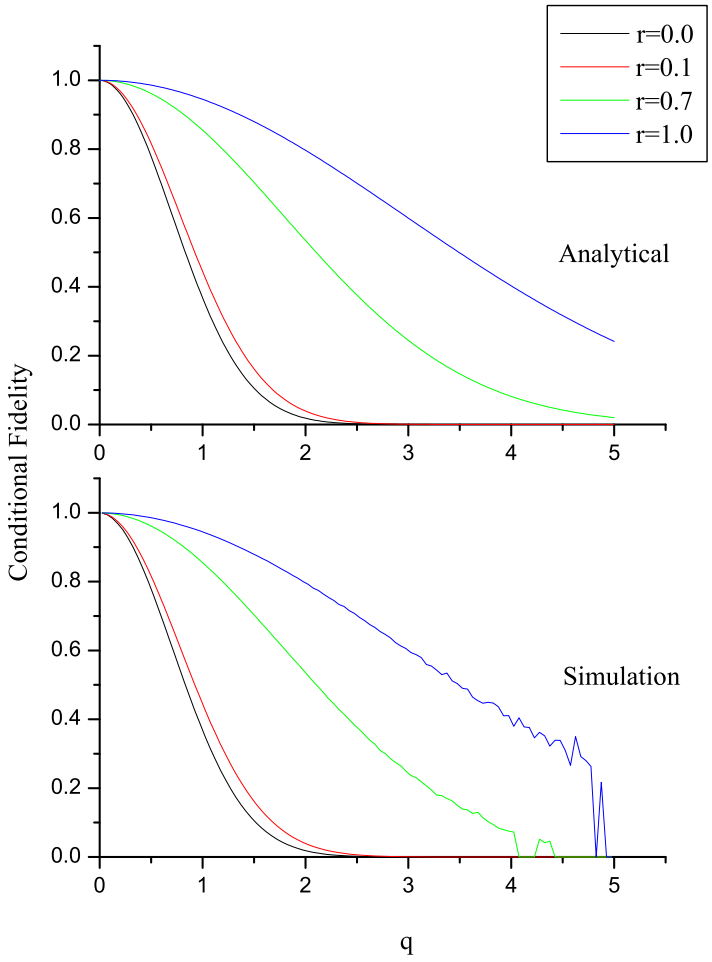

Figure 6.5: Radial conditional fidelity distribution for the vacuum state input. 100,000 trajectories.

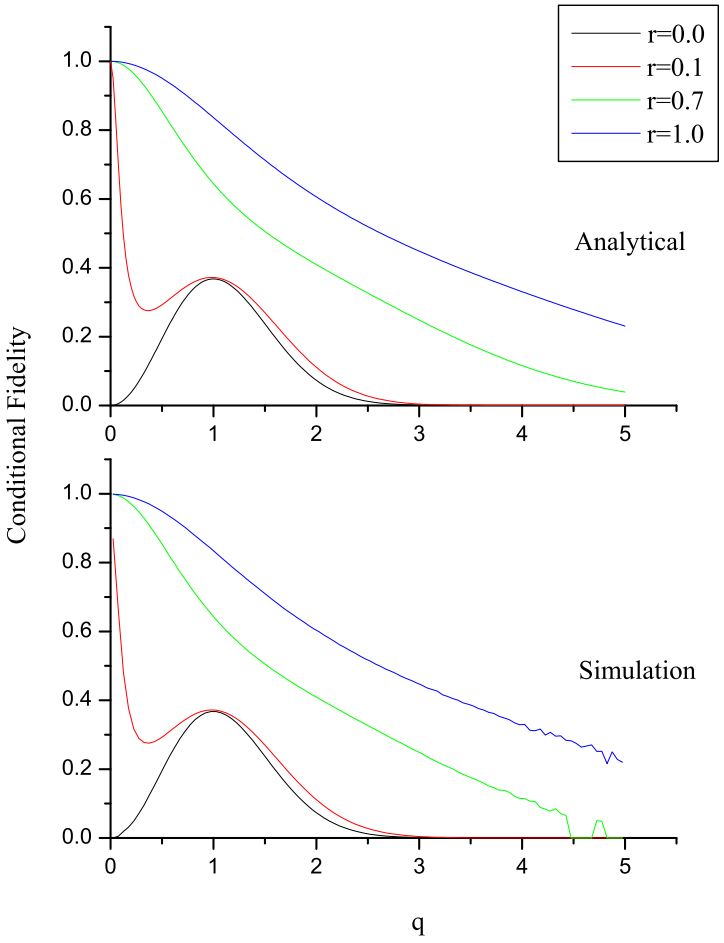

Figure 6.6: Radial conditional fidelity distributions for a one-photon Fock state input. 100,000 trajectories.

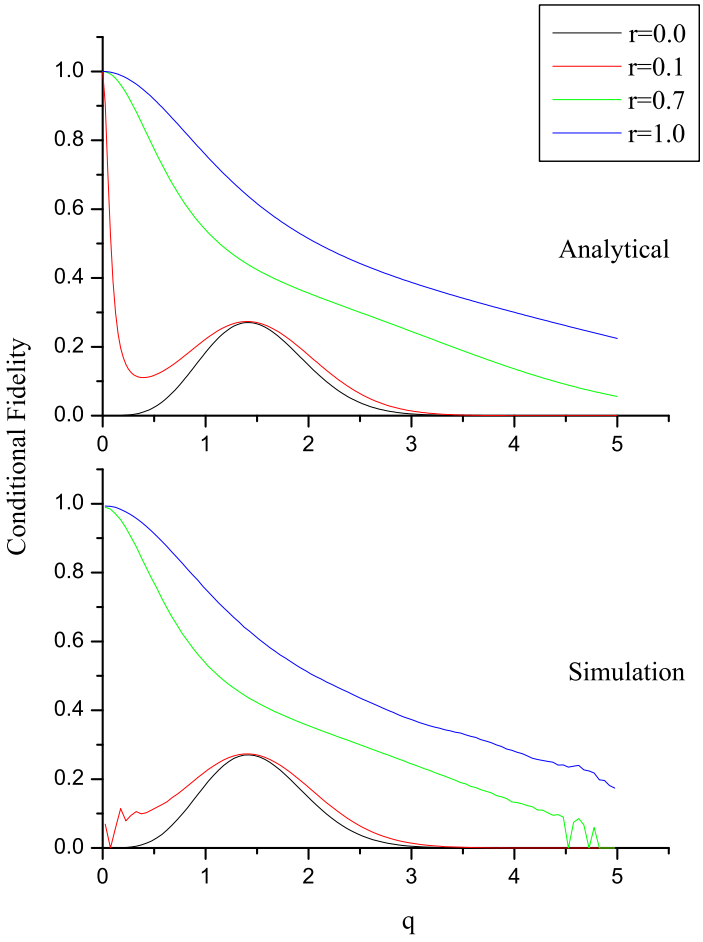

Figure 6.7: Radial conditional fidelity distributions for a two-photon Fock state input. 100,000 trajectories.

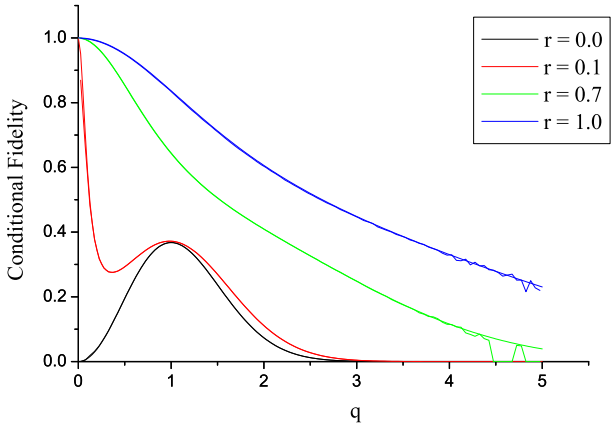

Figure 6.8: Radial conditional fidelity distributions for a one-photon Fock state input. Overlap of the simulation and analytical results. 100,000 trajectories.

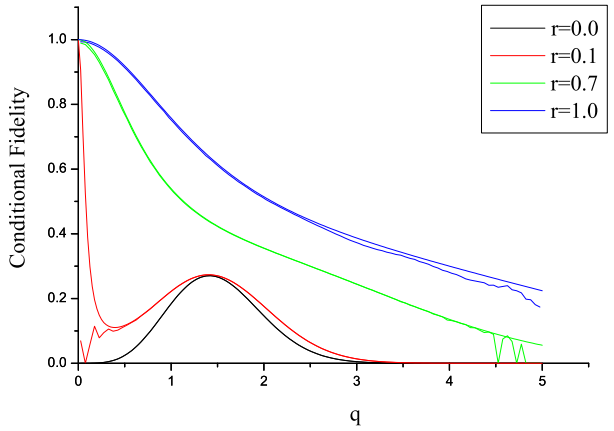

Figure 6.9: Radial conditional fidelity distributions for a two-photon Fock state input. Overlap of the simulation and analytical results. 100,000 trajectories.

The discrepancies for the vacuum and one-photon cases are due to the lack of simulation data, resulting in fluctuations or noise in the data. A sudden drop of fidelity to zero occurs because no data was obtained for that particular value of q. Looking at Figure 6.9, there is a clear difference between the numerical and analytical results, which is not due to the sampling noise; the simulation result for $r = 0.1$ goes down for small q, but the analytical result goes up steeply. Also the $r = 1.0$ case shows visible differences. These discrepancies must be due to numerical errors, since we have shown already that the stochastic Schrödinger equation agrees exactly with the expression obtained from the Wigner function analysis (for the conditional output states).

As it was said earlier, we are working in the interaction picture or a rotating frame. Does this affect the fidelity? The answer is 'NO'. This is because the input field as well as the output field oscillates in the Schrödinger picture, and so the input and the output oscillates at the same frequency. In experiments, the frequency of the local oscillator field is made to be the same as that of the input field, which essentially introduces the transformation to the rotating frame.

Analyzing the fidelity curves

A close look at Figures 6.5, 6.6 and 6.7 shows us a few interesting features. In the following discussion we accept that the simulation results are supposed to be identical to the analytical results and any discrepancies arise from factors such as the lack of simulation data (fluctuations), and numerical errors.

One thing we note immediately is that for a nonzero squeezing parameter teleportation is perfect, i.e., the fidelity is unity, if q = 0. This is true even if the squeezing parameter is very small, so that Alice's share of the EPR state is almost the vacuum state. Apart from this discontinuity the conditional fidelity curves seem to gradually expand from the $r = 0$ case as r is increased. The discontinuity stems from the fact that we are looking at the *conditional* fidelity, the fidelity between the input and the output once a particular measurement result is obtained. The information missing here is the probability of obtaining a particular measurement result. Indeed, if we look at the 'average fidelity' for a given q, defined as a product of the probability (of obtaining the q) and the conditional fidelity, there is no discontinuity; the probability of obtaining q = 0 decreases with r (see the next section). Going back to the conditional fidelity distribution, if $r \ll 1$, the fidelity curve is almost identical to the $r = 0$ case except near q= 0, where the measured result forces the

output state to be the same as the input Fock state.

Note that for the vacuum input there is no discontinuity. This is because if $r = 0$ the EPR state is two uncorrelated vacuum states; whatever Alice does, Bob always has a vacuum state. This is the classical limit of teleportation, in which no entanglement exists and the whole procedure reduces down to measurements of the x and p quadratures of the input state followed by the displacement, determined from the measured values, of the vacuum state. Anyway, the implication is that if the input state is in the vacuum state, the $r = \mathrm{q} = 0$ case gives perfect teleportation unlike the other input states.

We can also see that increasing r results in a higher conditional fidelity for a given input state. Furthermore, the conditional fidelities for higher r are always greater than those for lower r at every value of q. Intuitively, this makes sense, since a bigger value of r means a higher degree of entanglement, as discussed at the start of this chapter.

Another fact worth noting is that as the number of photons in the input state is increased, the conditional fidelity curves get narrower, meaning that the range of q for good teleportation decreases. A heuristic argument supporting this fact can be given as follows. To teleport a Fock state with a given number of photons, we require an approximately equal number of photons at Bob's location; but a large number of photons means a high value of r for the EPR state, and thus, we need a higher value of r to teleport a higher numbered Fock state.

The final fact we mention is the shift of the $r = 0$ and $r = 0.1$ curves in Figure 6.6 and Figure 6.7. This feature is easily seen by analyzing the $r = 0$ case. For $r = 0$ the output states are simply displaced vacuum states, displaced by $Q_x + iQ_y$; then, as the input photon number gets higher, we need a larger displacement to obtain a higher fidelity.

6.3 Probability distributions of Q_x and Q_y

The probability distributions of Q_x and Q_y tell us the likelihood of obtaining certain values of Q_x and Q_y. Figure 6.10 shows the probability distribution for a one-photon Fock state input with r=0.7, obtained from 200,000 trajectories. Note that the distribution is very noisy, and to get a better distribution we need to run a lot more trajectories. Looking at the radial probability distribution (using the cylindrical symmetry of the distribution) would help reduce the noisy fluctuations – since it is equivalent to averaging the distribution below over the circumference of a circle with a given radius – so we will work with radial probability distributions in this section.

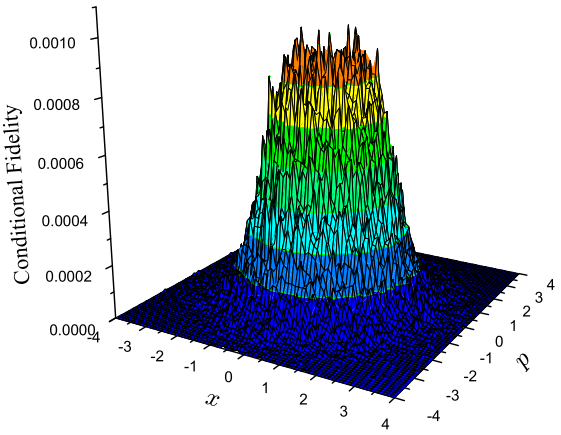

Figure 6.10: Probability distribution of Alice's measurements for a one-photon Fock state input and $r = 0.7$. 200,000 trajectories.

In the simulations all we have to do is add unity in the appropriate bin of q on each run, which can be done in the same way as we did when we extracted the conditional fidelity from the simulations. Analytically, the calculation is done with the Wigner function, which is equivalent to treating Alice's measurement scheme as an ideal measurement of x_d, p_e [9]. To find the probability distribution we proceed in a similar way to when we worked out W_{out} in Chapter 5. This time, however, we have to integrate out x_b and p_b, since the measurement results of Alice do not depend on what happens to Bob's field.[1] We could just integrate over W_{out}, but it

[1]This is because Alice's measurements are local measurements.

is easier to integrate over x_b and p_b first. Integrating $W_{\rm EPR}$ over the variables x_b and p_b, we obtain the Gaussian distribution

$$\frac{2}{\pi\cosh(2r)}\exp\left[\frac{-2(x_a^2+p_a^2)}{\cosh(2r)}\right].$$

Thus, the probability distribution is given by

$$\begin{aligned}P(x_d,p_e) = \frac{2}{\pi\cosh(2r)}\int dp_d dx_e W_{\rm in}\left(\frac{1}{\sqrt{2}}(x_d+x_e),\frac{1}{\sqrt{2}}(p_d+p_e)\right)\\ \times\exp\left[\frac{-(x_d-x_e)^2-(p_d-p_e)^2}{\cosh(2r)}\right],\end{aligned} \tag{6.3}$$

which, for a Fock state input [see Eq. (5.22)], becomes

$$\begin{aligned}P(q_x,q_y) = \frac{4}{\pi^2\cosh(2r)}\sum_{k=0}^{l}(-1)^{l-k}\binom{l}{k}\frac{1}{k!}2^k\int dxdp\left[(q_x+x)^2+(p+q_y)^2\right]^k\\ \times\exp\left\{-(q_x+x)^2-(p+q_y)^2-\frac{1}{\cosh(2r)}\left[(q_x-x)^2+(p-q_y)^2\right]\right\},\end{aligned} \tag{6.4}$$

where we have substituted q_x and q_y for x_d and p_e, respectively. This integral can be solved by a change of variables, $x' = x+q_x$, $p' = p+q_y$, which gives

$$\begin{aligned}P(q_x,q_y) = \frac{4}{\pi^2\cosh(2r)}\sum_{k=0}^{l}(-1)^{l-k}\binom{l}{k}\frac{1}{k!}2^k\int dx'dp'\left(x'^2+p'^2\right)^k\\ \times\exp\left\{-x'^2-p'^2-\frac{1}{\cosh(2r)}\left[(2q_x-x')^2+(2q_y-p')^2\right]\right\}.\end{aligned} \tag{6.5}$$

Looking at Eq. (B.1) and Eq. (B.3), we can see that this integral is equal to $K(k,1/2)$ with $\lambda = 1/2, B_x = 2q_x, B_p = 2q_y$ and $A = 1/2\cosh(2r)$. Using the result from Appendix B, we obtain

$$\begin{aligned}P(q_x,q_y) &= \frac{4}{\pi^2\cosh(2r)}\sum_{k=0}^{l}(-1)^{l-k}\binom{l}{k}\frac{1}{k!}2^k K(k,1/2),\\ &= \frac{4}{\pi^2\cosh(2r)}\sum_{k=0}^{l}(-1)^{l-k}\binom{l}{k}\frac{1}{k!}2^k\pi k!\left(\frac{\cosh(2r)}{1+\cosh(2r)}\right)^{k+1}\\ &\quad\times\exp\left[\frac{-4(q_x^2+q_y^2)}{1+\cosh(2r)}\right]L_k\left(\frac{-4(q_x^2+q_y^2)}{\cosh(2r)(1+\cosh(2r))}\right),\end{aligned} \tag{6.6}$$

$$= \frac{4}{\pi\,(1+\cosh(2r))} \exp\left[\frac{-4(q_x^2+q_y^2)}{(1+\cosh(2r))}\right] \sum_{k=0}^{l} (-1)^{l-k} \binom{l}{k} \times \left(\frac{2\cosh(2r)}{1+\cosh(2r)}\right)^k L_k\left(\frac{-4(q_x^2+q_y^2)}{\cosh(2r)(1+\cosh(2r))}\right). \quad (6.7)$$

Finally, to compare with the probabilities obtained from the simulations, we note that $\sqrt{2}q_x = Q_x, \sqrt{2}q_y = Q_y$.

As we did for the conditional fidelity distributions, three plots are shown in Figures 6.12, 6.13: for the vacuum, a one-photon and a two-photon Fock state input. The analytical curves are obtained by plotting Eq. (6.7). Again, the analytical and simulation results are shown on different axes. The two results agree well with one another, this time even for the two-photon Fock state input. To show how well they agree with one another, Figure 6.11 is shown below, which shows the overlap of the simulation and the analytical curves on the same axis.

The figures on the next two pages show the probability distribution for different inputs and different squeezing parameters. They show the trend that as the input photon number, or the squeezing parameter, increases, the peak of the graph shifts towards higher q. This makes sense, since the value of q tells us the strength of the input field plus Alice's share of the EPR pair, and the photon number of the input state (or the squeezing parameter) is proportional to the strength of the input state (or Alice's share of the EPR pair). The shift means that the larger the input photon number (or r), the smaller the chance of getting q = 0, i.e., perfect teleportation.

Note that as r is increased, the probability distribution gets broader. This is because the average photon number in Alice's share of the EPR pair increases with increasing r, and consequently a broader range of q becomes accessible for Alice.

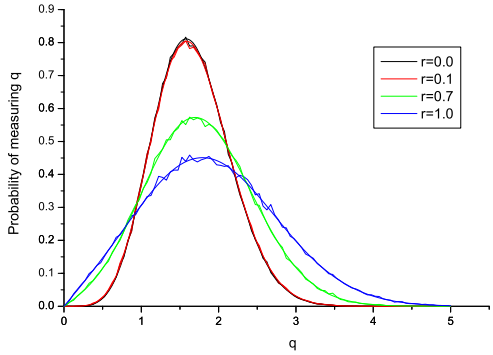

Figure 6.11: Radial probability distribution for a two-photon Fock state input and $r = 0.7$. Overlap of the simulation and analytical results. 200,000 trajectories.

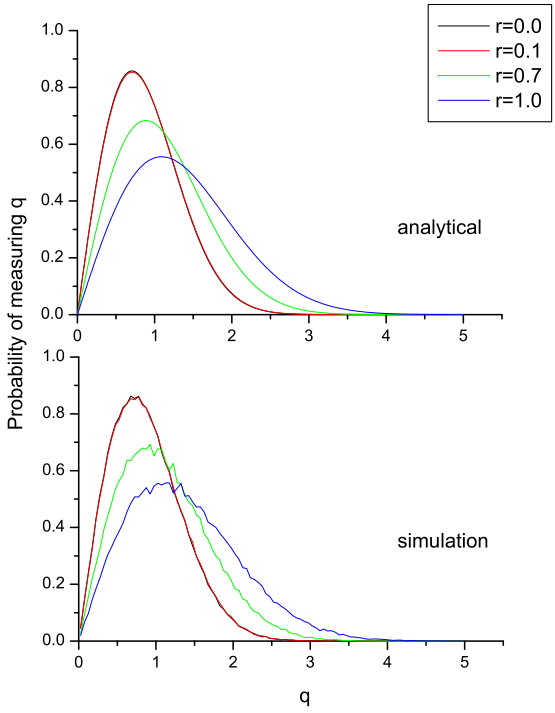

Figure 6.12: Radial probability distribution for the vacuum state input. 100,000 trajectories.

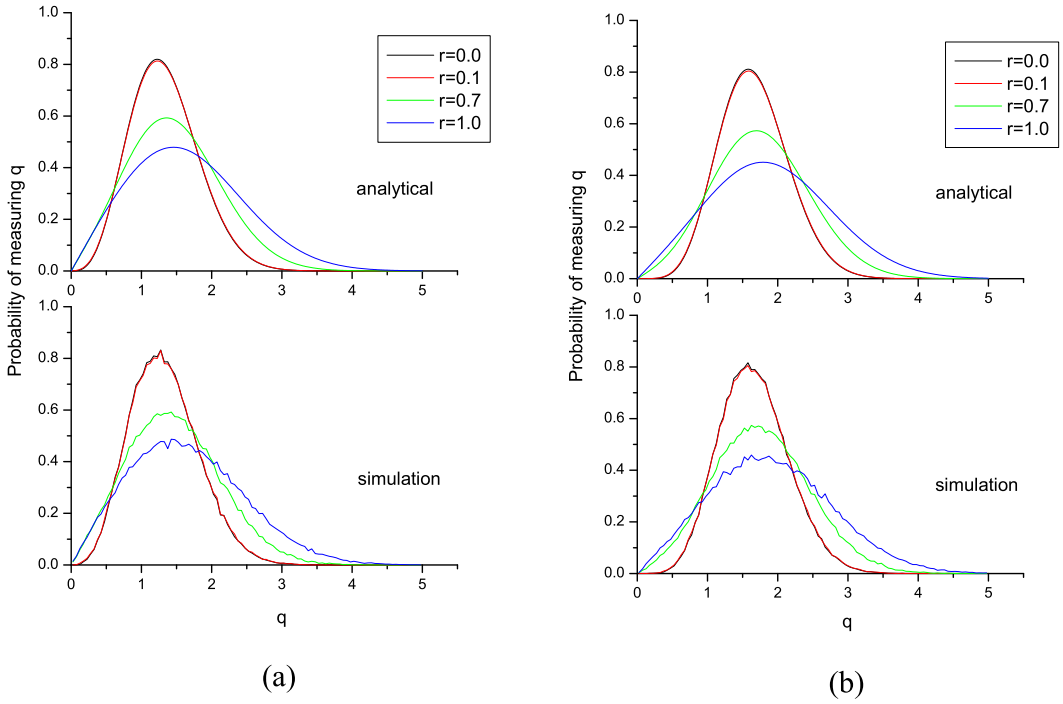

Figure 6.13: Radial probability distributions for: (a) a one-photon and (b) a two-photon Fock state input. 100,000 trajectories.

Chapter 7

Conclusion and future directions

7.1 Conclusion

In this thesis a single-mode continuous variable quantum teleportation protocol was introduced following the work of Braunstein and Kimble [9]. A quantum trajectory treatment of the protocol was developed, yielding a stochastic Schrödinger equation (SSE). Numerical simulation was used to solve the SSE, studying teleportation of Fock state inputs extensively. An analytical expression for the conditional output state, conditioned on the measurement results of Alice, was derived from the SSE, but an analytical expression for the probability distribution of Alice's measurements has not been found.

Also, as in the proposal of Braunstein and Kimble, Wigner functions were used to find analytical expressions for the conditional output state and the probability distribution of Alice's measurement results. The conditional output state thus found was shown to be equivalent to the conditional output state obtained from the SSE. This fact was proved for an arbitrary input state.

The Wigner representation of the conditional output state was used to give a visualization of the states. A few chosen single-shot results were shown, calculated both numerically and analytically, demonstrating clearly that as the squeezing parameter increases the quality of the teleportation also increases. The fidelity was introduced as a measure of the quality of teleportation, and the conditional fidelities (the fidelity between the input and the conditional output) for the Fock state inputs were investigated.

The study of Fock state teleportation revealed that the teleportation protocol behaves as we expected: as the squeezing parameter is increased (meaning higher

degree of entanglement for the EPR pair), the conditional fidelity increases. One unexpected property of the Fock state teleportation was that for any non-zero r, $Q_x = Q_y = 0$ always gives perfect teleportation. This fact was proved analytically, and the proof shows clearly that the property is unique to Fock state inputs; it is the perfect correlation in photon numbers of the EPR state that causes this effect.

The above property seemed strange, because it meant that even for very small r, for which the situation is almost identical to $r = 0$, there is a prominent difference in the conditional fidelity curve; a spike near q= 0. This discontinuity was found to have come from the fact that we are looking at the *conditional* fidelities, the fidelity *given* the measurement record was obtained. The key point here is that it is very unlikely to get q $\approx$ 0, and when we look at the 'average fidelity', the conditional fidelity multiplied by the probability density, there is no discontinuity.

The probability distributions of Alice's measurement results for the input Fock states were shown and analyzed. An analytical expression for the probability distribution was found from the Wigner function method given by Braunstein and Kimble and shown to agree with the simulation results. No proof has been given, however, that the expression found from the Wigner function method is equivalent to the SSE.

Our investigation showed that quantum trajectory theory gives the same answer as the Wigner function analysis for this protocol and either could be used to analyze it. We have concentrated on the single-shot quantities such as single-shot output states or conditional fidelities and obtained some specific results for Fock state teleportation.

7.2 Future directions

Improvements can be made to the simulation program. It was shown that the conditional output state obtained from the simulation does not match the analytical result for a two-photon Fock state input. We think the discrepancy arises from the numerical error and probably gets bigger for higher photon Fock state inputs and superposition states that contain them. Thus, to use the computer simulation for other states, the source of error has to be found first. Also the efficiency of the simulation program should be increased before it can be used to run a large number of trajectories for higher photon Fock state inputs or a large value of r, which requires a large number of basis states.

Another interesting thing is to prove the equivalence between the SSE and the Wigner analysis completely by calculating the probability distribution from the SSE. A similar proof is given by Howard Carmichael for the heterodyne detection scheme [34], in which case the probability distribution is equal to the Q function [17].

The effect of nonideal detectors could be studied, although in this case quantum trajectory theory cannot describe the evolution of a pure state and we must resort to density operators, which requires higher computational power. Nonideal detectors can be modeled by introducing beam splitters before the ideal detectors, as described in Braunstein and Kimble. These authors studied teleportation of an ensemble of coherent state superpositions in the nonideal case, but no single-shot results were calculated. A study of the teleportation of other non-classical fields (such as Fock states) in the nonideal case could be carried out.

Appendix A

Evaluation of Eq. (3.26)

We want to prove that

$$\int_0^\infty d\tau \exp[-i(\omega-\omega_0)\tau] = \pi\delta(\omega-\omega_0) + i\frac{P}{\omega_0-\omega}. \tag{A.1}$$

To prove it, we start from

$$\int_0^t d\tau \exp[-i(\omega-\omega_0)\tau] = \frac{\sin[(\omega-\omega_0)t]}{\omega-\omega_0} - i\frac{1-\cos[(\omega-\omega_0)t]}{\omega-\omega_0}, \tag{A.2}$$

and take the limit $t \to \infty$. We now consider a slowly varying function $f(\omega)$ and anticipate an integration with respect to ω over the product of this function and the above expression, i.e., we want to evaluate

$$\int_0^\infty d\omega f(\omega) \int_0^t d\tau \exp[-i(\omega-\omega_0)\tau], \tag{A.3}$$

in the limit $t \to \infty$. Then, from Eq. (A.2), we obtain two integrals. The first one is

$$\lim_{t\to\infty} \int_0^\infty d\omega f(\omega) \frac{\sin[(\omega-\omega_0)t]}{\omega-\omega_0}. \tag{A.4}$$

Note that in the limit $t \to \infty$, the sine function is oscillating rapidly, so unless $\omega = \omega_0$ the integral is very small. Thus, the slowly varying function $f(\omega)$ only contributes

near $\omega = \omega_0$, allowing us to take it out of the integration, i.e.,

$$\begin{aligned}\lim_{t\to\infty}\int_0^\infty d\omega f(\omega)\frac{\sin[(\omega-\omega_0)t]}{\omega-\omega_0} &= f(\omega_0)\lim_{t\to\infty}\int_0^\infty d\omega\frac{\sin[(\omega-\omega_0)t]}{\omega-\omega_0},\\ &= \pi f(\omega_0),\\ &= \int_0^\infty d\omega\pi\delta(\omega-\omega_0)f(\omega). \end{aligned} \tag{A.5}$$

The second line follows from evaluating the integral; the calculation can be found in Arfken and Weber [57] (see page 425)

The second integral we want to solve is

$$\begin{aligned}&\lim_{t\to\infty}\int_0^\infty d\omega f(\omega)\frac{1-\cos[(\omega-\omega_0)t]}{\omega-\omega_0}\\ &\qquad= \int_0^\infty d\omega\frac{f(\omega)}{\omega-\omega_0} - \lim_{t\to\infty}\int_0^\infty d\omega\frac{f(\omega)\cos[(\omega-\omega_0)t]}{\omega-\omega_0}. \end{aligned} \tag{A.6}$$

Let us have a look at the second expression on the second line. In the limit $t \to \infty$ the cosine term oscillates rapidly, making the integral negligible unless $\omega = \omega_0$. When $\omega \to \omega_0$, the cosine term approaches unity, making the integral the same as the first one on the second line. So the effect of the second integral is to subtract the singularity in the first integral, which is exactly what the Cauchy principal value does [57]. So we can write

$$\lim_{t\to\infty}\int_0^\infty d\omega f(\omega)\frac{1-\cos[(\omega-\omega_0)t]}{\omega-\omega_0} = P\int_0^\infty d\omega\frac{f(\omega)}{\omega-\omega_0}, \tag{A.7}$$

where P denotes the Cauchy principal value. Combining Eq. (A.2), Eq. (A.5), and Eq. (A.7) we get

$$\int_0^\infty d\tau\exp[-i(\omega-\omega_0)\tau] = \pi\delta(\omega-\omega_0) + i\frac{P}{\omega_0-\omega}, \tag{A.8}$$

thus proving Eq. (A.1).

Appendix B

Working out $K(\lambda, 1)$

To prove Eq. (5.24), we introduce a shorthand notation:

$$F(\lambda) = \int dxdp \exp\left[-2\lambda(x^2+p^2)\right] \exp\left\{-2A[(B_{x'}-x)^2+(B_{p'}-p)^2]\right\}, \quad \text{(B.1)}$$

with which we can define $K(n,\lambda)$ as

$$K(n) \equiv K(n,1), \quad \text{(B.2)}$$

where [see Eq. (5.23) for the definition of $K(n)$]

$$K(n,\lambda) = \left(\frac{-1}{2}\right)^n \frac{d^n F}{d\lambda^n} \equiv \left(\frac{-1}{2}\right)^n F^{(n)}(\lambda). \quad \text{(B.3)}$$

Note that Eq. (B.2) is only true if we have

$$A = \cosh(2r), \quad \text{(B.4a)}$$
$$B_x = Q_x + x\tanh(2r), \quad \text{(B.4b)}$$
$$B_p = Q_p + p\tanh(2r). \quad \text{(B.4c)}$$

$F(\lambda)$ can easily be evaluated, giving

$$\begin{aligned} F(\lambda) &= \frac{\pi}{2}\frac{1}{\lambda+A}\exp\left(-2AB^2 + \frac{2A^2B^2}{\lambda+A}\right), \\ &= \frac{\pi}{2}\frac{1}{\lambda+A}\exp\left(-\frac{2\lambda AB^2}{A+\lambda}\right), \end{aligned} \quad \text{(B.5)}$$

where $B^2 = B_x^2 + B_p^2$. We will assume that the general result can be written in the form

$$F^{(n)}(\lambda) = \frac{\pi}{2}\frac{(-1)^n n!}{(\lambda + A)^{n+1}} \exp\left(-\frac{2\lambda A B^2}{A+\lambda}\right) g_n\left(\frac{2A^2B^2}{\lambda + A}\right), \tag{B.6}$$

and solve for g_n. To this end, note first that $F^{(n+1)}$ is the derivative of $F^{(n)}$ with respect to λ, i.e.,

$$\begin{aligned} F^{(n+1)} &= \frac{dF^{(n)}}{d\lambda}, \\ &= \frac{\pi}{2}\frac{(-1)^n n!}{(\lambda + A)^{n+1}} \exp\left(-\frac{2\lambda A B^2}{A+\lambda}\right) \left[g_n\left(\frac{2A^2B^2}{\lambda + A}\right) \right. \\ &\quad \left. + \frac{2A^2B^2}{(n+1)(\lambda + A)} g_n\left(\frac{2A^2B^2}{\lambda + A}\right) - \frac{(\lambda + A)}{(n+1)} \frac{dg_n\left(\frac{2A^2B^2}{\lambda + A}\right)}{d\lambda} \right]. \end{aligned}$$

But from Eq. (B.6), we also have

$$F^{(n+1)} = \frac{\pi}{2}\frac{(-1)^{n+1}(n+1)!}{(\lambda + A)^{n+2}} \exp\left(-\frac{2\lambda A B^2}{A+\lambda}\right) g_{n+1}\left(\frac{2A^2B^2}{\lambda + A}\right). \tag{B.7}$$

Comparing Eq. (B.7) and Eq. (B.7), we obtain a relationship

$$\begin{aligned} g_{n+1}\left(\frac{2A^2B^2}{\lambda + A}\right) &= g_n\left(\frac{2A^2B^2}{\lambda + A}\right) + \frac{2A^2B^2}{(n+1)(\lambda + A)} g_n\left(\frac{2A^2B^2}{\lambda + A}\right) \\ &\quad - \frac{(\lambda + A)}{(n+1)} \frac{dg_n\left(\frac{2A^2B^2}{\lambda + A}\right)}{d\lambda}, \end{aligned} \tag{B.8}$$

which can be written, through a change of variable, in the form

$$g_{n+1}(x) = g_n(x) + \frac{x}{(n+1)} g_n(x) + \frac{x}{(n+1)} \frac{dg_n(x)}{dx}. \tag{B.9}$$

We now use the relations (Abramowitz and Stegun [53] Eq. (22.8.6) and Eq. (22.7.12))

$$x\frac{dL_n(x)}{dx} = n(L_n(x) - L_{n-1}(x)), \tag{B.10a}$$

$$(n+1)L_{n+1}(x) = (2n + 1 - x)L_n(x) - nL_{n-1}(x), \tag{B.10b}$$

where L_n is the Laguerre polynomial with integer n. These relations can be combined

to eliminate $L_{n-1}(x)$, giving

$$x\frac{dL_n(x)}{dx} = -(n+1-x)L_n(x) + (n+1)L_{n+1}(x). \tag{B.11}$$

This equation is equivalent to

$$x\frac{dL_n(-x)}{dx} = -(n+1+x)L_n(-x) + (n+1)L_{n+1}(-x), \tag{B.12}$$

and thus, by comparing Eq. (B.12) to Eq. (B.9), we see that $g_n(x) = L_n(-x)$. Substituting $g_n(x) = L_n(-x)$ into Eq. (B.6), and then substituting the result into Eq. (B.3) we obtain

$$K(n,1) = \left(\frac{-1}{2}\right)^n \frac{\pi}{2}\frac{(-1)^n n!}{(1+A)^{n+1}} \exp\left(-\frac{2AB^2}{1+A}\right) L_n\left(-\frac{2A^2B^2}{1+A}\right). \tag{B.13}$$

Appendix C

Two-mode squeezed state

In general, two-photon devices such as the non-degenerate parametric amplifier can produce the non-classical effect called squeezing. For example, a two-mode squeezed state can be produced by a non-degenerate parametric amplifier; the single-mode squeezed state introduced in Chapter 2 is obtained in the degenerate case. The effect of squeezing can be represented by the squeezing operator [13, 58]. In this section, we derive the Wigner function for the two-mode squeezed state by using the squeezing operator.

C.1 Preliminary

First we solve a useful integral using matrix notation. The result will be useful in calculating the Wigner function of the two-mode squeezed state. The integral is

$$\int dxdy \, \exp\left(\eta\alpha^T - \frac{1}{2}\eta\Lambda\eta^T\right), \tag{C.1}$$

where $\eta = (x, y)$, $\alpha = (\alpha_1, \alpha_2)$, and Λ is any 2 by 2 matrix. x and y are real values, and T denotes the transpose. Now assume that Λ is diagonalizable, i.e.,

$$\Lambda = U\mathcal{D}U^T, \tag{C.2}$$

where U is a unitary matrix and $\mathcal{D}$ is a diagonal matrix. Let us define x' such that $\eta U = (x', y') = \eta'$ and similarly $\alpha U = \alpha'$. Substituting these into Eq. (C.1), we obtain

$$\int dx'dy' \, \exp\left(\eta'\alpha'^T - \frac{1}{2}\eta'\mathcal{D}\eta'^T\right), \tag{C.3}$$

where the Jacobian is unity because the transformation is unitary.

Using $\mathcal{D} = \begin{pmatrix} d_1 & 0 \\ 0 & d_2 \end{pmatrix}$, Eq. (C.3) becomes two independent integrals of x' and y', as written in the first line of Eq. (C.4). Provided that d_1 and d_2 are positive, the integrals converge:

$$\begin{aligned} \int dx' \exp\left(\alpha_1' x' + \frac{1}{2} d_1 x'^2\right) \int dy' \exp\left(\alpha_2' y' + \frac{1}{2} d_2 y'^2\right), \\ &= \frac{2\pi}{\sqrt{d_1 d_2}} \exp\left(\frac{1}{2} \alpha U \mathcal{D}^{-1} U^T \alpha\right), \\ &= \frac{2\pi}{\sqrt{d_1 d_2}} \exp\left(\frac{1}{2} \alpha \Lambda^{-1} \alpha^T\right). \end{aligned} \tag{C.4}$$

Thus, the solution of Eq. (C.1) can be written as

$$\int dx dy \exp\left(\eta \alpha^T - \frac{1}{2} \eta \Lambda \eta^T\right) = \frac{2\pi}{\sqrt{d_1 d_2}} \exp\left(\frac{1}{2} \alpha \Lambda^{-1} \alpha^T\right). \tag{C.5}$$

C.2 Wigner function for a two-mode squeezed vacuum

C.2.1 Two-mode squeezing operator

The unitary two-mode squeezing operator is defined as [Eq. (5.5)]

$$S_{TM}(r) = \exp\left[r(a_1 a_2 - a_1^\dagger a_2^\dagger)\right], \tag{C.6}$$

where a's are annihilation operators. Our two-mode squeezed vacuum state is then,

$$|\psi\rangle = S_{TM}(r)|0\rangle. \tag{C.7}$$

Before we work out the Wigner function for this state, it is useful to determine how a and $a^\dagger$ are transformed by this unitary operator. Denoting

$$a_1(r) = S_{TM}^\dagger(r) a_1 S_{TM}(r), \tag{C.8}$$

$$a_2(r) = S_{TM}^\dagger(r) a_2 S_{TM}(r), \tag{C.9}$$

we obtain the differential equation

$$\begin{aligned}\frac{d}{dr}a_1(r) &= S_{TM}^{\dagger}(r)[a_1^{\dagger}a_2^{\dagger} - a_1a_2, a_1]S_{TM}(r),\\ &= -S_{TM}^{\dagger}(r)a_2^{\dagger}S_{TM}(r) = -a_2^{\dagger}(r),\end{aligned} \tag{C.10a}$$

and similarly

$$\frac{d}{dr}a_2(r) = -a_1^{\dagger}(r), \tag{C.10b}$$

$$\frac{d}{dr}a_1^{\dagger}(r) = -a_2(r), \tag{C.10c}$$

$$\frac{d}{dr}a_2^{\dagger}(r) = -a_1(r). \tag{C.10d}$$

Solving these differentials equations, we get

$$a_1(r) = a_1\cosh(r) - a_2^{\dagger}\sinh(r), \tag{C.11a}$$

$$a_2(r) = a_2\cosh(r) - a_1^{\dagger}\sinh(r), \tag{C.11b}$$

and the complex conjugates of these equations.

C.2.2 Wigner function

The Wigner function for a two-mode field is defined as

$$\begin{aligned}W(\alpha_1,\alpha_2) = \frac{1}{\pi^4}\int d^2\alpha_1 d^2\alpha_2 \mathrm{tr}\left[\rho\exp\{i(z_1^*a_1^{\dagger} + z_1a_1 + z_2^*a_2^{\dagger} + z_2a_2)\}\right],\\ \times\exp\{-i(z_1^*\alpha_1^* + z_1\alpha_1 + z_2^*\alpha_2^* + z_2\alpha_2)\},\end{aligned} \tag{C.12}$$

which is just a straight forward generalization of the Wigner function for a single-mode field. Using $\rho = |\,\psi\rangle\langle\psi|$, where $|\,\psi\rangle$ is a two-mode squeezed vacuum state [Eq. (C.7)], the trace in the integral becomes

$$\langle 0,0|\exp\{i[z_1^*a_1^{\dagger}(r) + z_1a_1(r) + z_2^*a_2^{\dagger}(r) + z_2a_2(r)]\}|0,0\rangle. \tag{C.13}$$

Substituting in Eqs. (C.11) and rearranging the equation we get

$$\langle 0,0|\exp\{i[z_1^*(r)a_1^{\dagger} + z_1(r)a_1 + z_2^*(r)a_2^{\dagger} + z_2(r)a_2]\}|0,0\rangle, \tag{C.14}$$

where $z_1(r) = z_1\cosh(r) - z_2^*\sinh(r)$ and $z_2(r) = z_2\cosh(r) - z_1^*\sinh(r)$. Using the Baker-Hausdorff relation this expectation value can be written as

$$\langle 0,0|e^{iz_1^*(r)a_1^\dagger}e^{iz_1(r)a_1}e^{iz_2^*(r)a_2^\dagger}e^{iz_2(r)a_2}|0,0\rangle \exp\left[-\frac{1}{2}(|z_1(r)|^2+|z_2(r)|^2)\right], \\ = \exp\left[-\frac{1}{2}(|z_1(r)|^2+|z_2(r)|^2)\right]. \quad \text{(C.15)}$$

Substituting Eq. (C.15) into Eq. (C.12), we obtain

$$W(\alpha_1,\alpha_2) = \frac{1}{\pi^4}\int d^2\alpha_1 d^2\alpha_2 \exp\left[-\frac{1}{2}(|z_1(r)|^2+|z_2(r)|^2)\right] \\ \times \exp\left[-i(z_1^*\alpha_1^* + z_1\alpha_1 + z_2^*\alpha_2^* + z_2\alpha_2)\right]. \quad \text{(C.16)}$$

Now we write this integral in terms of $z_1 = x_1 + ip_1$ and $z_2 = x_2 + ip_2$:

$$|z_1(r)|^2+|z_2(r)|^2 = (|z_1|^2+|z_2|^2)\cosh(2r) - \sinh(2r)(z_1z_2 + z_1^*z_2^*), \\ = \cosh(2r)(x_1^2+x_2^2+p_1^2+p_2^2) - 2\sinh(2r)(x_1x_2 - p_1p_2). \quad \text{(C.17)}$$

Then,

$$W(\mu,\nu) = \frac{1}{\pi^4}\int dx_1dp_1dx_2dp_2 \exp\left[-\frac{1}{2}\cosh(2r)(x_1^2+x_2^2+p_1^2+p_2^2)\right] \\ \times \exp\left[-\sinh(2r)(x_1x_2-p_1p_2)\right]\exp\left[-i(x_1\mu_1+p_1\nu_1+x_2\mu_2+p_2\nu_2)\right], \quad \text{(C.18)}$$

where $\mu_1 = \alpha_1 + \alpha_1^*$, $\nu_1 = i(\alpha_1 - \alpha_1^*)$, $\mu_2 = \alpha_2 + \alpha_2^*$, and $\nu_2 = i(\alpha_2 - \alpha_2^*)$. We now look at the x_1, x_2 integration only, since the p_1, p_2 integration is the same as the x_1, x_2 part. Thus, we need to solve

$$\mathcal{I} = \frac{1}{\pi^2}\int dx_1dx_2 \exp\left\{-\frac{1}{2}[\cosh(2r)(x_1^2+x_2^2) - 2\sinh(2r)x_1x_2]\right\} \\ \times \exp\left\{-i(x_1\mu_1+x_2\mu_2)\right\}. \quad \text{(C.19)}$$

To solve this, we cast it into the matrix form

$$\mathcal{I} = \int dx_1dx_2 \exp\left(\eta\mu^T - \frac{1}{2}\eta\Lambda\eta^T\right), \quad \text{(C.20)}$$

where $\eta = (x_1\ x_2)$, $\mu = (-i\mu_1\ -i\mu_2)$, and $\Lambda = \begin{pmatrix} \cosh(2r) & -\sinh(2r) \\ -\sinh(2r) & \cosh(2r) \end{pmatrix}$. Λ has a determinant of one, thus it is invertible, and it has the eigenvalues e^{2r} and e^{-2r}.

Using Eq. (C.5) and $\Lambda^{-1} = \begin{pmatrix} \cosh(2r) & \sinh(2r) \\ \sinh(2r) & \cosh(2r) \end{pmatrix}$, we obtain

$$\mathcal{I} = \frac{2}{\pi} \exp\left\{-\frac{1}{2}[(\mu_1^2 + \mu_2^2)\cosh(2r) + 2\sinh(2r)\mu_1\mu_2]\right\}. \tag{C.21}$$

Similar working for the p_1, p_2 integration gives us

$$W = \frac{4}{\pi^2} \exp\left\{-\frac{1}{2}[(\mu_1^2 + \mu_2^2 + \nu_1^2 + \nu_2^2)\cosh(2r) + 2\sinh(2r)(\mu_1\mu_2 - \nu_1\nu_2)]\right\}. \tag{C.22}$$

Finally, substituting the μ's and ν's in terms of α's and expanding the cosh and sinh in terms of e^{2r} and e^{-2r}:

$$W = \frac{4}{\pi^2} \exp\left\{-e^{-2r}[(x_1 - x_2)^2 + (p_1 + p_2)^2] - e^{2r}[(x_1 + x_2)^2 + (p_1 - p_2)^2]\right\}. \tag{C.23}$$

This is the Wigner function for a two-mode squeezed vacuum state. Note that as r increases W tends to $C\delta(x_1 + x_2)\delta(p_1 - p_2)$.

Appendix D

Properties of the characteristic function

In this appendix we prove a few properties used in Section 5.3.4.

D.1 Property 1

$$\int dudv\chi_\psi(-u,-v)\chi_\phi(u,v) = \pi|\langle\psi|\phi\rangle|^2. \tag{D.1}$$

We can prove this property by using Eq. (2.49). Rewriting this equation using real variables, we get

$$\chi_s(u,v) = \int dxdpW\left(x,p\right)\exp\left[2i(xu-pv)\right]. \tag{D.2}$$

Substituting into the l.h.s of Eq. (D.1) gives

$$\begin{aligned}
&\int dudv\chi_\psi(-u,-v)\chi_\phi(u,v)\\
&= \int dudvdxdpdx'dp'W_\psi\left(x,p\right)W_\phi\left(x',p'\right)\exp\left[2iu(x-x')-2iv(p-p'))\right],\\
&= \pi^2\int dxdpdx'dp'W_\psi\left(x,p\right)W_\phi\left(x',p'\right)\delta(x-x')\delta(p-p'),\\
&= \pi^2\int dxdpW_\psi\left(x,p\right)W_\phi\left(x,p\right).
\end{aligned} \tag{D.3}$$

We can now use the well-known property[1]

$$\pi \int dxdpW_{\psi}(x,p)\, W_{\phi}(x,p) = |\langle\psi|\phi\rangle|^2 \tag{D.4}$$

which gives us

$$\int dudv\chi_{\psi}(-u,-v)\chi_{\phi}(u,v) = \pi|\langle\psi|\phi\rangle|^2. \tag{D.5}$$

Thus, we have proved Eq. (D.1).

D.2 Property 2

$$\chi_{\psi}(u,-v) = \chi_{\psi'}(u,v), \tag{D.6}$$

where, if $|\psi\rangle = \sum_{m=0}^{\infty} c_m|m\rangle$, $|\psi'\rangle = \sum_{m=0}^{\infty} c_m^*|m\rangle$. First, note that

$$\chi_{\psi}(u,-v) = \chi_{\psi}(z^*,z) = \sum_{m,n=0}^{\infty} c_n^* c_m \langle n|e^{iz^*a+iza^{\dagger}}|m\rangle. \tag{D.7}$$

Then, using (See Eq. (4.28) of Carmichael [19])

$$e^{iz^*a^{\dagger}+iza} = \sum_{m,n=0} \frac{(iz^*)^n(iz)^m}{n!m!}(a^{\dagger n}a^m)_s, \tag{D.8}$$

where s stands for symmetric ordering, we can write

$$\chi_{\psi}(u,-v) = \sum_{m,n,k,l=0}^{\infty} c_n^* c_m \frac{(iz^*)^l(iz)^k}{l!k!}\langle n|(a^{\dagger k}a^l)_s|m\rangle. \tag{D.9}$$

Because the expectation value is real, we have

$$\langle n|(a^{\dagger k}a^l)_s|m\rangle = \langle m|(a^{\dagger k}a^l)_s^{\dagger}|n\rangle = \langle m|(a^{\dagger l}a^k)_s|n\rangle, \tag{D.10}$$

[1] See, for example, Schleich [17] or Carmichael [19]. The latter uses the same definition of the Wigner distribution as given in this thesis; the result can be seen from Eq. (4.84) and Eq. (4.75b) in the book.

where the second equality follows from the property of symmetric operators. Substituting this into Eq. (D.9), we obtain

$$\begin{aligned}\chi_\psi(u,-v) &= \sum_{m,n,k,l=0}^{\infty} c_n^* c_m \frac{(iz^*)^l (iz)^k}{l!k!} \langle m|(a^{\dagger l} a^k)_s|n\rangle, \\ &= \left(\sum_{m=0}^{\infty} c_m \langle m|\right) e^{iz^* a^\dagger + iza} \left(\sum_{n=0}^{\infty} c_n^* |n\rangle\right), \\ &= \chi_{\psi'}(u,v), \end{aligned} \tag{D.11}$$

where $|\psi'\rangle$ is as defined below Eq. (D.6).

D.3 Property 3

$$\chi_\psi(u,v) = \chi_{\psi_*}(-u,-v), \tag{D.12}$$

where $|\psi_*\rangle = \sum_{m=0}^{\infty}(-1)^m c_m |m\rangle$. Again, we use Eq. (D.8) and write

$$\chi_\psi(u,v) = \sum_{m,n,k,l=0}^{\infty} c_n^* c_m \frac{(iz^*)^k (iz)^l}{k!l!} \langle n|(a^{\dagger k} a^l)_s|m\rangle. \tag{D.13}$$

Now, note that for a given m, and n, the only terms that survive are given by $l-k = m-n$. Given this we can write

$$\begin{aligned}\chi_\psi(u,v) &= \sum_{m,n,k,l=0}^{\infty} (-1)^{(m-n)+(l-k)} c_n^* c_m \frac{(iz^*)^k (iz)^l}{k!l!} \langle n|(a^{\dagger k} a^l)_s|m\rangle, \\ &= \sum_{m,n,k,l=0}^{\infty} (-1)^n c_n^* (-1)^m c_m \frac{(-iz^*)^k (-iz)^l}{k!l!} \langle n|(a^{\dagger k} a^l)_s|m\rangle, \\ &= \left(\sum_{n=0}^{\infty} (-1) c_n^* \langle n|\right) e^{-iz^* a^\dagger - iza} \left(\sum_{m=0}^{\infty} (-1)^m c_m |m\rangle\right), \\ &= \chi_{\psi_*}(-u,-v), \end{aligned} \tag{D.14}$$

hence proving Eq. (D.12).

D.4 Property 4

We want to prove Eq. (5.52). To this end, we expand the characteristic function and rearrange the equation:

$$
\begin{aligned}
&\chi_{\rm in}(u,-v)\exp\left[-2\sqrt{2}i\,(q_x u+q_y v)\right],\\
&=\langle{\rm in}|\exp\left[iu(a+a^\dagger)+v(a-a^\dagger)\right]|{\rm in}\rangle\exp\left[-2\sqrt{2}i\,(q_x u+q_y v)\right],\\
&=\langle{\rm in}|\exp\left\{iu[(a-\sqrt{2}q_x)+(a^\dagger-\sqrt{2}q_x)]+v[(a-i\sqrt{2}q_y)-(a^\dagger+i\sqrt{2}q_y)]\right\}|{\rm in}\rangle,\\
&=\langle{\rm in}|\exp\Big\{iu[(a-\sqrt{2}q_x-i\sqrt{2}q_y)+(a^\dagger-\sqrt{2}q_x+i\sqrt{2}q_y)]\\
&\qquad\qquad +v[(a-i\sqrt{2}q_y-\sqrt{2}q_x)-(a^\dagger+i\sqrt{2}q_y-\sqrt{2}q_x)]\Big\}|{\rm in}\rangle,\\
&=\langle{\rm in}|\exp\left\{iu[(a-\tilde{Q})+(a^\dagger-\tilde{Q}^*)]+v[(a-\tilde{Q})-(a^\dagger-\tilde{Q}^*)]\right\}|{\rm in}\rangle,\\
&=\langle{\rm in}|D^\dagger(-\tilde{Q})\exp\left[iu(a+a^\dagger)+v(a-a^\dagger)\right]D(-\tilde{Q})|{\rm in}\rangle, \qquad \text{(D.15)}
\end{aligned}
$$

where $\tilde{Q}=\sqrt{2}(q_x+iq_y)$, and D is the displacement operator. Thus, defining $|{\rm in}-\tilde{Q}\rangle=D(-\tilde{Q})|{\rm in}\rangle$, we have proved that

$$
\chi_{\rm in}(u,-v)\exp\left[-2\sqrt{2}i\,(q_x u+q_y v)\right]=\chi_{{\rm in}-\sqrt{2}\tilde{q}}(u,-v). \qquad \text{(D.16)}
$$

Appendix E

Stochastic calculus

In this appendix, we show that the stochastic Schrödinger equation (SSE)

$$d|\chi(t)\rangle = \left[d\tilde{Q}^* c + d\tilde{Q} a\right] |\chi(t)\rangle, \tag{E.1}$$

has the solution

$$|\chi(t)\rangle = \exp\left(-2ac\int_0^t dt' e^{-2t} + \tilde{Q}a + \tilde{Q}^* c\right) |\chi(0)\rangle, \tag{E.2}$$

where $\tilde{Q}$ is a stochastic quantity which we will write as $\tilde{Q} = f(t)dt + dW_x + idW_y$. Here, $f(t)$ denotes an arbitrary, but not stochastic, function of t, and $dW_{x,y}$ denote (independent) Wiener increments. The solution was provided by Carmichael [59].

To solve the equation we have to know whether it is to be interpreted as the Ito or Stratonovich SDE (stochastic differential equation). In our case, the SSE has to be interpreted as an Ito SDE, since our SSE has been derived on the assumption that dWs are white noises. If we had derived the SSE for a real noise (non-white noise) process, and then had taken the limit of white noise, we would have to interpret the SSE as a Stratonovich SDE. The way to see that our SSE is an Ito SDE is to derive the master equation back from the SSE. To derive the master equation, we have to use the fact that:

1. $|\chi(t)\rangle$ is statistically independent to the Wiener increment dW, where the Wiener increment is the future increment.

2. $dW_i dW_j = \delta_{ij} dt$, where $i, j \in \{x, y\}$ and the higher order terms are zero.

The second fact is called the Ito rule, and is unique of the solutions of Ito SDEs

[35]. The derivation of the master equation, starting from the SSE for homodyne detection scheme is given in [60].

We will now prove that Eq. (E.2) is indeed the solution of Eq. (E.1), using the Ito rules. The solution can be best seen by first assuming that the answer can be obtained using ordinary calculus, i.e., we assume that the answer is

$$|\chi(t)\rangle = \exp\left(\tilde{Q}a + \tilde{Q}^* c\right)|\chi(0)\rangle, \tag{E.3}$$

and checking if this answer is right even when $\tilde{Q}$ is treated as a stochastic quantity.

Taking the differential of both sides, we need to consider

$$d\left[\exp\left(\tilde{Q}a + \tilde{Q}^* c\right)\right] = \exp\left[(\tilde{Q} + d\tilde{Q})a + (\tilde{Q}^* + d\tilde{Q}^*)c\right] - \exp\left(\tilde{Q}a + \tilde{Q}^* c\right). \tag{E.4}$$

To this end, we expand the first term on the r.h.s to obtain

$$\begin{aligned}\exp\left[(\tilde{Q} + d\tilde{Q})a + (\tilde{Q}^* + d\tilde{Q}^*)c\right] &= \exp\left(\tilde{Q}a\right)\exp\left(\tilde{Q}^* c\right) \\ &\times \left(1 + d\tilde{Q}a + \frac{1}{2}(d\tilde{Q})^2 a^2 + \cdots\right)\left(1 + d\tilde{Q}^* c + \frac{1}{2}(d\tilde{Q}^*)^2 c^2 + \cdots\right),\end{aligned} \tag{E.5}$$

and note that according to the Ito rule we have

$$(d\tilde{Q})^2 = (d\tilde{Q}^*)^2 = 0, \tag{E.6a}$$

$$d\tilde{Q}d\tilde{Q}^* = 2e^{-2t}dt. \tag{E.6b}$$

Equation (E.6a) follows from the fact that dW_x and dW_y are independent, hence $dW_x dW_y = 0$ from the Ito rule. $dW_i^2 = dt$ is used to derive both Eq. (E.6a) and Eq. (E.6b). Higher order terms vanish as in ordinary calculus. Putting Eq. (E.6a) and Eq. (E.6b) into Eq. (E.5), we obtain

$$\begin{aligned}&\exp\left[(\tilde{Q} + d\tilde{Q})a + (\tilde{Q}^* + d\tilde{Q}^*)c\right] \\ &\quad = \exp\left(\tilde{Q}a\right)\exp\left(\tilde{Q}^* c\right)\left(1 + d\tilde{Q}a + d\tilde{Q}^* c + 2e^{-2t}dtac\right),\end{aligned} \tag{E.7}$$

which means that

$$d|\chi(t)\rangle = \left(d\tilde{Q}a + d\tilde{Q}^* c + 2e^{-2t}dtac\right)|\chi(t)\rangle. \tag{E.8}$$

Thus, we need an extra term in Eq. (E.3). The extra term needed is exactly $\exp\left(-2ac\int_0^t dt' e^{-2t'}\right)$, thus proving that Eq. (E.2) is the solution of Eq. (E.1).

Appendix F

Computer codes

F.1 Main code

Code for solving the SSE. It calculates the output state, conditional fidelity and probability distribution.

```
C    code for quantum trajectory of continuous variable quantum teleportation
C    for a fock state input

      integer timestep, n, base, inputbase, dispbase
      parameter(timestep=10000,n=50000,base=20,inputbase=1,dispbase=10)
      !base  = largest number for  fock state basis for squeezed state
      real*8 kappa,dt,probjump,r(2),avgno(0:timestep),ksqrt
      real*8 model(0:timestep),rsqz,avgnumber(0:timestep),dtsqrt,sqrt2
      real*8 norm,Qx,Qy,dQx,dQy,adga(0:timestep-1),bdgb(0:timestep-1)
      real*8 inputcoeff(0:inputbase),cnorm,cdgcexpt(0:timestep-1)
      real*8 adgaexpt(0:timestep-1),bdgbexpt(0:timestep-1)
      real*8 bmodel(0:timestep-1),amodel(0:timestep-1),tr,tra
      real*8 cdgc(0:timestep-1),qxreg,qyreg,newfrequency(-40:40,-40:40)
      real*8 frequency(-40:40,-40:40),fid(-40:40,-40:40)
      real*8 fiddist(-40:40,-40:40,1:10000),radiusreg
      real*8 newradialfreq(1:50),radialfreq(1:50),radialfid(1:50)

      complex*16 wavefn(0:inputbase,0:base,0:base),alpha
      complex*16 apsi(0:inputbase,0:base,0:base)
      complex*16 adgpsi(0:inputbase,0:base,0:base)
      complex*16 bpsi(0:inputbase,0:base,0:base)
      complex*16 bdgpsi(0:inputbase,0:base,0:base)
      complex*16 adgapsi(0:inputbase,0:base,0:base)
      complex*16 bdgbpsi(0:inputbase,0:base,0:base)
      complex*16 rho(0:dispbase,0:dispbase),output(0:base)
      complex*16 aexpt,bexpt,adgexpt,bdgexpt,dispoutput(0:dispbase)
      complex*16 displace(0:base,0:base)
      complex*16 cdgcpsi(0:inputbase,0:base,0:base)
      complex*16 avgrho(0:dispbase,0:dispbase)

      integer i,jumpno,ISEED,j,k,l,p,Qxint,Qyint,radiusint

      !---set parameters---!
      kappa = 1.0D0
      ksqrt = dsqrt(kappa)
      dt = 0.001D0
      dtsqrt = dsqrt(dt)
      sqrt2 = dsqrt(dfloat(2))
      rsqz = 0.7D0      !squeezing parameter
      !---------------------!

      open(1,file='rho.dat')
      open(3,file='fiddist.dat')
      open(4,file='radialfidelity.dat')

      do j=1,n          !loop for ensemble

      if(mod(j,5000)==0)then
      print *,j
      endif
      Qx = 0
```

```
      Qy = 0


      wavefn = 0 !reset
      !--set up initial two-mode vacuum squeezed states--!
      wavefn(:,0,0) = dfloat(1)/cosh(rsqz)
      do k=1,base
        wavefn(:,k,k) = -tanh(rsqz)*wavefn(:,k-1,k-1)
      enddo
!-------------------------------------------------!


      !-----set up initial input state-----!
      inputcoeff(inputbase) = 1
      do i=0,inputbase
      wavefn(i,:,:) = inputcoeff(i)*wavefn(i,:,:)
      enddo
!-----------------------------------!
      do i = 1,timestep            !loop for alice's measurements
       r(1) = gasdev(15)
       r(2) = gasdev(17)

  !---calculate a|psi>,a+|psi>,b|psi>,b+|psi>---!

  !a,a+ and a+a
      do k=1,inputbase
       adgpsi(k,:,:) = dsqrt(dfloat(k))*wavefn(k-1,:,:)
       apsi(k-1,:,:) = dsqrt(dfloat(k))*wavefn(k,:,:)
       adgapsi(k,:,:) = k*wavefn(k,:,:)
      enddo
      adgapsi(0,:,:) = 0
      apsi(inputbase,:,:) = 0
      adgpsi(0,:,:) = 0
  !b,b+ and b+b
      do k=1,base
       bdgpsi(:,k,:) = dsqrt(dfloat(k))*wavefn(:,k-1,:)
       bpsi(:,k-1,:) = dsqrt(dfloat(k))*wavefn(:,k,:)
       bdgbpsi(:,k,:) = k*wavefn(:,k,:)
       cdgcpsi(:,:,k) = k*wavefn(:,:,k)
      enddo
      bdgbpsi(:,0,:) = 0
      bpsi(:,base,:) = 0
      bdgpsi(:,0,:) = 0
      cdgcpsi(:,:,0) = 0
!-----------------------------------------!



!-----start computing scaled charges-----!

    !---first compute expectation values and norm---!
      norm = sum(wavefn*conjg(wavefn))
      aexpt = sum(conjg(wavefn)*apsi)
      adgexpt = conjg(aexpt)
      bexpt = sum(conjg(wavefn)*bpsi)
      bdgexpt = conjg(bexpt)
  !-----------------------------------------!
!-------check photon numbers after homodyne measurement------------!
      adgaexpt(i-1) = sum(conjg(wavefn)*adgapsi)/norm
      bdgbexpt(i-1) = sum(conjg(wavefn)*bdgbpsi)/norm
      cdgcexpt(i-1) = sum(conjg(wavefn)*cdgcpsi)/norm
  !-------------------------------------------------------------------!

      dQx = dt*ksqrt*((aexpt+adgexpt) + (bexpt+bdgexpt))/norm +dtsqrt*r(1)
      dQy = -dt*ksqrt*imag((adgexpt-aexpt) - (bdgexpt-bexpt))/norm +dtsqrt*r(2)
      Qx = Qx + dQx*exp(-i*kappa*dt)
      Qy = Qy + dQy*exp(-i*kappa*dt)
  !-----------------------------------------!


  !--use stochastic schrodinger equation to evolve wavefn--!
      wavefn = wavefn-kappa*(adgapsi + bdgbpsi)*dt + ksqrt*(dcmplx(dQx,-dQy)*apsi +dcmplx(dQx,dQy)*bpsi)
  !-----------------------------------------------------!

      enddo !end of alice's measurements

      adga = adga + adgaexpt
      bdgb = bdgb + bdgbexpt
      cdgc = cdgc + cdgcexpt
      output = wavefn(0,0,:)

  !-----run victor's measurement,displacement-----!
      alpha = dcmplx(Qx,Qy)
```

```
  !---number state representation of displacement op---!
      displace(0,0) = exp(-alpha*conjg(alpha)/2)
      do k = 1,dispbase
       displace(k,0) = alpha/dsqrt(dfloat(k))*displace(k-1,0) !calculate first column,<m|a>, where |a> is coherent state
       displace(0,k) = -conjg(alpha)/dsqrt(dfloat(k))*displace(0,k-1) !calculate first row, <-a|n>
      enddo

      do k=1,dispbase
  !--<k|D(a)|k>--!
      displace(k,k) =  (displace(k-1,k-1)*dsqrt(dfloat(k)) + alpha*displace(k-1,k))/dsqrt(dfloat(k))
  !--------------!

      do l=k+1,dispbase
       displace(l,k) = (displace(l-1,k-1)*dsqrt(dfloat(k)) + alpha*displace(l-1,k))/dsqrt(dfloat(l)) !column
       displace(k,l) = (displace(k-1,l-1)*dsqrt(dfloat(k)) - conjg(alpha)*displace(k,l-1))/dsqrt(dfloat(l)) !row
      enddo
    enddo

!-----------------------------------------------------!

  !---now apply the displacement to output field---!

      do i=0,dispbase
       dispoutput(i) = sum(displace(i,0:base)*output)
      enddo
  !-----------------------------------------------!
      cnorm = sum(dispoutput*conjg(dispoutput))
      do k=0,dispbase
       do l=0,dispbase
        rho(k,l)=dispoutput(k)*conjg(dispoutput(l))/cnorm
       enddo
      enddo
      avgrho = avgrho + rho
  !----end of victor's measurement,displacement-------!

  !----------- fidelity distribution ------------------!
      if(Qx.gt.0)then
       if(Qx.gt.(4.0))then
        Qx = 4.0
       else
        Qx = Qx + 0.05
       endif
      else
       if(Qx.lt.(-4.0))then
        Qx = -4.0
       else
        Qx = Qx - 0.05
       endif
      endif

      if(Qy.gt.0)then
       if(Qy.gt.(4.0))then
        Qy = 4.0
       else
        Qy = Qy + 0.05
       endif
      else
       if(Qy.lt.(-4.0))then
        Qy = -4.0
       else
        Qy = Qy - 0.05
       endif
      endif
      Qxint = int(Qx*10)
      Qyint = int(Qy*10)
      fid(Qxint,Qyint) = fid(Qxint,Qyint) + real(dispoutput(inputbase)*conjg(dispoutput(inputbase))/cnorm)
      frequency(Qxint,Qyint) = frequency(Qxint,Qyint) + 1
      fiddist(Qxint,Qyint,frequency(Qxint,Qyint)) = real(dispoutput(inputbase)*conjg(dispoutput(inputbase))/cnorm)
  !-------------------end of calculating fidelity distribution --------------!

  !-------------radially symmetric conditional fidelity-------------------------!
      radius = dsqrt(Qx**2+Qy**2)
      radiusint = 1 + int(radius*10)
      if(radius.LE.5)then
       radialfid(radiusint) = radialfid(radiusint) + real(dispoutput(inputbase)*conjg(dispoutput(inputbase))/cnorm)
       radialfreq(radiusint) = radialfreq(radiusint) + 1
      endif
  !-------------end of radially symmetric conditional fidelity------------------!
     enddo !end of ensemble run

  !----------fidelity as a function of qx and qy--------------------------------!
      newfrequency = frequency
      do i=-40,40
       qxreg = i*0.1d0
```

```
       do j=-40,40
        qyreg = j*0.1d0
      if(frequency(i,j)==0)then
         newfrequency(i,j) = 1
        endif
        write(3,300) qxreg,qyreg,fid(i,j)/newfrequency(i,j),frequency(i,j)
       enddo
      enddo


  !---------fidelity as a function of radius r------------------!
      newradialfreq = radialfreq
      do i=1,50
       radiusreg = i+0.05
       if(radialfreq(i)==0)then
        newradialfreq(i) = 1
       endif
       write(4,400) radiusreg,radialfid(i)/newradialfreq(i),radialfreq(i)
      enddo
      do i=0,dispbase
       do j=0,dispbase
        write(1,100) avgrho(i,j)
       enddo
      enddo
      close(1)
      close(3)
      close(4)
 !-------------------------------------------------------------------------!
      do i=0,dispbase
tr = tr + avgrho(i,i)

enddo
print *,tr
100   format( e20.10)
200   format( 5e20.10)
300   format( 4e20.10)
400   format( 3e20.10)

end


! randomnumber generators

      FUNCTION gasdev(idum)
      INTEGER idum
      REAL gasdev
c      USES ran3
      INTEGER iset
      REAL fac,gset,rsq,v1,v2,ran1
      SAVE iset,gset
      DATA iset/0/
      if (idum.lt.0) iset=0
      if (iset.eq.0) then
 1       v1=2.*ran3(idum)-1.
         v2=2.*ran3(idum)-1.
         rsq=v1**2+v2**2
         if(rsq.ge.1..or.rsq.eq.0.)goto 1
         fac=sqrt(-2.*log(rsq)/rsq)
         gset=v1*fac
         gasdev=v2*fac
         iset=1
      else
         gasdev=gset
         iset=0
      endif
      return
      END




      FUNCTION ran3(idum)
      INTEGER idum
      INTEGER MBIG,MSEED,MZ

      REAL ran3,FAC
      PARAMETER (MBIG=1000000000,MSEED=161803398,MZ=0,FAC=1./MBIG)

      INTEGER i,iff,ii,inext,inextp,k
      INTEGER mj,mk,ma(55)
      SAVE iff,inext,inextp,ma
      DATA iff /0/
      if(idum.lt.0.or.iff.eq.0)then
         iff=1
```

```
        mj=abs(MSEED-abs(idum))
        mj=mod(mj,MBIG)
        ma(55)=mj
        mk=1
        do 11 i=1,54
           ii=mod(21*i,55)
           ma(ii)=mk
           mk=mj-mk
           if(mk.lt.MZ)mk=mk+MBIG
           mj=ma(ii)
11      continue
        do 13 k=1,4
           do 12 i=1,55
              ma(i)=ma(i)-ma(1+mod(i+30,55))
              if(ma(i).lt.MZ)ma(i)=ma(i)+MBIG
12         continue
13      continue
        inext=0
        inextp=31
        idum=1
      endif
      inext=inext+1
      if(inext.eq.56)inext=1
      inextp=inextp+1
      if(inextp.eq.56)inextp=1
      mj=ma(inext)-ma(inextp)
      if(mj.lt.MZ)mj=mj+MBIG
      ma(inext)=mj
      ran3=mj*FAC
      return
      END
```

F.2 Wigner plot

This code takes a density operator as input and produces the Wigner distribution as its output.

```
C This program is a little modification to howard's wigner function plotting program
C this program creates Wigner.dat from rhoss.dat, which is a given denstiy matrix
C rho is such that rhonm = conjg(rhomn)
      parameter (mphoton=10,nn=mphoton+1)
      parameter (xmin=-4.0,xmax=4.0,ymin=-4.0,ymax=4.0)
      parameter (nxstep=50,nystep=50)

      double complex rho(0:mphoton,0:mphoton)
      double precision logfact(0:mphoton),tr
      double precision xstep,ystep,x,y,xy,logxy,logfactor
      double precision Qfn,sumQfn,Wig,sumWig,sign
      double complex al,logal,logal1(0:mphoton)
      double complex clogfactor,clogfactor1,clogfactor2
      double precision mumax,numax,mustep,nustep,mu,nu,munu
      double precision factorn,factorm

      integer i,j,n,m,k,l,nwig,minusn,minusl,ii
      pi=3.14159265358979323

      open(unit=1,action='read',file='rhoss.dat',status='old')
      do i=0,mphoton
       do j=0,mphoton
        read(1,100)rho(i,j)
100     format( e20.10)
       end do
      end do
      close(unit=1)
      !print *,rho
      do i=0,mphoton
       tr = tr+rho(i,i)
      enddo
      print *,tr

      logfact(0)=0.0
      do n=1,mphoton
       logfact(n)=logfact(n-1)+0.5*log(real(n))
      end do

      open(4,file='Wigner.dat',status='unknown')


      sumWig=0.0
```

```
      xstep=(xmax-xmin)/real(nxstep)
      ystep=(ymax-ymin)/real(nystep)
      do i=0,nxstep
         x=xmin+real(i)*xstep
         do j=0,nystep
            y=ymin+real(j)*ystep

            xy=x*x+y*y
            al = cmplx(x,y)

            Wig=0.0
            xy=2.0*xy
            logxy=log(2.0*xy)
            minusn=-1
            do n=0,mphoton
               minusn=-minusn
               logfactor=-xy-logxy
               minusl=-1
               do l=0,n
                  minusl=-minusl
                  logfactor=logfactor+logxy
                  sign=real(minusn*minusl,8)
                  Wig=Wig+sign*(rho(n,n))*exp(logfactor+2.0D00*(logfact(n)-logfact(n-l)-2.0D00*logfact(l)))

               end do
            end do
           !print *,Wig
            logal=log(2.0*al)

            logal1(0)=0.0

            do n=1,mphoton
               logal1(n)=logal1(n-1)+logal
            end do

            do n=1,mphoton
               minusn=-1


               do m=0,n-1
                  minusn=-minusn
                  minusl=-1
                  do l=0,m

                     minusl=-minusl
                     clogfactor=-xy+logal1(l)+conjg(logal1(n-m+l))+logfact(n)+logfact(m)
     *                          -2.0*(logfact(n-m+l)+logfact(m-l)+logfact(l))
                     sign=real(minusn*minusl)

                     Wig=Wig+2.0*sign*real(exp(clogfactor)*rho(n,m))

                  end do
               end do
            end do
            Wig=2.0*Wig/pi
            sumWig=sumWig+Wig

            write(4,300)x,y,Wig
         end do
      end do

      close(4)


      print *,sumWig*xstep*ystep
  300 format(3(2x,e12.5))

stop
end
```

Bibliography

[1] A. Einstien, B. Podolsky, and N. Rosen, "Can Quantum-Mechanical Description of Physical Reality Be Considered Complete?" Phys. Rev. **47**, 777 (1935).

[2] C. H. Bennett, "Quantum Information" Physica Scripta **T76**, 210 (1998).

[3] C. H. Bennett and S. J. Wiesner, "Communication via One- and Two-Particle Operators on Einstein-Podolsky-Rosen States" **69**, 2881 (1992).

[4] C. H. Bennett, G. Brassard, C. Crepeau, R. Jozsa, A. Peres, and W. K. Wootters, "Teleporting an Unknown Quantum State via Dual Classical and Einstein-Podolsky-Rosen Channels" Phys. Rev. Lett. **70**, 1895 (1993).

[5] A. Furusawa, J. L. Sorensen, S. L. Braunstein, C. A. Fuchs, H. J. Kimble, and E. S. Polzik, "Unconditional quantum teleportation" Science **282**, 706 (1998).

[6] P. van Loock, Samuel L. Braunstein, and H. J. Kimble, "Broadband teleportation" Phys. Rev. A **62**, 022309 (2000).

[7] S. L. Braunstein, C. A. Fuchs, and H. J. Kimble, "Criteria for continuous-variable quantum teleportation" J. Mod. Opt. **47**, 267 (2000).

[8] Lev Vaidman, "Teleportation of quantum states" Phy. Rev. A **49**, 1473 (1994).

[9] Samuel L. Braunstein and H. J. Kimble, "Teleportation of Continuous Quantum Variables" Phys. Rev. Lett. **80**, 869 (1998).

[10] W. P. Bowen, N. Treps, B. C. Buchler, R. Schnabel, T. C. Ralph, H. Bachor, T. Symul, and P. K. Lam, "Experimental investigation of continuous-variable quantum teleportation" Phys. Rev. A **67**, 032302 (2003).

[11] Eugen Merzbacher, *Quantum Mechanics*, 3rd ed. (John Wiley & Sons, 1998).

[12] Marlan O. Scully and M. Suhail Zubairy, *Quantum Optics* (Cambridge university press, 1997).

[13] D. F. Walls and G. J. Milburn, *Quantum Optics* (Springer-Verlag, 1994).

[14] P. A. M. Dirac, *The Principles of Quantum Mechanics*, 4th ed. (Oxford Science Publications, 1957).

[15] Leonard Mandel and Emil Wolf, *Optical coherence and quantum optics* (Cambridge university press, 1995).

[16] H. P. Yuen and V. W. S. Chan, "Optical Communication with Two-Photon Coherent States-Part III: Quantum Measurements Realizable with Photoemissive Detectors" IEEE Trans. Inf. Theory **IT-26**, 78 (1980).

[17] Wolfgang P. Schleich, *Quantum Optics in Phase Space* (Wiley-vch, 2000).

[18] E. P. Wigner, "On the Quantum Correction for Thermodynamic Equilibrium" Phys. Rev. **40**, 746 (1932).

[19] H. J. Carmichael, *Statistical Methods in Quantum Optics*, Vol. 1, 2nd ed. (Springer, 2002).

[20] C. M. Caves, "Quantum-mechanical noise in an interferometer" Phys. Rev. D **23**, 1693 (1981).

[21] D. F. Walls, "Squeezed States of Light" **306**, 141 (1983).

[22] R. Loudon and P. L. Knight, "Squeezed Light" J. Mod. Opt. **34**, 709 (1987).

[23] H. P. Yuen and V. W. S. Chan, "Noise in homodyne and heterodyne detection" Opt. Lett. **8**, 177 (1983).

[24] H. J. Carmichael, *An Open Systems Approach to Quantum Optics* (Springer-Verlag, 1993).

[25] R. Loudon, *The Quantum Theory of Light* (Oxford Science Publications, 1983).

[26] R. J. Glauber, "The Quantum Theory of Optical Coherence" Phys. Rev. **130**, 2529 (1963).

[27] C. W. Gardiner and P. Zoller, *Quantum Noise*, 2nd ed. (Springer, 1999).

[28] P. L. Kelley and W. H. Kleiner, "Theory of Electromagnetic Field Measurement and Photoelectric Counting" Phys. Rev. **136** (1964).

[29] I. R. Senitzky, "Dissipation in quantum mechanics. The harmonic oscillator." Phys. Rev. **119**, 670 (1960).

[30] I. R. Senitzky, "Dissipation in quantum mechanics. The harmonic oscillator. II" Phys. Rev. **124**, 642 (1961).

[31] William H. Louisell, *Quantum Statistical Properties of Radiation* (John Wiley & Sons, 1973).

[32] G. Lindblad, "On the Generators of Quantum Dynamical Semigroups" Commun. Math. Phys. **48**, 119 (1976).

[33] C. W. Gardiner and M. J. Collett, "Input and output in damped quantum systems: Quantum stochastic differential equations and the master equation" Phys. Rev. A **31**, 3761 (1985).

[34] H. J. Carmichael, *Statistical Methods in Quantum Optics*, Vol. 2 (Springer, unpublished).

[35] C. W. Gardiner, *Handbook of Stochastic Methods*, 3rd ed. (Springer, 2003).

[36] W. K. Wootters and W. H. Zurek, "A single quantum cannot be cloned" **299**, 802 (1982).

[37] J. J. Sakurai, *Modern Quantum Mechanics*, Revised ed. (Addison Wesley, 1994).

[38] E. Schrödinger, "Discussion of probability relations between separated systems" Proceedings of the Cambridge Philosophical Society **31**, 555–563 (1935).

[39] John. S. Bell, *Speakable and unspeakable in quantum mechanics* (Cambridge university press, 1987).

[40] S. J. Freedman and J. F. Clauser, "Experimental test of local hidden-variable theories" Phy. Rev. Lett. **28**, 938 (1972).

[41] A. Aspect, J. Dalibard, and G. Roger, "Experimental test of Bell's inequalities using time-varying analyzers" Phys. Rev. Lett. **49**, 1804 (1982).

[42] G. Weihs, T. Jennewein, C. Simon, H. Weinfurter, and A. Zeilinger, "Violation of Bell's inequality under strict Einstein locality conditions" Phys. Rev. Lett. **81**, 5039 (1998).

[43] J. F. Clauser, M. A. Horne, A. Shimony, and R. A. Holt, "Proposed Experiment to Test Local Hidden-Variable Theories" Phy. Rev. Lett. **23**, 880 (1969).

[44] D. Bouwmeester, J. Pan, K. Mattle, M. Eibl, H. Weinfurter, and A. Zeilinger, "Experimental quantum teleportation" Nature **390**, 575 (1997).

[45] D. Boschi, S. Branca, F.De Martini, L. Hardy, and S. Popescu, "Experimental realization of teleporting an unknown pure quantum state via dual classical and Einstein-Podolsky-Rosen channels" Phys. Rev. Lett. **80**, 1121 (1998).

[46] M.G. Raymer, J. Cooper, H. J. Carmichael, M. Beck, and D. T. Smithey, "Ultrafast measurement of optical-field statistics by dc-balanced homodyne detection" J. Opt. Soc. Am B **12** (1995).

[47] Roy J. Glauber, "Coherent and Incoherent States of the Radiation Field" Phys. Rev. **131**, 2766 (1963).

[48] E. C. G. Sudarshan, "Equivalence of semiclassical and quantum mechanical descriptions of statistical light beams" Phys. Rev. Lett. **10**, 277 (1963).

[49] T. W. Marshall, "Random Electrodynamics" Proc. R. Soc. London **276**, 475 (1963).

[50] H. J. Carmichael and H. Nha, "Continuous variable teleportation within stochastic electrodynamics" in P. Hannaford, A. Sidorov, H. Bachor, and K. Baldwin, eds. *Proceedings of the XVI international conference laser spectroscopy*, pages 324–333 (World Scientific, 2003).

[51] http://www.library.cornell.edu/nr/cbookfpdf.html, "Numerical recipes books online, Chapter 7.1 and 7.2".

[52] S. M. Barnett and P. M. Radmore, *Methods in Theoretical Quantum Optics* (Oxford Science Publications, 1997).

[53] Milton Abramowitz and Irene A. Stegun, *Handbook of Mathematical Functions* (Dover, 1970).

[54] John Von Neumann (translated by Robert T. Beyer), *Mathematical foundations of quantum mechanics* (Princeton: Princeton University Press, 1955).

[55] C. H. Bennett, D. P. DiVincenzo, J. A. Smolin, and W. K. Wootters, "Mixed-state entanglement and quantum error correction" Phys. Rev. A **54**, 3824 (1996).

[56] G. Giedke, M. M. Wolf, O. Kruger, R. F. Werner, and J. I. Cirac, "Entanglement of formation for symmetric gaussian states" Phys. Rev. Lett. **91**, 107901 (2003).

[57] G. B. Arfken and H. J. Weber, *Mathematical Methods for Physicists*, 5th ed. (Harcourt Academic Press, 2001).

[58] C. M. Caves and B. L. Schumaker, "New formalism for two-photon quantum optics. I. Quadrature phases and squeezed states" Phys. Rev. A **31**, 3068 (1985).

[59] H. J. Carmichael, "Private communication".

[60] H. M. Wiseman and G. J. Milburn, "Quantum theory of field-quadrature measurements" Phy. Rev. A **47**, 642 (1993).